Characterization and mapping of irrigated crop classes at territory level

Mukhtar Adamu Abubakar

THÈSE DE DOCTORAT D'AVIGNON UNIVERSITÉ

École Doctorale 536
Agrosciences et sciences

INRAE - Institut National de Recherche pour l'Agriculture, l'Alimentation et l'Environnement
Unité EMMAH – (Environnement Méditerranéen et Modélisation des Agro-Hydrosystèmes)

Par

Mukhtar Adamu Abubakar

Characterization and Mapping of Irrigated Crop Classes at Territory Level

Présentée et soutenue publiquement le 29 November, 2023 devant le jury composé de :

Valerie LE DANTEC Maître de conférence, Université Paul Sabatier (HDR) , Toulouse	Rapportrice
Hervé QUENOL Directeur de Recherches, LETG, Université Rennes	Rapporteur
Nicolas DELBART Professeur, LIED, Université Paris Cité	Examinateur
Vincent SIMONNEAUX Ingenieur de Recherche IRD, CESBIO Toulouse	Examinateur
André CHANZY, Directeur de Recherches, UMR 1114 EMMAH, INRAE-AU	Directeur de thèse
Dominique COURAULT, Directrice de Recherches, UMR 1114 EMMAH, INRAE-AU	Co-Directrice de thèse

Dedication

To the memory of my late grandparents ADAMU ABDULLAHI, AISHA ABUBAKAR, MUKHTAR MUHAMMAD, KHADIJAH HABIBU.

To my dear father ABUBAKAR, who inspired and made me what I am today, who gave me all the love, support, and encouragement for what I would remain grateful for.

To my dear mother ASMA'U, who has never ceased to surround me with her affection and her most delicate attentions all along my life and to whom I have an unwavering devotion.

To my soul partner, my patient and understanding wife SUMAIYA who has been a great source of motivation and inspiration.

To my two lovely angels, baby HUSNA (ASMA'U) and baby HAMRA (AISHA). May God bless you.

To my dear brothers ADAM, ISAH, KABEER, ABDUL JALIL, ABUBAKAR, and BILAL who shared all my moments with a lot of joy and encouragement.

To my parents-in-law LADAN and AISHA, brothers and sisters-in-law, and my entire extended family members.

Mukhtar

Dédicaces

À la mémoire de mes grands-parents décédés ADAMU ABDULLAHI, AISHA ABUBAKAR, MUKHTAR MUHAMMAD, KHADIJAH HABIBU.

À mon cher père ABUBAKAR, qui m'a inspiré et a fait de moi ce que je suis aujourd'hui, qui m'a donné tout l'amour, le soutien et l'encouragement dont je lui suis reconnaissant.

À ma chère mère ASMA'U, qui n'a cessé de m'entourer de son affection et de ses attentions les plus délicates tout au long de ma vie et à qui je voue une dévotion inébranlable.

À mon âme sœur, mon épouse SUMAIYA, patiente et compréhensive, qui a été une grande source de motivation et d'inspiration.

À mes deux adorables anges, le bébé HUSNA (ASMA'U) et le bébé HAMRA (AISHA). Que Dieu vous bénisse.

À mes chers frères ADAM, ISAH, KABEER, ABDUL JALIL, ABUBAKAR et BILAL qui ont partagé tous mes moments avec beaucoup de joie et d'encouragement.

À mes beaux-parents LADAN et AISHA, à mes beaux-frères et belles-sœurs et à tous les membres de ma famille élargie.

Mukhtar

ACKNOWLEDGEMENT

Firstly, I would like to thank Almighty ALLAH for giving me the grace to endure from the beginning to the end.

I expressed my deepest gratitude and appreciation to my team of supervisors Mr. André Chanzy and Mrs. Dominique Courault for guiding me throughout my thesis period with crucial advice, significant remarks, continuous support, and patience. It was a great privilege and honour working with you and once again thank you for your time. I would also like to show my gratitude to Mr. Fabrice Flamain, Mr. Guillaume Pouget, Ms. Veronique Desfonds, Mrs. Marie Weiss, and Mr. Ayoub Nachite for their support and assistance (directly or indirectly) during the period of stay study. My sincere regards go to the entire staff and students of the INRAE AVIGNON-EMMAH-CLIMAT/SOL units

My deepest appreciation to Mrs. Emmanuelle Vaudour, Mr. Gilles Vercambre, Mr. Lionel Jarlan, and Mr. Stéphane Ruy for their tireless external yearly assessments of my PhD. All your contributions and suggestions have enormously improved the content of my PhD thesis.

My sincere appreciation to the thesis committee members Mrs. Valerie Le Dantec, Mr. Hervé Quenol, Mr. Nicolas Delbart, and lastly Mr. Vincent Simonneaux for their remarks and participation.

I would like to express my deepest appreciation for all the good shared memories experienced during my stay in France. Such a happy experience has occupied my thoughts with cheerful days and it will go down in history as a source of support and encouragement. Thanks to all my close friends Muhammed Awwal Atta, Coffi Belmys Cakpo, and Kamran Irfan to mention a few.

I would also like to show my gratitude to the entire staff and students of Nasarawa State University Keffi (NSUK), Faculty of Agriculture. To all the staffs (academic and non-academic) of the Agronomy Department (Prof. Ajayi, Prof. Haruna, Prof. Jayeobe, Prof. Ogara, Dr. Ibrahim, Dr. Amana, Engr. Ogbe, Mr. Jibrin) I sincerely appreciate all your supports.

Thanks, my lovely family for your continuous support.

REMERCIEMENTS

Tout d'abord, je voudrais remercier ALLAH tout-puissant de m'avoir donné la grâce de tenir le coup du début à la fin

J'exprime ma profonde gratitude et mon appréciation à mon équipe de superviseurs, M. André Chanzy et Mme Dominique Courault, pour m'avoir guidé tout au long de ma période de thèse avec des conseils cruciaux, des remarques significatives, un soutien continu et de la patience. Ce fut un grand privilège et un honneur de travailler avec vous et je vous remercie encore une fois pour le temps que vous m'avez consacré. Je tiens également à exprimer ma gratitude à M. Fabrice Flamain, M. Guillaume Pouget, Mme Véronique Desfonds, Mme Marie Weiss et M. Ayoub Nachite pour leur soutien et leur assistance (directe ou indirecte) durant la période de mon séjour d'étude. Mes sincères salutations vont à l'ensemble du personnel et des étudiants des unités INRAE AVIGNON-EMMAH-CLIMAT/SOL.

Je remercie vivement les membres qui ont participé au comité de suivi de ma thèse Mme Emmanuelle Vaudour, M. Gilles Vercambre, M. Lionel Jarlan et M. Stéphane Ruy pour leurs évaluations externes annuelles de mon doctorat. Toutes vos contributions et suggestions ont énormément amélioré le contenu de ma thèse de doctorat.

Je remercie sincèrement les membres du comité de thèse, Mme Valérie Le Dantec, M. Hervé Quenol, M. Nicolas Delbart, et enfin M. Vincent Simonneaux, pour leurs remarques et leur participation.

J'aimerais exprimer ma profonde gratitude pour tous les bons souvenirs partagés pendant mon séjour en France. Une expérience aussi heureuse a occupé mes pensées pendant des jours joyeux et restera dans l'histoire comme une source de soutien et d'encouragement. Merci à tous mes amis proches, Muhammed Awwal Atta, Coffi Belmys Cakpo et Kamran Irfan, pour n'en citer que quelques-uns.

Je tiens également à exprimer ma gratitude à l'ensemble du personnel et des étudiants de la Faculté d'agriculture de l'Université d'État de Nasarawa à Keffi (NSUK). Ajayi, Haruna, Jayeobe, Ogara, Ibrahim, Amana, Ogbe, Jibrin), j'apprécie sincèrement votre soutien.

Merci à ma charmante famille pour son soutien constant

Funding

This study was funded by Petroleum Technology Development Funds (PTDF) under The Federal Ministry of Petroleum Resources, Nigeria, Overseas Scholarship Scheme (2019/2020). Which is also partly funded by the French National Research Institute for Agriculture, Food, and Environment (INRAE-Avignon) under a part of the IRRIWEL and Kaust Projects.

Financement

Cette étude a été financée pour la plus grande partie par les Fonds de développement de la technologie pétrolière (PTDF) dans le cadre du Ministère fédéral des ressources pétrolières, Nigeria, programme de bourses d'études à l'étranger (2019/2020). Elle a aussi bénéficié de financements complémentaires de projets menés sur les sites étudiés (projet EU Irriwell et Kaust). Elle a été soutenue par l'Institut national de recherche sur l'agriculture, l'alimentation et l'environnement (INRAE-Avignon).

Characterization and Mapping of Irrigated Crop Classes at Territory Level

Abstract

The occurrence and intensity of water shortages due to climate change are increasing worldwide including the Mediterranean region, and are thus becoming a major threat to agricultural production. Efficient management of agricultural water resources is therefore a crucial concern, particularly in irrigated areas. Accurate assessments of plant water requirements using tools for estimating evapotranspiration (ET) on a regional scale could contribute to the sustainable management of limited water resources in regions already facing water shortages. Implementing these tools requires precise knowledge of irrigated crops, their location as well as their foliar development. To this end, remote sensing provides important information on the dynamics of plant cover via vegetation indices (NDVI) or the estimation of biophysical variables (e.g. Leaf Area Index (LAI)), which are variables describing characteristics of plant cover linked to ET.

The general aim of this thesis is to evaluate methods using Sentinel-2 data to map irrigated crops and their leaf development. The study is based on two Mediterranean areas, namely the Crau plain and the Ouvèze-Ventoux irrigated zone. In this work, the algorithms used for mapping surfaces and characterising plant cover are all based on the analysis of LAI time series estimated by remote sensing to identify the phenological and agronomic traits of the plant cover observed. The main innovation lies in the use of these traits to characterise plant cover rather than injecting the raw time series (reflectances or vegetation indices) into the classification algorithms as is generally done. This work is divided into three parts: (i) the first concerns the mapping of irrigated grasslands in the Crau. (ii) the second part is dedicated to the mapping of irrigated woody crops (orchards, vineyards, and olive groves) (iii) finally, the third part focused mainly on the characterisation of vineyards by looking for two important characteristics, namely the management of the inter-row and the characterisation of the foliar index of the vine, which requires the subtraction of the contributions of the inter-row to the LAI as seen by the satellite. For the first part of the work (on irrigated grassland), a mowing detection algorithm was designed using the temporal LAI signal derived from Sentinel 2 observations. The algorithm includes a filter to eliminate noise in the signal that could lead to false detection of mowing. A pixel is classified as irrigated grassland if at least two mowings are detected. We obtained a very satisfactory Kappa index of between 0.94 and 0.99 depending on the year. In the second stage of the work, a classification based on phenological metrics (PMs) derived from the Sentinel 2 time series was developed. The PMs correspond to the parameters of an analytical model (double logistic) used to characterise the phases of growth and decline in LAI, as well as the plateau corresponding to the maximum development of the canopy. The PMs are calculated from the LAI time series averaged over the agricultural plot and then fed into the classification algorithm (random forest RF). The Kappa indices vary from 0.86 to 0.95 depending on the year. These results are much better than those obtained by applying the RF algorithm to the LAI time series (Kappa ranging from 0.3 to 0.52). Finally, in the last part of this thesis, the proposed method is based on two hypotheses, namely the temporality of the vine's leaf development and the fact that the inter-

row grass cover is dry or absent in summer. This makes it possible to fit a theoretical vine leaf development curve based on an analytical curve of the double logistic type and to identify the contribution of the inter-row to LAI by subtracting the theoretical vine curve from the observed LAI time series. We were thus able to separate the inter-rows with different management practices such as grassed, partial grassed, and tillage.

This study demonstrates the value of using phenological traits (or points characterising the phenological stages) rather than the raw values derived from the raw temporal profiles of the remote sensing data (less data is used and the method can be reproduced from one year to the next). This is an interesting feature that reduces the workload involved in collecting reference information.

Caractérisationa et cartographie des classes de cultures irriguées au niveau du territoire

Résumé

L'occurrence et l'intensité des pénuries d'eau dues au changement climatique augmentent dans le monde et dans la région méditerranéenne et devient ainsi une menace majeure pour la production agricole. Une gestion efficace des ressources en eau agricole est donc une préoccupation cruciale, en particulier dans les territoires irrigués. Des évaluations précises des besoins en eau des plantes grâce à des outils permettant d'estimer l'évapotranspiration (ET) à l'échelle régionale pourraient contribuer à une gestion durable des ressources en eau limitées dans des régions déjà confrontées à des pénuries d'eau. La mise en œuvre de ces outils requiert une connaissance précise des cultures irrigués, leur localisation ainsi que leur développement foliaire. Pour cela, la télédétection apporte des informations importantes sur la dynamique des couverts végétaux via les indices de végétation (NDVI) ou l'estimation de variables biophysiques (par exemple l'indice Foliaire (LAI)), qui sont des variables décrivant des caractéristiques des couverts végétaux relié à l'ET. L'objectif général de cette thèse est d'évaluer des méthodes utilisant les données Sentinel-2 pour cartographier les cultures irriguées, ainsi que leur développement foliaire. L'étude s'appuie sur deux territoires méditerranéens à savoir la plaine de la Crau et la zone irriguée Ouvèze-Ventoux. Dans ce travail les algorithmes utilisés pour la cartographie des surfaces et la caractérisation des couverts végétaux s'appuient tous sur l'analyse des séries temporelles de LAI estimée par télédétection afin d'identifier des traits phénologiques et agronomiques des couverts végétaux observés. L'innovation principale réside dans l'exploitation de ces traits pour caractériser les couverts végétaux plutôt que d'injecter les séries temporelles brutes (réflectances ou indices de végétation) dans les algorithmes de classification comme cela est généralement fait. Ce travail comprend trois parties : (i) la première a porté sur la cartographie des prairies irriguées en Crau. (ii) la deuxième partie est dédiée à la cartographie des cultures irriguées ligneuses (vergers, vignes et oliveraies) (iii) enfin, la troisième partie s'est principalement concentrée sur la caractérisation des vignes en recherchant deux caractéristiques importantes qui sont la gestion de l'inter-rang et la caractérisation de l'indice foliaire de la vigne qui nécessite de soustraire les contributions de l'inter-rang au LAI vue par le satellite.

Pour la première partie du travail (sur les prairies irriguées), un algorithme de détection de la fauche a été conçu en utilisant le signal LAI temporel dérivé des observations de Sentinel 2. L'algorithme comprend un filtre pour éliminer le bruit dans le signal qui pourrait conduire à une fausse détection de la fauche. Un pixel est classé comme étant une prairie irriguée si deux fauches au moins sont détectées. Nous avons

obtenu un indice de Kappa très satisfaisant compris entre 0,94 et 0,99 selon les années. Dans la seconde étape de travail, une classification basée sur les métriques phénologiques (PM) dérivées des séries temporelles de Sentinel-2 a été développée pour effectuer la classification. Les PM correspondent aux paramètres d'un modèle analytique (double logistique) qui permet de caractériser les phases de croissance, de décroissance du LAI ainsi que le plateau correspondant au développement maximum du couvert. Les PM sont calculées sur les séries temporelles de LAI moyennées sur la parcelle agricole pour être ensuite introduites dans l'algorithmes de classification (random forest RF). Les indices Kappa varient de 0,86 à 0,95 selon les années. Ces résultats sont bien meilleurs que ceux obtenus en appliquant l'algorithme RF aux séries temporelles LAI (Kappa compris entre 0,3 et 0,52). Enfin, dans la dernière partie de ce travail de thèse, la méthode proposée se base sur deux hypothèses, à savoir la temporalité du développement foliaire de la vigne et le fait que le couvert herbacé de l'inter-rang est sec ou absent en été. Cela permet d'ajuster une courbe théorique du développement foliaire de la vigne basée sur une courbe analytique de type logistique double et d'identifier la contribution de l'inter-rang au LAI en soustrayant que la courbe théorique de la vigne à la série temporelle de LAI observée. Ainsi Nous avons réussi à séparer les inter rangs avec différentes pratiques de gestion comme l'enherbement, l'enherbement partiel et le travail du sol.

Cette étude démontre l'intérêt d'utiliser des traits phénologiques (ou points caractérisant les stades phénologiques) plutôt que les valeurs brutes issues des profils temporels brutes des données de télédétection (moins de données sont utilisées et la méthode peut être reproduite d'une année sur l'autre). Il s'agit d'une caractéristique intéressante qui permet de réduire la charge de travail liée à la collecte d'informations de référence.

Table of Contents

Lists of figures

Lists of Tables

Preface

This PhD thesis was conducted involving the French National Institute for Agriculture, Food and the Environment (INRAE), Avignon, and the University of Avignon (UA) under the full supervision of Mr. André Chanzy and Mrs. Dominique Courault.

This PhD thesis report is an outcome of four years of non-stop hard work (the first University inscription was in October 2019 at the University of Avignon), conducted at the French National Institute for Agriculture, Food and the Environment (INRAE) in Avignon at the Mediterranean Environment and Modelling of Agroecosystems (EMMAH) laboratory: Territorial dynamics, functioning of agricultural areas and modelling (DREAM) team.

While undertaking this PhD thesis, three times steering committees were conducted. The involved committee members were Mrs. Emmanuelle Vaudour (Assistant Professor at AgroParisTech), Mr. Gilles Vercambre (Senior Researcher at INRAE-Avignon), Mr. Lionel Jarlan (Research Director at Institue of Research for Development).

While undertaking this PhD thesis work, I profited from the Petroleum Technology Development Funds (PTDF) Overseas Scholarship (48 months); partly funded by INRAE-Avignon and international projects (10 months) including all field trip travel expenses.

Introduction

Contextual background

The most significant component of agricultural production on the Earth's surface is water with 50% of the complete water extractions on an average basis in the Mediterranean region (Fader et al., 2016). However, this region is facing water shortages (including rainfall and other forms of precipitations) due to the negative impact of climate change and global warming which has led to increased irrigation practices and consequently created water use conflicts and irrigation restrictions by policy and decision makers to preserve the scarce resource (Pageot et al., 2020). For instance, in Southern France, some regions have been already faced with irrigation water restrictions. This was the case for instance in the Crau area where more than half of the region is dedicated to agriculture with various irrigated crops as permanent grasslands via flooding, (Courault et al., 2010; Merot et al., 2008a), or intensive market garden and orchards (Séraphin et al., 2016). Another region in Southern France, in the North of the Vaucluse department, is the Ouvèze-Ventoux watershed. This area already suffered from water restrictions which are expected to be stronger by 2030 with new regulations on water withdrawals for agriculture from the Ouvèze River that must be reduced by 30% to preserve the biologic quality of the River. In this region, the farmer's vulnerability to the reduction of water access is a key issue. Dealing with water shortage needs management improvements of the water resources in these watersheds with a precise assessment of the irrigation needs that take the climatic requirements, the soil characteristics, and plant requirements into account.

In the past years, the region has had to cope with repeated droughts and water shortages This will be amplified with an increase in irrigated surface since rainfed crops might require irrigation to sustain the production. This is typically the case in vineyards. The worsening tensions on water resources are leading to changes in the rules for sharing water, the implementation of which must be based on an objective assessment of water requirements to ensure that the consequences are shared equitably between the various water users.

Precise geospatial data on irrigated land extents improves our comprehension of agricultural water use, local land surface processes, conservation or depletion of water resources, and hydrological budget components. Therefore, accurate optimization of water resources by providing the exact required water by crop remains one of the obvious ways to avoid over-exploitation of the scarce (water) resource. Thus, to supervise plant water needs across terrains with vast spatial extents, remote sensing (RS) is an interesting tool that provides spatial data concerning two main parameters for assessments of irrigation i.e. crop type and crop development. On the one hand, the irrigation scheduling strategy is dependent on crop type with water needs depending on the phenology and the management of the crop quality. With this later, suboptimal water supply might be sought to improve the harvested organ quality. On the other hand, evapotranspiration (ET) is governed by crop development and the resulting leaf area. The ability of remote sensing to supervise vegetation and its physical features has long been recognized for the past years (Tucker, 1979). RS offers large coverage of areas under irrigation in many spectral regions and with a frequent temporal revisit (Figure 1) that surveys phenological traits (emergence, vegetative growth) and agronomic traits (date of sowing, harvest). Therefore, the accessibility of remote sensing information and image classification approaches makes it achievable to perform high-quality characterization for crop

types by utilizing limited field information that can aid in predicting management systems like water supply (Peña and Brenning, 2015).

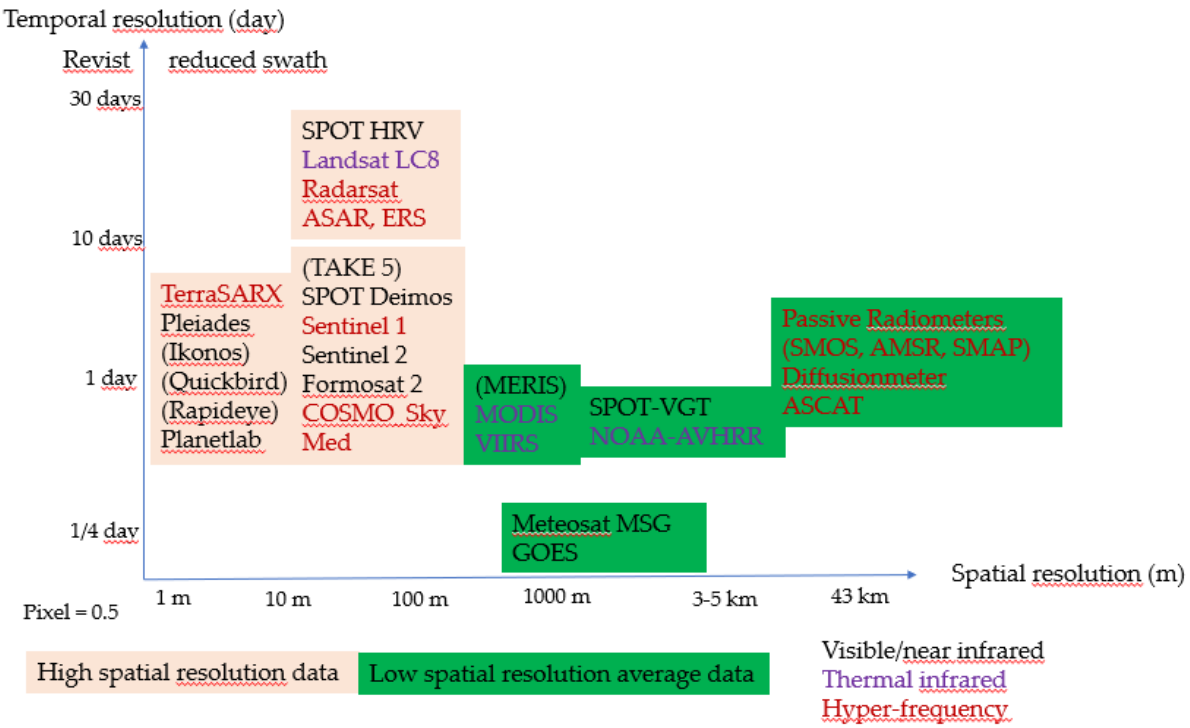

Figure 1: The most frequently used satellite sensors in the agricultural field and their spatial resolution on the abscissa and temporal (revisit) resolution on the ordinate (inspired by Courault et al. (2020)).

Irrigated perennial woody fruit trees are among the major irrigated crops in Southern France and there is a need to accurately identify these (irrigated woody fruit trees) crop types with a specific complexity due to heterogeneous canopy and RS signal that gathers contributions of the tree canopy and the herbaceous background. Concerning the mapping of irrigated field crops (like maize, sunflower, soybean, potatoes, sorghum, etc.) using RS data, undeniable progress has been made in that aspect (Bazzi et al., 2022; Courault et al., 2008; Demarez et al., 2019a). However, the delineation of irrigated woody fruit trees using RS remains farfetched (there are few related conducted works) due to the strong variability existing even among the same crop type due to variation in management practices (like presence or absence of inter-row grass, etc.) among other things. The limitation of horticultural maps based on remote sensing might also be ascribed to the complexities linked to the separation of different tree crop types or species spectrally to acquire precise maps (Usha and Singh, 2013). The utilization of SITS (satellite image time series) has offered encouraging results on crop identification. Through the utilization of SITS, the temporal profiles of targeted crops are generated from multispectral images generated within the temporal window of interest mostly the complete growing season. Such multitemporal pattern is linked to the crop's phenology like their seasonal patterns or stages of inter/intra annual changes, whose date of onset and offset can be used to characterize a given crop among other types of crops planted within the same agricultural area. The improvement of satellite missions, with more frequent acquisition and thus enhanced SITS has been boosting the chances of accurately

classifying various crop types (Masialeti et al., 2010; Odenweller and Johnson, 1984; Pena et al., 2017; M.A. Peña and Brenning, 2015)

We have also seen that characterising LAI is an important factor in assessing crop water requirements. While characterisation of LAI by remote sensing gives good results for crops with homogeneous cover (Weiss et al., 2002; Weiss and Baret, 1999), it is much more difficult to know the LAI of the tree stratum of an orchard, a vineyard, or an olive grove. Remote sensing shows the overall canopy cover, which includes the herbaceous cover under the canopy or in the inter-row. Being able to estimate these two components is a real challenge.

Thanks to the launch of the recent Sentinel satellite missions that provide various possibilities to handle such challenging issues (crop type delineations including background contributions) as they offer real-time satellite images with high spatial (10 m) resolution and temporal revisits of 5 days which remain cost-free and open source.

PhD objectives, and methodological approach

The broad objective of my PhD thesis is to develop methods using remote sensing data for mapping irrigation characteristics at the territory level to assess water consumption according to the specific needs of the different cropping systems. Therefore, there is a need to map the cropping systems and in particular those being irrigated. Two study areas namely Crau and Ouveze-Ventoux respectively located in Southern France, characterized by a Mediterranean climate were chosen to evaluate the developed methods. The areas are characterized by a diversity of irrigated cropping systems with gardening, orchards, vineyards, olive groves, and irrigated grasslands. The water requirements are very different due to the irrigation system (flooded irrigation in grasslands, drip or micro sprinkler in orchards, vineyards, and olive groves) and crop cycles. Woody crops are characterized by mixed surfaces that contain the canopy of interest (tree), in general along rows, and the background which is managed differently either by tilling the inter-row or leaving grass. As irrigation needs are determined by the vegetation coverage of the tree canopy, there is a need to delineate remote sensing data on the contribution of the canopy and that of the background. **Mapping the different irrigated crops and delineating the canopy and background contributions are the two main key (specific) objectives of this thesis.** To achieve these goals, I wish to take profit from the temporal characteristics of new remote sensing Sentinel missions, which allows the characterization of the crop dynamic in detail. It is assumed that such time series together with agronomic knowledge can provide robust features that can be used to characterize relevant irrigation characteristics

Thus, this manuscript is structured into five main chapters:

- The first chapter made a state-of-the-art of the general notions associated with the characterisation and mapping of irrigated fields using a remote sensing approach.
- The second chapter made a description of the two study areas and the data used.
- The third chapter shows the results of mapping irrigated permanent grasslands using temporal profiles of the leaf area index (LAI) of Sentinel-2 (S2) data (published paper 1).

- The fourth chapter showed the mapping of orchards, vineyards, and olive perennial woody crops using temporal profiles of leaf area index (LAI) and green chlorophyll vegetation index (GCVI) based on phenology metrics (published paper 2).
- The fifth chapter analysed remote sensing data (S2) and aimed to characterise canopy leaf area and inter-row management of some selected vineyards in Ouveze-Ventoux using LAI of S2 data and leaf surface from field visits (published paper 3).
- Lastly, the general conclusions and perspectives of the research were presented
- .

Chapter 1

State of the art on characterisation and mapping of irrigated fields using remote sensing approach.

This chapter presented the state-of-the-art for delineating irrigated fields using optical and microwave, remote sensing. Incorporation of several kinds of irrigation mapping using time series by exploiting the significance of some key agronomic and phenology traits by emphasizing irrigated grassland, orchards, and vineyards. I also presented the different literature on the characterisation of orchards and grapevines using high-resolution satellite sensors. I made a synthesis of the different satellite missions used from low, medium to high-resolution satellites of optical (in the visible and near-infrared domain) and microwave domains.

Several specific possibilities are offered by Earth-Observation (EO) satellites to supervise features linked to irrigation such as land use/land cover, soil moisture, or vegetation phenology. Over the past decades, there has been a growing interest in utilizing satellite Earth Observations (EO) to capture data linked to irrigation scale and reoccurring frequency. This has created an expansion of studies utilizing the latest EO program capable of quantifying surface variables with proportional high spatial resolutions below 1km (https://defence-industry-space.ec.europa.eu/eu-space-policy/copernicus_en) (Massari et al., 2021).

1.1 Irrigation characterisation and mapping using optical satellite sensors

On a recorded history dating back to precisely 1972, research studies commenced with the utilization of optical remotely sensed images of Landsat-1 satellite (with 80 m spatial resolution and 18 days temporal revisit) to delineate areas under irrigation (using center pivot sprinkler system) and evaluate water use (Hoffman et al., 1975) in the United States. In 1984, the launching of Landsat-5 (with 30 m spatial resolution and seven spectral bands) was achieved and a comparative satellite named SPOT a.k.a. "*Satellite pour l'Observation de la Terre*" (with 20 m spatial resolution and six days revisit within the green, red, and near-infrared bands) was launched by France in 1986 (Mulla, 2013).

Optical sensors (multispectral and hyperspectral) are widely utilized to calculate several vegetation indices by a proper description of various biophysical features (Jin et al., 2017).

Vegetation indices (VI) derived from multispectral reflectance can be exploited to acquire data on phenology, vegetation water content, and biomass over a growing season. Interpretation of the VI times series can bring advanced information on crop systems (Beniaich et al., 2022), management practices (Abubakar et al., 2023), irrigation needs (Darouich et al., 2022), and risk assessments on soil erosion (Rizzi et al., 2021).

Information via optical satellite sensors like Landsat, MODIS (Moderate Resolution Imaging Spectroradiometer), AVHRR (Advanced Very High Resolution Radiometer), MERIS (Medium, Resolution Imaging spectrometer), and, SPOT have already been widely utilized to identify irrigated cropland areas by utilizing the variations in spectral behaviours among irrigated and non-irrigated cropland fields (Deines et al., 2017; Loveland et al., 2000; Ozdogan et al., 2010; Sharma et al., 2018). The proxy used to map irrigated areas using optic data depends on the differences in spectral signatures between irrigated and non-irrigated surfaces. Due to the wettest conditions in irrigated fields, they mostly retain more photosynthesis and denser biomass consequently creating variations within the spectral and temporal signature among irrigated fields and comparable non-irrigated fields. Such variations are probably seen using multispectral vegetation indices like normalized difference vegetation index (NDVI) where Pervez and Brown (2010) adopted three assumptions which are (i) irrigated crops have higher yearly NDVI values in comparison to non-irrigated crops (ii) the growing peak NDVI values at any time will vary for each crop and for each geographical location of the USA (iii) the NDVI difference between irrigated and non-irrigated crops will be under non-optimal precipitation condition (droughts) with an overall accuracy of 92%. In a similar research study Xiang et al. (2019) used normalized water vegetation index (NDWI) to delineate irrigated cropland and forests by adopting two basic hypotheses, (i) canopy moisture of irrigated cropland (using land surface water index (LSWI)) is higher than forest (ii) the variation in land surface water index is higher in arid regions than in humid regions. Pageot et al. (2020) used normalized difference red-edge (NDRE) showing interesting properties with the possibility of taking into account the variations in canopy development (speed and amplitude) with good accuracy. Chen et al. (2018) used green index (GI) obtained from Landsat, MODIS, or Sentinel-2 sensors was also utilized widely to characterize and delineate irrigated fields. Deines et al. (2017a), have used random forest (RF) classification based on the temporal features of vegetation signals like the maximum and range of variation of the proposed vegetation index. During 18 years, training might be restricted to wet and dry years, from which an outstanding overall accuracy (OA) was derived (> 0.9). Different crop growth patterns can occur due to irrigation in comparison to rainfed agriculture entirely (Thenkabail et al., 2005) as plant development (NDVI), which is greater in irrigated areas.

However, the transfer of the approach according to optical information is constrained in humid regions with frequent cloud cover (Karakizi et al., 2018). Timely detection of irrigated crops is of utmost significance for the irrigation calendar, however, coverage due to clouds could seriously lower the availability (the numbers) of optical images consequently making identification of irrigated crops very challenging (Demarez et al., 2019b).

1.2 Irrigation characterisation and mapping using microwave satellite sensors

One of the advantages offered by microwave sensors is that they are not affected by weather conditions (like clouds, dust, etc.). Microwave signal (backscattering with an active system, emission with a passive system) is sensitive to the moisture content of both soil and vegetation and thus, possesses the ability to estimate quantities related to irrigation. Additionally, microwave RS is responsive (sensitive) to several factors that require parameterization during retrieval which include soil texture, characteristics of vegetation coverage, topography, surface temperature, and the atmosphere. These feature heterogeneities might complicate the retrieval more and put its physical basis in jeopardy. Therefore, the resolution (spatial) of the measurement might play a crucial role in retrieving the physical consistency (Lee and Anagnostou, 2004).

Passive microwave remote sensors also known as radiometers quantify the naturally emitted electromagnetic radiations from the surface of the Earth as brightness temperature (T_B) and have been a good application for supervising global surface variables. The passive microwave radiometer is liable to be more responsive (sensitive) to near-surface soil moisture (Lee and Anagnostou, 2004). However, the spatial resolution of the spaceborne radiometer is coarse (e.g. 50 km with SMOS) which might be a strong limitation. In the past few years, the introduction of microwave satellite soil moisture products was presented as a tool for detecting irrigated territories. Kumar et al. (2015) conducted one of the early studies using microwave sensors. They made comparisons of soil moisture distribution of modelled datasets which did not integrate irrigation data against several satellite soil moisture products with coarse spatial resolution. Assuming the satellite signals are impacted by the irrigation (signals), it might be anticipated that will also display soil moisture conditions that are wetter than the results of land surface model simulation driven by climate data only. The researchers concluded that despite the encouraging results obtained for irrigation detection across some specific areas, the spatial discrepancy between satellite inferred from coarse resolution satellite and model data and the effect of vegetation, topography, and frozen soil created unreliability across most locations. Lawston et al. (2017), revealed that aside from temporal signature, the seasonal irrigation schedule across three large areas under irrigation in the US (United States) might be detected when utilizing the SMAP (Soil Moisture Active Passive) enhanced 9km product. They identify soil moisture anomalies to detect irrigation. It works in semi-arid where the contrast between irrigated and non-irrigated areas is strong and when the irrigated areas are large enough and not embedded in complex topography.

Another new opportunity for delineating agricultural fields under irrigation is provided by SAR data (active microwave). SAR sensors are more responsive (sensitive) to surface features like plant structure and surface roughness (Lee and Anagnostou, 2004). In recent years, the Sentinel-1 (S1) satellite has been incorporated into land use delineation methods across several environmental contexts (Massari et al., 2021) thanks to the very interesting characteristics of the S1 mission with 5 days revisit period; a global coverage at 10 x 10 m pixel size across two C-band polarizations VV and VH. Various methods were suggested to delineate areas under irrigation by taking multitemporal data from S1 backscattering to identify specific signal changes in areas under irrigation (El Hajj et al., 2017;

Gao et al., 2017). Gao et al. (2018) suggested a method according to direct assessments of multi-temporal radar signals on individual agricultural fields via various metrics like the mean, standard deviation, correlation length, and fractional dimension. The method permits the separation of three classes namely non-irrigated fields, irrigated crops, and trees with a precision of almost 80% across a site in Catalonia, Spain. These satisfactory results based on S1 information were replicated for the mapping of irrigated fields using a deep learning algorithm (Bazzi et al., 2020). Sentinel 1 sensors also allow the collection of high-resolution soil moisture estimates that are significant for the management of irrigation (but for crops with NDVI below 0.7), the methods are based on machine learning techniques such as NN (neural networks), change detection approaches, and as well direct inversion technique of semi-empirical physical models (Bauer-Marschallingere et al., 2019; Bousbih et al., 2018; El Hajj et al., 2017; Gao et al., 2017; Santi et al., 2019). The potential of microwave supervision to retrieve information on irrigation timing was also investigated in some research. For instance, Le Page et al. (2020) suggested evaluating the timing of irrigation at the plot scale by making comparisons between surface soil moisture derived from the model via coefficient obtained from S2 to measurements of local surface soil moisture and products of soil moisture obtained from S1 and S2 (El Hajj et al., 2017). The research was conducted across six maize fields in South-West France and displayed that the best retrieval of irrigation would be fulfilled with measurement (local) of surface soil moisture for each 3-4 days. The authors also observed that the approach is not sufficient for small irrigation event timing of less than 10 mm due to the frequency of the six daily measurements of S1, and there might be confusion between irrigation and rainfall events.

However, the mapping of irrigated fields using SAR data can be constrained in regions experiencing frequent events of rainfall occurrences (Bazzi et al., 2022, 2020) because irrigation and rainfall have a similar impact on the surface soil moisture which correlates with the coefficient of radar backscattering (Bazzi et al., 2021). In addition, the SAR C-band data was disclosed to be more responsive (sensitive) to canopy density in densely vegetated fields like wheat and grasslands than soil moisture (Bazzi et al., 2022; El Hajj et al., 2019; Nasrallah et al., 2019) however, when the NDVI value is above 0.7, the SAR C-band is not capable of penetrating canopy cover and thus the C-band appears non-sensitive to surface soil moisture (El Hajj et al., 2019). Concerning densely vegetated cover, the penetration of radiation in the C-band through the canopy is reduced significantly. In this regard, irrigation events detection using the backscattering coefficient increase might be challenging (Bazzi et al., 2021). For instance, El Hajj et al. (2019) and Nasrallah et al. (2019), displayed that the contribution of soil in the C-band SAR backscattered signal is insignificant around the heading growth stage in wheat because of the C-band's low penetration signal to the surface of the soil. In this regard, irrigation events detection using the backscattering coefficient increase might be challenging (Bazzi et al., 2021).

1.3 Irrigation characterization and mapping using optic and microwave sensors

Studies (Julien et al., 2011; Ozdogan and Gutman, 2008) have shown that dense time series of optical data permits crop-type delineation and characterization across different climates and under heterogeneous cropping systems. However, because cloud coverage affects optical data,

crop delineation performance might be reduced in some instances, even with a temporal revisit of 5 days. On the contrary, since microwave data are not impeded by cloud coverage, the unifying data utilization of high-resolution optic and microwave sensors might offer synergies to identify irrigated plots as well as the timing intervals of the occurred irrigation events. Various studies have pinpointed the possibility of merging (synergy) optic and microwave data which might improve the detection of crop types that are affected by cloud coverage while using optical data alone (Inglada et al., 2016; Sonobe et al., 2017; Whyte et al., 2018).

Ferrant et al. (2019, 2017) utilized a random forest (RF) classifier by merging radar and optical (Sentinel-1 and Sentinel-2) data across Southern India to explore the profits of high spatial resolution and multiple satellite approaches. The input resolution permitted the recovery of irrigated fields for the dual climatic seasons of India at 10 and 20 m spatial resolutions. Implying that synergy among radar and optical monitoring using RF algorithm further slightly enhanced irrigation assessments. Demarez et al. (2019) employed random forest via synergetic use of 6 Landsat-8 bands every 16 days (optical) and synthetic aperture radar (SAR) information, highlighting that the dual merging marginally enhanced the precision of the classification in comparison to the performance when used separately (with one source) on summer crops. When Landsat 8 alone was used the kappa index was 0.85 while when Sentinel-1 data was used alone the kappa index was 0.70 and for the synergy (Landsat 8 and Sentinel-1) the kappa was 0.89 implying the adding value was not much. Likewise, Pageot et al. (2020) adopted a method that supported precipitation data, gaining the same marginal outcome (kappa index for SAR, optical, and the synergy in 2017 was 0.63, 0.72, and 0.75 while for 2018 was 0.54, 0.65, 0.66). They also disclosed that the utilization of precipitation information boosted the capability and that the combination of high temporal resolutions with monthly composite led to the same achievements while decreasing computation duration. Inglada et al. (2016) when Landsat 8 alone was used gained an initial kappa accuracy of 0.70 and had a marginal gain of 0.06 kappa accuracy improvements after combining Landsat 8 and Sentinel-1 (kappa index of 0.76). In another study conducted by Whyte et al. (2018), they used optical and radar data with yet again very marginal differences with a kappa index of 0.72 whereas a kappa index of 0.71 was obtained when optical data were used alone.

1.4 Irrigation characterization and mapping using agronomic and phenology traits.

1.4.1 Characterization of the cropping system

Crop delineations according to RS observation have been a critical requirement for crop supervision, and biophysical and biochemical parameter estimation (like yield and water requirements). Therefore, classical methods of crop classification have been adopted such as clustering, decision-trees, parcel-based, machine, or deep learning methods (Ashourloo et al., 2020). However, the aforementioned approaches mostly need huge training data of different crops as training samples while such data provision is in general time-consuming, expensive, and labour-demanding (Ashourloo et al., 2019). Additionally, these conventional classifiers used VI during classification and the difficulty comes mainly from the fact that these vegetation covers have a great diversity of development because of the age of the plantation, their density, the mode of management such as pruning, and the confusion that there can be

with other plant covers (non-irrigated meadows, wetlands...). On the contrary, phenology-based approaches derived from SITS (satellite image time series) are valuable sources for uniform and rapid supervision of agricultural fields that might be independent of ground data (Ashourloo et al., 2020). By utilizing such data, changes in the crop reflectance signatures during the growth period might be adopted to automatically identify and separate crops without the need for huge training data samples (Ashourloo et al., 2018).

Usually, plant phenology is evaluated at the ground scale (known as ground phenology (GP)) which requires observation visually for phenology incidence (Figure 2) however, it is labour and time-demanding (Misra et al., 2020). Thus, observations via spaceborne are engaged to supervise plant spatial and temporal development at the landscape level which is also referred to as LSP (land surface phenology) (Zeng et al., 2020). LSP refers to the seasonal manner of changes in vegetated land surface examined using RS information (Reed et al., 2009). Metrics of LSP are mostly linked to overall inter-annual variations, that are interpreted from optic RS data like SOS (start of the season), POS (peak of the season), EOS (end of season or senescence), LOS (length of season) (de Beurs and Henebry, 2004; Reed et al., 2009), including other transitional phases like maturity and senescence (Zhang et al., 2003). These phenological metrics are generally computed from NDVI or other related vegetation indices (for instance (de Beurs and Henebry, 2004; White et al., 2009)) and refer to the DOY (day of the year). Nevertheless, the NDVI possesses some limitations like less sensitivity to vegetation photosynthesis dynamics (Wang et al., 2017). On the contrary, quantitative vegetative variables like LAI (for instance (Mateo-Sanchis et al., 2021; Verger et al., 2016)) when engaged to a lesser scale, might aid a better precision accuracy in the retrieval of LSP metrics, particularly croplands (Wang et al., 2017; Wang et al., 2017).

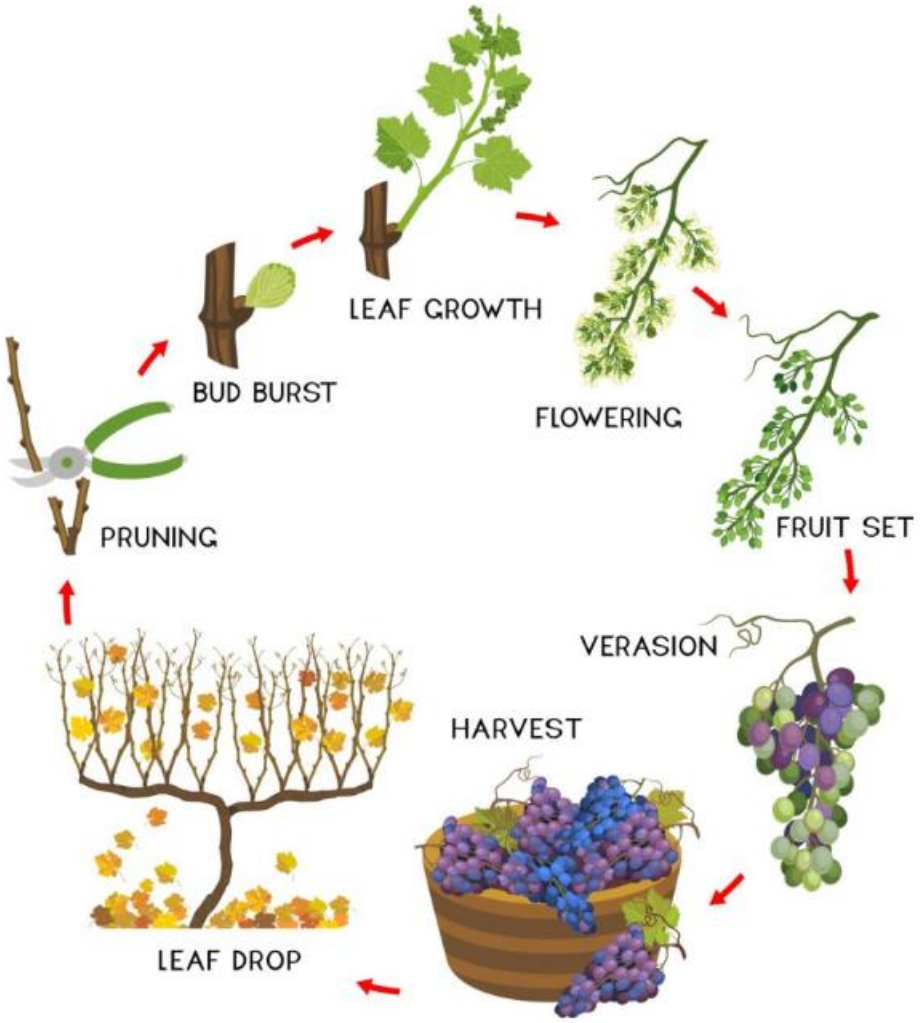

Figure 2: Phenological stages of grapevine (Caffarra, 2023)

Even though optical RS has displayed encouraging results in monitoring phenology, several optical sensors have various limitations concerning resolution (spatial and temporal) (Misra et al., 2020). For instance, optical data of the Landsat mission is faced with cloud coverage (for Landsat 7) that affects its use to examine LSP and requires synergy with other datasets that possess higher resolution to defeat such constraints (Melaas et al., 2016). According to Vrieling et al. (2018), despite the spatial and temporal resolution, the accessibility of data provided by Landsat 8 is still limited because of its sole orbit and sufficiently fine to document rapid changes occurring like the green-up of cropland. Having Landsat data being not too frequent (due to the 16 days revisit periods), needing huge computational inputs for processing, and the difficulties of gap fillings in Landsat 7, most especially in cloudy terrains, other sensors like MODIS, AVHRR, SPOT-VEGETATION, and MERIS with coarse, received popularity because high-quality sets of data were readily accessible with less processing difficulty (Bolton et al., 2020; Zhu et al., 2019). Nevertheless, several LSP studies carried out using data from these sensors, despite giving frequent monitoring, are faced with the problem of mixed pixels

and thus, restricted their application across complex terrains (Chen et al., 2018; Misra et al., 2018). Aside from atmospheric interference (like clouds, aerosol e.t.c.) and algorithmic corrections that change (contaminate) the true spectral data (Ahl et al., 2006), two crucial geographic uncertainties might complicate the detection of SOS (start of the season) due to the coarse spatiotemporal resolutions in products of VI (like MODIS, SPOT VGT). The first uncertainty source pertains to the temporal mismatch of remotely sensed information with ground data. For instance, VI products of MODIS might fail to match ground dates due to vegetation growth among green-up and the maturity is an active and fast event (for instance using an 8 or 16-day MODIS products to determine 10-12 day growth duration (Ahl et al., 2006)). The second uncertainty source is the mixed pixel effect which is equally referred to as the point vs pixel problem (Reed et al., 1994; White et al., 2009). They arise due to (i) a pixel within the VI products might possess unknown constituents of vegetation species or types of land covers and, (ii) these vegetation species vary in their responsiveness (sensitivity) to climate changes regarding SOS (Badeck et al., 2004; Duchemin et al., 1999; Schwartz and Reed, 1999). As the pixel-based SOS trend can be induced by the variation in the sole variable or a group of variables (like species composition, species SOS) contained in a mixed pixel, it is far from clear regarding the exact mechanism that reads the phenological results. Even though mixed pixels cannot be avoided, cautious handling of pixel complexity might aid in evaluating the variation in the computed LSP (Granero-Belinchon et al., 2020; Tian et al., 2020). The fused datasets of the different Landsat satellite missions like Landsat 7, 8, and probably 9 when operational might offer an official ground coverage of 8 days (https://landsat.gsfc.nasa.gov/satellites/landsat-9/), and are therefore among the leading options for data sampling at higher resolution (spatial and temporal). Although, going by the cost challenges and image retrieval during Landsat commercialization between 1984 to 2008 (Zhu et al., 2019), the cost-free accessible wide-swath coarser resolution sensors like MODIS and AVHRR were focused with much interest among the phenology community.

To counter some of the shortcomings of these sensors with lower resolution (spatial), satellite sensors from collections of similar sensors with a decametric spatial and 5 days temporal resolution like S2 (cost-free), RapidEye (expensive), and Planet might aid in improving the computation and comprehension of LSP. The ESA (European Space Agency) S2 satellite sensors accessible from 2016 (S2A) and 2017 (S2B) to duplicate the data retrieval at fine spatial resolution (10 m) and temporal revisit (5 days). One of the main advantages of the S2 data is the temporal resolution with improved ground sampling and overlaying areas (for S2A and 2B orbits) attaining even better temporal sampling, which is essential for terrains where cloud coverage might be often (Immitzer et al., 2016). It is noticed that, for similar terrain, S2 can retrieve roughly more than ten times pixels in comparison to Landsat 8, going by its decametric spatial resolution and 5 days temporal resolution from the dual sensors (S2A and S2B), thus allowing enhanced space ability to supervise vegetation (Addabbo et al., 2016; Griffiths et al., 2019). Prior research utilizing simulated S2 bands derived from hyperspectral data displayed encouraging results in the supervision of vegetation greenness and land cover. Such studies also discovered bands of S2 to be adaptable with various optic sensors like VIIRS, MODIS, MERIS, RapidEye, and Landsat (Hill, 2013; Veloso et al., 2017). Likewise, utilization of S2-like bands from other optic sensors, Veloso et al. (2017) observed the resulting output to

be highly linked to fresh biomass and GAI (green area index), and capable of retrieving short phenological phases, consequently aiding accurate supervision of crop advancements. S2 allows the advantages of supervising and examining plant phenology extensively (Delegido et al., 2011) and the use of S2 for phenological-related studies has increased immensely in the past few years.

Multitemporal data can be used to map crop conditions, agronomic activities, and phenology of plots under irrigation which can serve as added information for decision-making (Karantzalos et al., 2017). For instance, Ashourloo et al. (2018) used the RS time series of Landsat 8 information to obtain phenological patterns of alfalfa fields in Iran and the United States of America (USA) for automatic mapping independent of training data. The spectral reflectance values (from different bands) of alfalfa were compared among other crops in a growing season by finding suitable relationships for demonstrating the features of alfalfa and also differentiating it from other crops with an overall accuracy ranging from 90-94%. In another study, Ashourloo et al. (2019) made a classification of canola fields in Iran and the United States of America (USA) by proposing a new index (canola index) based on temporal changes in the green and red band that are linked to some agronomic activities (harvesting period) and phenological features (flowering period). The comparison with conventional classification approaches like Maximum Likelihood (ML) and Support Vector Machine (SVM) has shown an interest in using agronomic traits to identify a given crop with improved accuracy. A similar attempt was established in extensive agricultural fields to separate potato field classes from other crop classes by Ashourloo et al. (2020). The authors based their mapping criteria on spectral indices linked to phenological (flowering and peak of greenness) and agronomic traits (harvesting periods of early and late potato fields) leading to good classification accuracy (Kappa = 0.8) with little training data. The authors of Julien et al. (2011) made a land-use map based on the annual behaviour of both the land surface temperature (LST) and the NDVI. The classification was performed on characteristics of the LST/NDVI yearly relationship and produced good results for the identification of irrigated fields (kappa = 0.85). With irrigated perennial woody fruit trees, classification was done by Kordi and Yousefi (2022) to map apple orchards, vineyards, and annual crops in Iran. Phenology traits were utilized by choosing the optimum data by merging Sentinel 1, Landsat 8 images, and DEM (digital elevation model) with a total precision of 89% attained. These researches have displayed that good results can be achieved with perennial woody fruit tree delineation. The standards of the achieved results came from the number of images used, the choice of selected dates used, and the complementarity among spectral indices within the optical domain and textural indices obtained from SAR images. The classification standards also came from the uniqueness of the signatures of the different covers. In this regard, the phenology makes it realistic to aim at the dates of observation to be regarded particularly during stages of greenness and senescence. In previous studies, phenology is not directly utilized as a criterion for classification but more to consider optimum or key specific dates. The utilization of phenology or agronomic traits might offer advantages in time series assessments since they are relatively independent of the acquisition dates. This can be fascinating in a condition where partial cloud coverage is often present in the temperate zone, which might affect the time series

homogeneity from one location to another within the area to be mapped. This can significantly affect the learning process of the algorithm.

1.4.2 Characterization of the main canopy leaf area

Knowledge concerning biophysical features (canopy) of vegetation is significant for describing water models among others. In situ (ground) measurements of these biophysical features are labour-demanding, time-consuming, and might even be destructive. Thus, achieving spatial and temporal sampling is difficult for a reliable continuous supervision of the Earth's surface. This is the reason why satellite repeatability is needed for environmental modelling, for instance, Weiss and Baret (1999) compared the retrieval performance of different biophysical variables (including LAI) from the accumulation of large swath satellite data (VEGETATION/SPOT4 sensor). The LAI is the main vegetation structure variable controlling canopy reflectance and is among the main drivers of canopy primary production processes because it represents the size interference between the plant and atmosphere for energy and mass exchange. Thus, it is of crucial interest for evapotranspiration models. The top of the canopy (LAI) bidirectional reflection distributive function (BDRF) of the homogenous canopy (like field crops) was estimated with good accuracy (Weiss et al., 2002; Weiss and Baret, 1999).

However, in the case of perennial woody crops like orchards and vineyards, the computation of the canopy LAI is faced with the problem of mixed pixels. For instance, Khaliq et al. (2019) highlighted the advantages of low-altitude UAV (unmanned aerial vehicles) drones over decametric S2 data in comparative multispectral vineyard imagery. They consider three elements of the vineyard environments i.e. the complete cropland surface, only the grapevine canopies, and, the inter-row terrain only. The results indicated that the decametric resolution imagery failed to directly describe the vineyard variability due to the contribution of inter-row background to the remotely sensed data might affect the computation of the NDVI leading to crop descriptors that are biased. On the contrary, UAV imagery computed vigour maps consider only the canopy pixels leading to be linked to the in-field assessment in comparison to the decametric S2 data.

However, it is important to note that data from UAV drones can be very expensive especially when acquired daily (high temporal revisits). However, by using S2 data some studies still disclosed the potential of S2 sensors to characterize inter-row patterns of row plantations for instance, Palazzi et al. (2022) exploited decametric S2 data to delineate inter-row signals of grapevine fields using a photo interpretation and, cluster analysis(Object-based) classification approach. The results pin-pointed that vineyards can be classified based on the different inter-row soil management (i.e. conventional tillage and permanent grass cover) with the best accuracies obtained using NDVI and NDWI. The obtained results indicated that a seasonality effect might be involved in the selection of the most appropriate bands or index that well describes the development of soil coverage at a certain time of the year. Data concerning the management of vineyards is normally difficult to find and might need in-field measurements. The choice of an unsupervised classification approach of remotely sensed information over a given duration might be a crucial and rapid tool, for permitting the users to characterize a certain area without the need to create training data.

According to Palazzi et al. (2022), results from the cluster analysis show that open-sourced satellite data regardless of being characterized by a resolution (geometrical) that fails to permit discrimination among grapevine rows and inter-rows; might still be crucial to determine variations concerning soil management of the latter part of the vineyard. Free-sourced information like S2 is indeed characterized by a 5-day temporal revisit, permitting the user to reconstruct growth patterns among vineyards that might be linked to either the grapevine plants or ground coverage that might be found in the inter-rows. In such a way, cluster analysis might offer information concerning the vigour variations occurring within the vineyard (both from a spatial and temporal point of view) permitting one to differentiate parts of the field with different vigour. That might be due to the presence of grapevine plants that failed to grow than the presence of portions of bare soil within the inter-rows, both indicators of poor management practices. Such information might be crucial for crop supervision events using satellite sensors.

1.5 Synthesis

Numerous studies have used active microwave satellite sensors to generate soil moisture at field-to-region scales because of their spatial resolution (i.e. higher). However, the retrieval of SAR-based soil moisture again poses several drawbacks which include the concern regarding the estimation of surface roughness and vegetation water parameterization. During synergy between optic and microwave sensors, we observe from most studies that there was not much-adding value to most of the obtained accuracy, the gain remains very marginal with optic data when used alone having the highest precision.

Considering the availability of cost-free satellite sensors like the Sentinel-2 (optic) which provide data at decametric spatial (10 m) and 5 days temporal revisits, the analysis of cropping patterns and land use during a growing season can easily be observed using spectral vegetation indices like NDVI or biophysical variables like LAI. Despite the challenges of cloud coverage faced with optic remote sensing, the quick temporal revisit of the Sentinel-2 mission the temporal evolution can lead to identifying some key unique features during growing seasons such as a decrease or increase in biomass or NDVI/LAI, harvest, or mowing practices, the start of the season (greenness), the length of the season, the end of the season or senescence to mention a few. Such capacity to analyze some key unique agronomic or phenology traits (features) can aid in identifying fields with similar features like crop type and land use. The main advantage of the use of temporal traits is that it requires a minimum (or zero training data if expert knowledge is used) during delineation to identify different land uses and it enhances classification reliability.

Chapter 2
Study Sites and Data

In this chapter, the overall description of the two (2) study sites (geographic location, climate, soil, etc.) was presented. Also, the remote sensing data used during this thesis were described. The different exploited vegetation indices and biophysical variables were also detailed for 2016 to 2022. The data on ground monitoring about phenology and canopy development was also presented in this chapter.

2.1 Description of the Study Sites

2.1.1 Geographical positions

The study was conducted across two different locations in South-East France namely the Ouveze-Ventoux and the Crau area (Figure 3). These study sites are representative of the Mediterranean with a strong diversity of cropping systems including irrigated permanent grasslands, fruit orchards (cherries plums, peaches apricots etc.), vineyards (table and wine grapes), and olive groove orchards.

The Crau (a flat plain) is located around 43° 38' N and 5° 00' E (5m a.s.l) close to the Rhône delta having a surface area of 600 km² (Abubakar et al., 2022). The Crau is restricted to the North by the Alpilles relief and bounded to the East by the Miramas Hills and the Rhône Delta to the West an area referred to as "Camargue", and to the South by the Mediterranean Sea (Séraphin et al., 2016; Trolard et al., 2016).

The Ouveze-Ventoux site is positioned around 44° 10' N and 5° 16' E (with its lowest and highest elevation as 230 and 630 m a.s.l) and covers 59 km² (Abubakar et al., 2023). Forest and semi-natural environments occupy roughly 57.7% (Tuffery et al., 2021) of the area showing a high environmental diversity.

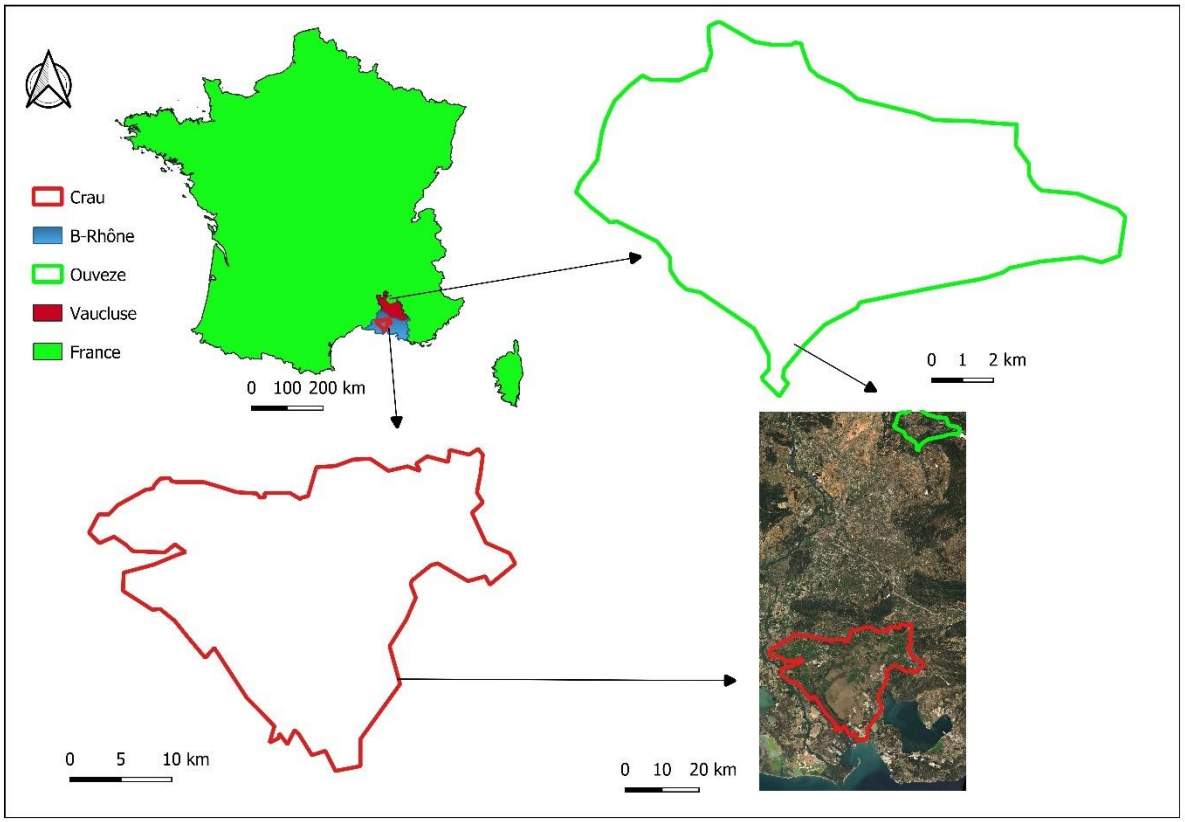

Figure 3. Geographical locations of the two study sites in South East France.

2.1.2 Climate

The Crau is characterized by a meso-Mediterranean climate with a summer drought period of three months, a winter that is mild having an average temperature of 7°C and occasional frost, with rain precipitation of 400-600mm per annum mostly in the autumn (50%). Having a very high hour sunshine per annum of > 2800 and wind that can be very strong for some periods. The wind is a significant element of the Crau climate with about 300 days of wind per year, this includes 70 days having a wind speed above 20km.h^{-1} majorly as a result of Mistral which is a North/North-Western wind (Jaunatre, 2012). The wind (Mistral) participates in the desertification of soil and sunlight decreases temperatures in the winter. An additional significant component of the Mediterranean climate is the high inter-annual variation: for instance, from 1997-2006, a meteorological station in the South of Crau documented an average annual precipitation of 561mm however having a minimum of 394mm and a maximum of 823mm (Bourrelly et al., 1983).

The Ouveze-Ventoux climate has the typical Mediterranean climate identified by cold and moist winters and dry and hot summers. Annual precipitation is about 750 mm per year, annual mean temperature of 12.6°C according to the Vaison la Romaine data (https://fr.climate-data.org/europe/france/provence-alpes-cote-d-azur/vaison-la-romaine-65550/#climate-table). The lowest relative humidity of the year is in July (48.82%) and the

month with the highest humidity is January (77.71 %). The fewest rainy days are expected in July, while the wettest days are measured in November.

2.1.3 Soil description

The soils in the Crau sites are calcic luvisols having an irragric upper horizon consisting of 5% stones, over an average loamy sand layer of 15-75%, and a petro-calcic horizon (FAO-UNESCO, 1981). The thickness of the upper layer is 0.1-0.4m having roots dominating the 0.3 m upper layer of which the root density rapidly decreases with depth until the permeable pudding stone hampers growth. It is shallow at about 60-80 cm and stony with 20% at the surface soil and about 90% subsurface (around 80 cm deep) creating a water holding capacity that is very low and as well poor in organic matter and mineral elements except for the irrigated layers which were deposited by irrigation water.

The soils in Ouveze-Ventoux have a depth of 80cm-1m that has a coarse stoney fraction of 48-63%, therefore, leading to low soil water capacity retention. The subsoil in Ouveze-Ventoux consists of Pliocenic calcareous loamy sands. The topsoil ranges between 1.5% and 3% (Van Der Perk et al., 2004). The soils in Ouveze-Ventoux developed in tertiary molassic deposits and according to the FAO system of soil classification it is classified as calcaric regosols with sandy loam and loamy sand as the dominant textures (van Dijck and van Asch, 2002).

2.1.4 Irrigation

Irrigation practices in the Crau are more than 4 centuries old dating back to the 16th century (Séraphin et al., 2016). In the Crau area, there are 13500 ha of grasslands irrigated using flooding techniques and 8500 ha of orchards (fruit and olives) using drip irrigation. A few field crops are irrigated using sprinkling techniques (pivot) and there is a growing surface of greenhouses. Flood irrigation is carried out from March to September with variable water turns according to a local association called ASA (*Association Syndicale Autorisée*) from 8 to 12 days. Below a certain flow threshold and the estimated level at the outlet of Serre-Ponçon, there may be water restrictions that are applied (this has been the case in recent years in 2015-2022). Gravity irrigation brings water often in excess in comparison with the plant's real needs; water supply canals are provided by the ASAs. This irrigation technique contributes significantly to the recharge of the groundwater of about 75%, which is important for the region's industries, domestic (280,000 inhabitants), and, intensive irrigation of orchard and market garden production (Séraphin et al., 2016; Trolard et al., 2016). In recent years, due to recurrent droughts, water distribution in the region has been restricted, impacting groundwater supply, local production, and economic development as a result. Urban expansion (in particular the establishment of numerous logistics platforms near *Fos sur mer* in these irrigated areas makes surfaces waterproof and reduces water supply to the groundwater table (Courault et al., 2010).

In the Ouveze-Ventoux site, irrigation is done either by drip system or using a micro sprinkler under the canopy. Marginally very few fields are irrigated using sprinklers near the Ouveze river bed. Irrigation is generally carried out for most crops from April to October. For the grapevines, irrigation stops earlier to allow the fruit to ripen and have more sugar at the end of August to early September.

2.1.5 Water resource for irrigation

The site of Crau Plain lacks a natural network of Rivers and every water surface transfer happens via a dense canal of irrigation network from the Durance. The absence of a network of rivers is due to the very plain relief in addition to the high percolation ability of natural surfaces where an outcrop of puddingstones with roughly no soil layer (Dellery, 1964). The agricultural sector has the right to use 200 million m^3 of water from the Serre Ponçon Lake, in summer. These are determined when the reconstructed natural flow of the Durance River is higher than a threshold. The management of 200 million is, therefore, a strong issue. Flooding irrigation, mainly for grassland irrigation (Figure 4 (a and b)) is the major source of recharge of the Crau aquifer (75%), which is used to supply orchards, olive trees, and greenhouses.

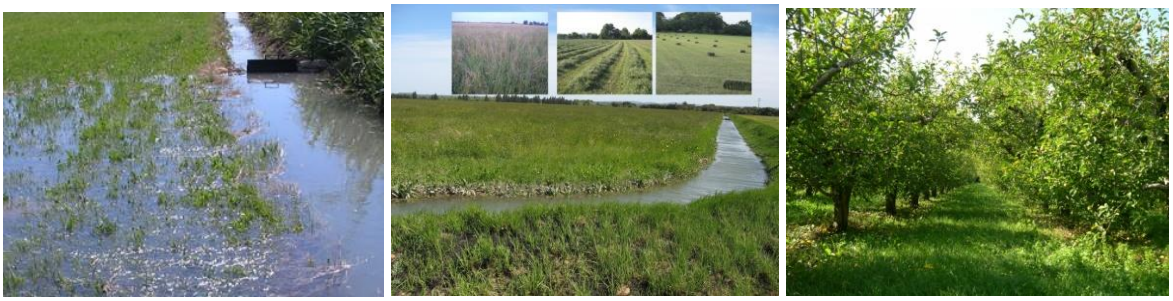

a) **b)** **c)**

Figure 4. Flooded grassland (a), surface channel network (b), and orchards (c) in the Crau area. (photos @courault and flamain)

In the Ouveze-Ventoux site, the main water source for irrigation water is the Ouvèze River with a right of 200 L/s. Water is pumped in reservoirs at different altitudes (from 250m to 520 m) to distribute water over the basin within a network of pipes to deliver pressurized water as shown in Figure 5.

a) **b)** **c)**

Figure 5. Vineyard irrigation for table vine (a), drip, and micro-sprinkler on cherry trees (b and c) (photos @courault).

2.2 Ground data

Different ground data were used during this thesis like the already existing field segmentation, land use maps, the use of Goeportail and Google Earth to check and verify

different occasions on the field, and vineyard monitoring to support the last phase of the work. Surveyed plots were located and observed crops were reported including other relevant agricultural management practices like irrigation, inter-row grass, levelling, etc.

2.2.1 Land use map and field boundaries

Plot boundaries were demarcated across the two study sites (Crau and Ouvèze-Ventoux) resulting in polygons. The map was initiated with the cadastre, which we then corrected manually to delimit homogeneous spatial entities in terms of their use hereafter referred to as plot (the boundaries were fine-tuned using an aerial picture to isolate homogeneously managed surfaces). The whole area was therefore segmented and used for this study. The resulting layer was then used to aggregate classification results produced at pixel scale over the plot's polygons.

2.2.1 Vineyards field monitoring of phenology and canopy development

Ground monitoring of grapevine trees was conducted in the Ouvéze-Ventoux site for two years (2021 and 2022) and the goal is to track the temporal dynamic of the leaf area of both compartments as shown below (Figure 6).

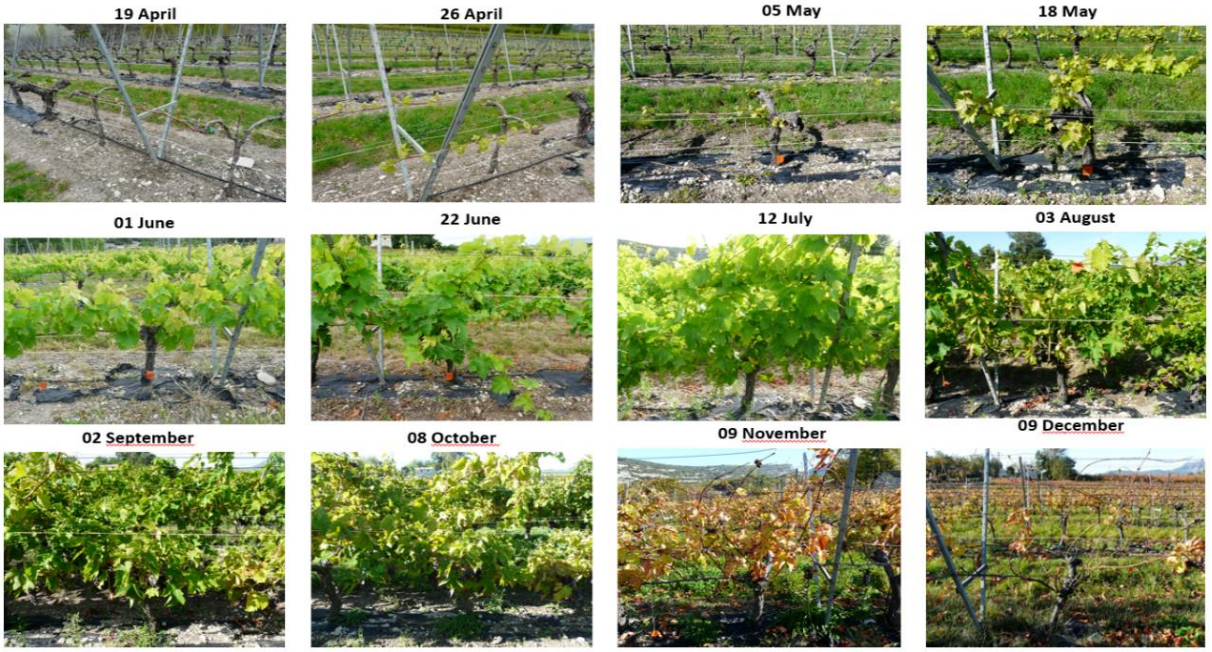

Figure 6. Grapevine ground canopy monitoring for the year 2021

Eleven (11) plots of grapevines (4 table grapevines and 7 wine grapevines) were selected (Figure 7) across the study area (brief descriptions in Table 1). In each plot, five grapevine tree stands were randomly chosen to observe phenology and characterize the leaf development. On each grapevine tree, a branch was selected to count the leaves during the whole growing season (11 field visits every year) to characterize the dynamic of the leaf development. The standard protocol was to count the leaves number on the main branches and the sub-branches. In addition, specific observations were made to establish allometric relationships to infer leaf surface area from the leaf counts. Therefore, at three dates across the grapevine cycle (20-05-2022; 05-07-2022, and 07-10-2022) the leaf lengths (from the petiolar

sinus to the end of the apical lobe) of every leaf on a selection of monitored branches (from 58 to 30) were measured. The lengths thus measured were then converted into surface area using a relationship between length and surface area established on sets of leaves of different sizes taken from each of the plots. The results showed that a single relationship is sufficient to characterize the leaf area of the different grapevine varieties monitored in this work. At the end of the process, we obtained three allometric relationships for each of the leaf length measurement dates linking the leaf surface (cm^2 per branch) to the leaf number. Figure 8 exhibits a variation of the relationship across the year and thus the different relationships were estimated as follows. Up to March 20th, we used the allometric function established the 20-05-2022. From March 21st to October 6th we applied the second relationship established the 05-07-2022 and finally the relationship obtained the 07-10-2023 as applied after October 7th. The estimated leaf surface per branch was then averaged at the field level and then normalized using the maximum value of every time series.

Figure 7. Displaying the eleven selected grapevine plots for ground-based monitoring

Table 1. Descriptions of the eleven selected grapevine plots

S/N	Plot ID	Variety	Inter-row management strategies	Irrigation
1	45	Table grapevine	Grassy	Irrigated
2	203	Wine grapevine	Partially tilled	Non-irrigated
3	204	Wine grapevine	Constantly tilled	Non-irrigated
4	1901	Table grapevine	Grassy	Irrigated
5	2026	Wine grapevine	Tilled	Non-irrigated
6	2335	Wine grapevine	Tilled	Non-irrigated
7	3064	Table grapevine	Grassy	Irrigated
8	3121	Table grapevine	Tilled	Irrigated
9	3138	Wine grapevine	Tilled	Non-irrigated
10	3140	Wine grapevine	Tilled	Non-irrigated
11	3358	Wine grapevine	Partially tilled	Non-irrigated

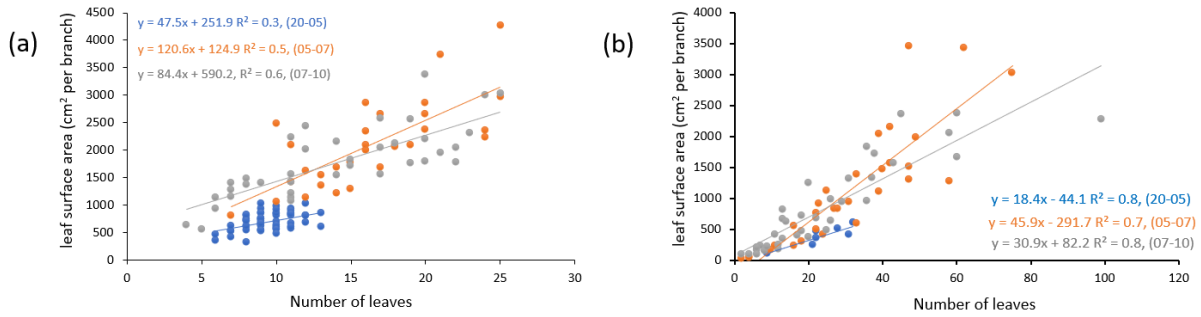

Figure 8. The three linear allometric relations (a) for main branches and (b) sub-branches used for the conversion of leaves number to surface area.

2.2.2 *Assessments of background coverage*

Standardized RGB photos were taken (Figure 9) using a digital camera to characterize the background coverage using vertical views in three locations in the plot inter-row, the location remaining the same across the season to maintain the same ROI (region of interest). To estimate the degree of soil surfaces covered by the background vegetation as shown in Figure 10, the percentage of the ground cover was estimated using the SegVeg model for semantic segmentation of RGB photos into soil background portion, green vegetation portion, and senescent portion as described by Serouart *et al*. (2022). It conforms with the U-net model that delineates vegetation from the background (after training across a dataset that is very large and diverse). Pixels of the vegetation are subsequently classified using a Support Vector Machine (SVM) shallow machine learning approach trained on grids extracted pixels applied to the RGB photos. We used an already trained SegVeg model (Serouart et al. 2022) leading to a vegetation cover fraction ranging from 0 to 1. The presence of senescent vegetation (pruned residues or dried grasses) was not considered in the vegetation cover. A qualitative assessment of the results was done leading to the removal of images with blurry shadows from the analysis because it leads to a biased assessment as shown below (Figure 11).

Figure 9: horizontal (a) and vertical (b) view photos of plots showing the background coverage.

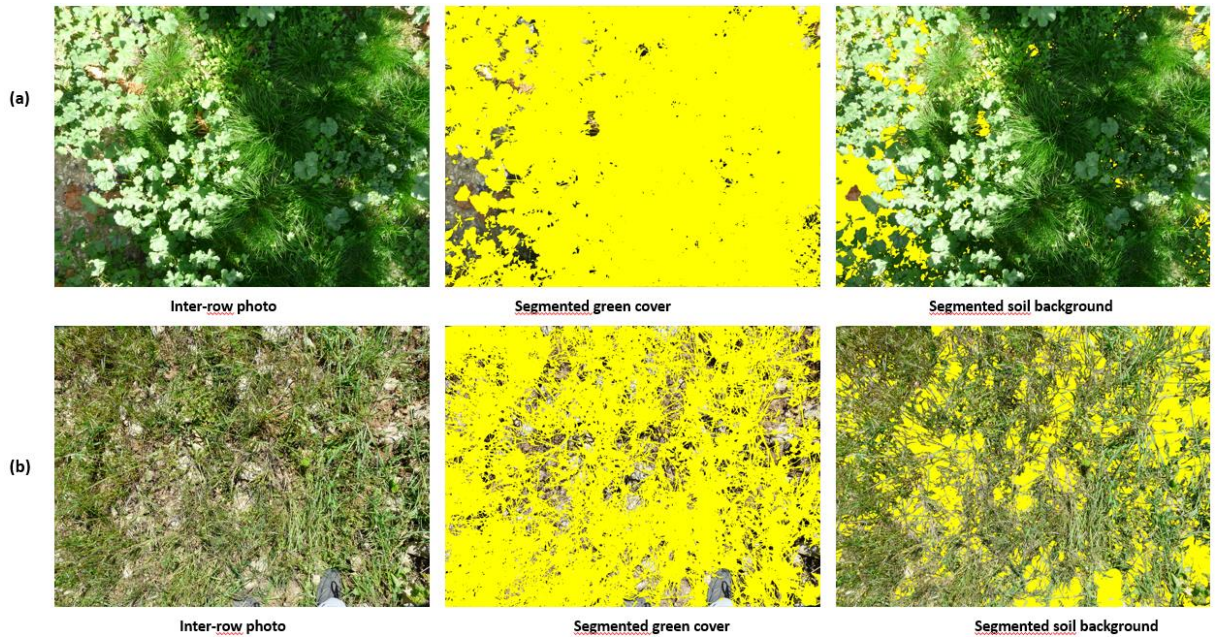

Figure 10. The percentage of the inter-row green cover estimate using the SegVeg model.

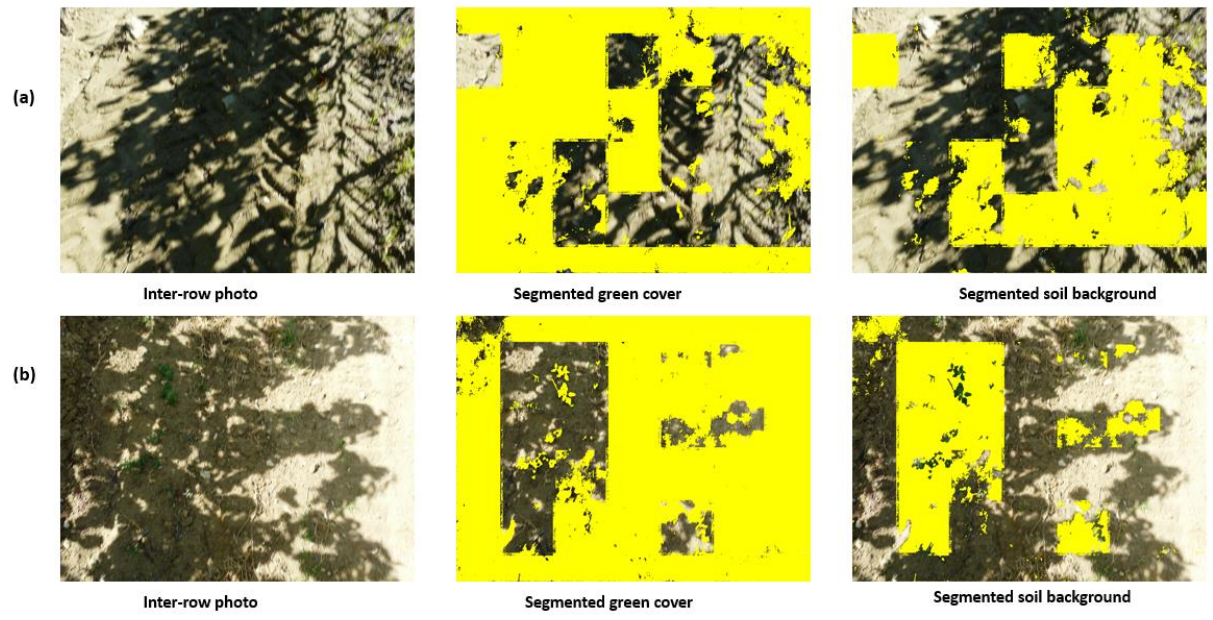

Figure 11: The percentage of the inter-row green cover estimate using the SegVeg model affected by blurry shadows.

2.3 Rainfall conditions at the experimental site.

Among the components of weather, only rainfall data was used in this study. The rainfall data used in this study were extracted from the weather station of Entrecheaux for both years (2021 and 2022) which is closest to the selected monitored grapevine fields. The cumulated rainfall value for 2021 was 664.8 mm and for 2022 was 754.8 mm respectively (Figure 12). In particular, the year 2022 was wetter (more precipitation) than 2021 but also had the driest summer. Rainfall data analysis was useful to examine grass dynamics, especially in the summertime when grass regrowth might be stimulated by a rainfall event.

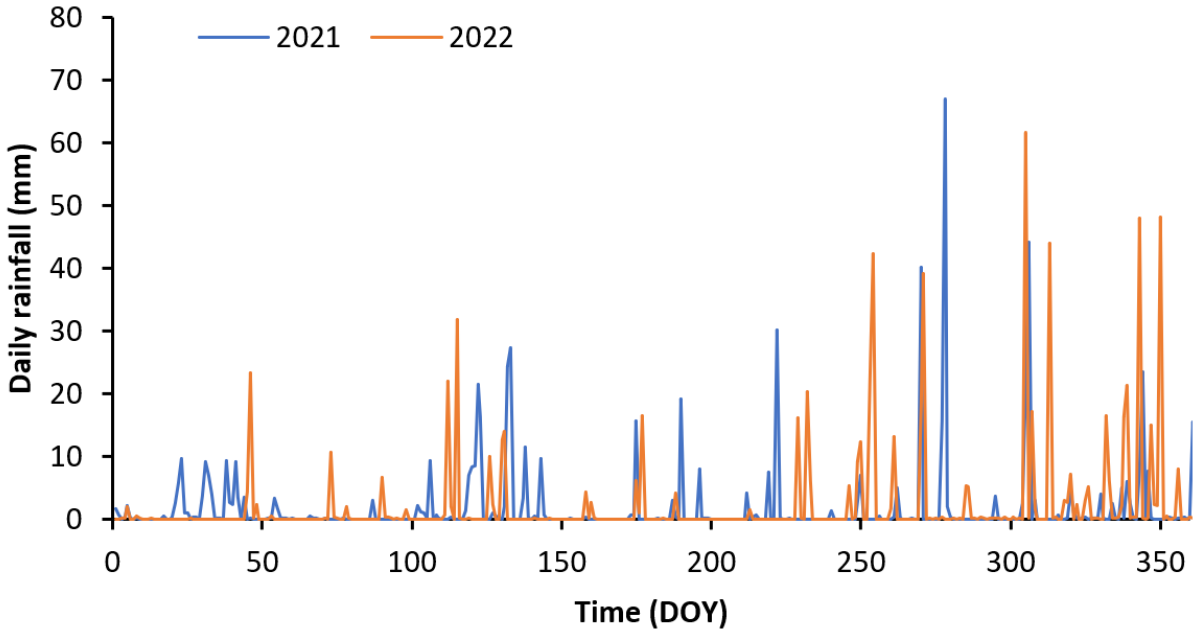

Figure 12: cumulative daily rainfall for the years 2021 and 2022 in the Ouvèze-Ventoux site.

2.4 Remote sensing data

2.4.1 Satellite Imagery

In our study, time-series of Sentinel-2 optical images were utilized and were obtained from both Sentinel-2A and Sentinel-2B of all dates in a given year (for 2016-2021), all within the visible (B2, B3, and B4), the near-infrared (B8) and mid-infrared (B11 our B12) bands. We utilized the open-source service center to obtain images (https://www.theia-land.fr/, accessed on 17 May 2022), it offers cloud treatments (cloud mask described in Hagolle et al. (2017)) to eliminate pixels influenced by clouds (images with > 30% cloud cover), and for this obvious reason, the number of images utilized vary across study sites and years as well because there were different level of cloudiness in each site. Since Sentinel-2B satellites were functional in the time of 2017, fewer data (dates) were obtained from the 2016-2017 year. Table. 2. Below is a depiction of the number of cloud-free images used for each year across the two study sites.

Table 2. Number of cloud-free available images across the two study sites used for the classification

S/N	Year	Crau	Ouveze-Ventoux
1	2016	43	39

2	2017	49	45
3	2018	55	52
4	2019	56	51
5	2020	52	49
6	2021	51	50
7	2022	-	51

2.4.2 Vegetation indices and biophysical variables

Various vegetation indices and biophysical variables were utilized for spectral and temporal analysis which was subdivided into those highlighting greenness like the popular normalized difference vegetation index (NDVI), enhanced vegetation index (EVI), green chlorophyll vegetation index (GCVI) to those highlighting moisture like normalized difference moisture index (NDMI), land surface water index (LSWI), and finally on biophysical variables like leaf area index (LAI), fraction vegetation cover (FCOVER) and the fraction of absorbed photosynthetically active radiation (FAPAR) as summarized in Table. 2. The biophysical variables used in this study were computed with the BVNET algorithm by utilizing the B2, B3, B4, and B8 bands (from 10-meter resolutions) as described in Weiss et al. (2002). The algorithm is robust and has been fused into the S2 toolbox developed by the European Space Agency, It operates on the principles of neural network calibrated (trained) on simulated spectral reflectance utilizing a radiative transfer model (Weiss et al., 2002) and time series of LAI implemented across every 10 m spatial resolution.

2.4.3 Plot pixel average

In each plot (polygon) across the two study sites, a buffer of 20 meters (two pixels) was removed to avoid the impact of mixed pixels at the plot boundary. The plot mean was computed by averaging the vegetation indices of all pixels in a given buffered polygon using the zonal statistics function in R [("Zonal statistics in R | GeoProfesja," 2016)] which was the values taken for the land classification (i.e. at the indices level). The minimum number of pixels being considered in each plot is one from the cloud-free images. A minimum of thirty-nine (39) cloud-free images were used from 2016 to 2022.

Table 3. List of tested vegetation indices and biophysical variables

Full name	Index	Formula	Reference
Canopy greenness-related vegetation indices			
Normalized Difference Vegetation Index	NDVI	$\frac{NIR - RED}{NIR + RED}$	(Rouse Jr et al., 1973)
Green Normalized Difference Vegetation Index	GNDVI	$\frac{NIR - GREEN}{NIR + GREEN}$	(Gitelson et al., 1996)
Enhanced Vegetation Index	EVI	$2.5 * \frac{NIR - RED}{NIR + C1 * RED - C2 * BLUE + L}$	(A. Huete et al., 2002)
Transformed Soil Adjusted Vegetation Index	TSAVI	$a * \frac{NIR - a * RED - b}{RED + a * (RED + a(NIR - b) + c * (1 + a^2)}$	(Baret et al., 1989)
Atmospherically Resistant Vegetation Index	ARVI	$\frac{NIR - (RED - 1 * (BLUE - RED))}{NIR + (RED - 1 * (BLUE - RED))}$	(Kaufman and Tanre, 1992)
Green Chlorophyll Vegetation Index	GCVI	$\frac{NIR}{GREEN} - 1$	(Gitelson et al., 2006)
Water-related vegetation indices			
Normalized Difference Moisture Index	NDMI	$\frac{NIR - SWIR12}{NIR + SWIR12}$	(Gao, 1995)
Land Surface Water Index	LSWI	$\frac{NIR - SWIR1}{NIR + SWIR1}$	(Xiao et al., 2005)
Biophysical variables			
Leaf Area Index	LAI		(Weiss et al., 2002)
Fraction Vegetation Cover	FCOVER		(Weiss et al., 2002)
Fraction of Absorbed Photosynthetically Active Radiation	FAPAR		(Weiss et al., 2002)

Chapter 3

Detection of irrigated permanent grasslands with Sentinel-2 based on temporal patterns of the leaf area index (LAI)

3.1 Intention note

Conventional crop mapping methods are often based on ground observations to train supervised classification algorithms. Thanks to the frequent acquisition made possible by recent satellite missions (Sentinel 2), temporal patterns can be also explored since they depend on both phenology and crop management (Bazzi et al, 2021, Courault et al, 2010). Some of these patterns are specific to a given crop and can therefore be used to map it (Bazzi et al, 2021). In this study, this approach has been applied to identify the irrigated permanent grasslands (IPG) in the Crau region (Southern France).

The irrigated grasslands have an important economic role in the region (unique production with a certified label IPG), by irrigation made by flooding between March and October which contributes to 70% of the ground table recharge. (Courault et al., 2010; Merot et al., 2008b). Grasslands are mowed three times per year. This agricultural practice is clearly identifiable in the temporal profile of the leaf area index (LAI) derived from Sentinel 2 images. The signal decreases sharply when the canopy is mown. The grass then grows back rapidly, and the observed drop is then followed by an increase in LAI, leading to a specific temporal pattern for the leaf area index (LAI). We have therefore proposed an algorithm based on the detection of mowing based on the analysis of the temporal LAI derived from Sentinel 2 observations. The algorithm comprises different steps, first a filtering on the period and to fix minimum and maximum LAI values corresponding to grasslands. The number of minima is calculated for each year. A pixel is classified as grassland if the number of detected mowings is greater or equal to 1. Five years (2016-2020) were studied. The detection of the number of mowings was calculated at the pixel level, then the results were aggregated at the plot level. An evaluation dataset comprising 780 plots was used to assess the performance of the classification. The mapping of irrigated grasslands obtained with this method was compared with other classifications obtained by supervised methods. The results showed that the method based on the mowing analysis gives higher scores than other supervised classification methods that largely include training data sets. Analysis of changes in land use shows that the misclassified plots concern mainly grasslands managed less intensively or with high intra-plot heterogeneity due to irrigation failures or grazing throughout certain periods of the year. A change in land use can be observed and detected by this method, but long time series are required to confirm the changes observed and to remove the ambiguities associated with the heterogeneity of grasslands.

Résumé

Les méthodes conventionnelles de cartographie des cultures sont souvent basées sur le recueil d'observations de terrain pour entraîner les algorithmes de classifications supervisées. Grâce à l'acquisition fréquente permise par les missions satellitaires récentes (Sentinel 2), nous pouvons identifier des modèles temporels qui dépendent à la fois de la phénologie et de la gestion des cultures. Certains de ces modèles sont spécifiques à une culture donnée et peuvent donc être utilisés pour la cartographier. Cette approche a été appliquée pour identifier les prairies permanentes irriguées (PPI) dans la région de la Crau (sud de la France), qui jouent un rôle crucial dans la recharge des nappes phréatiques. Les prairies en Crau sont généralement fauchées trois fois dans l'année entre mai et octobre. Cette pratique culturale est clairement identifiable sur les profils temporels de l'indice foliaire (LAI) dérivés des images Sentinel 2. Le signal décroit brusquement lorsque le couvert est fauché. Puis l'herbe repousse rapidement, et la chute observée est ensuite suivie d'une croissance du LAI, ce qui conduit à une signature temporelle spécifique de de ce type de couvert. Nous avons donc proposé un algorithme fondé sur la détection des fauches basée sur l'analyse du LAI dérivé des observations Sentinel 2. L'algorithme comprend différentes étapes, un premier filtrage sur les périodes considérées en fixant également un minimum et maximum de valeurs de LAI correspondant aux prairies. Le nombre de minima est calculé pour chaque année. Un pixel sera classé en prairie si le nombre de fauches détectées est au moins supérieur ou égal à 2. Cinq années (2016-2020) ont été étudiées. La détection du nombre de fauche a été calculée au niveau du pixel, puis les résultats ont été agrégés au niveau de la parcelle. Un ensemble de données comprenant 780 parcelles a été utilisé pour évaluer les performances de la classification. Nous avons obtenu un indice de Kappa compris entre 0,94 et 0,99 selon les années. La cartographie des prairies irriguées obtenues avec cette méthode a été comparées à d'autres classifications obtenues par méthode supervisée. Les résultats obtenus montrent que la méthode basée sur l'analyse des fauches donne de meilleurs scores que les autres méthodes de classification supervisées qui demandent des données d'entraînement. L'analyse des changements l'utilisation des sols montre que les parcelles mal classées concernent des prairies gérées de façon moins intensive ou présentent une forte hétérogénéité intra-parcellaire due à des défauts d'irrigation ou à un pâturage à certaines périodes de l'année. Un changement réel d'utilisation des terres peut être détecté par cette méthode, mais cela demande de longues séries chronologiques pour confirmer les changements observés et lever les ambiguïtés liées à l'hétérogénéité des prairies.

Mots clés : irrigation ; télédétection ; Sentinel-2 ; prairies ; indice de surface foliaire cartographie

3.2 Graphical Abstract

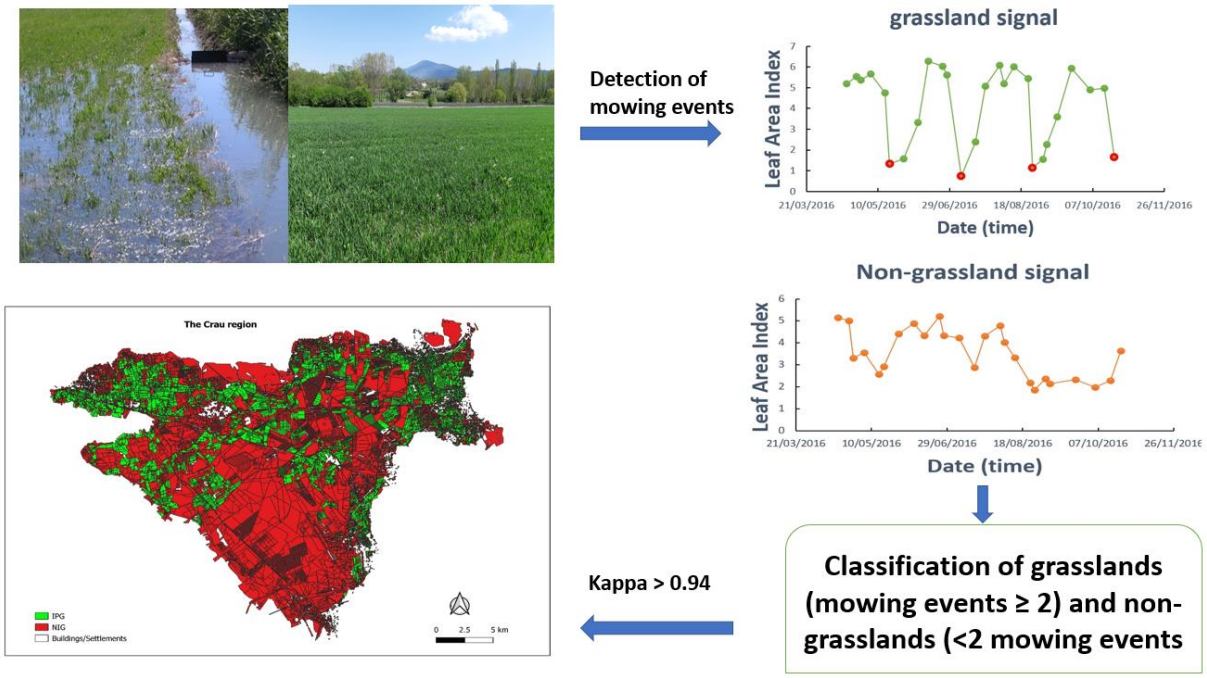

Detection of Irrigated Permanent Grasslands with Sentinel-2 based on temporal patterns of the Leaf Area Index (LAI).

Mukhtar Adamu Abubakar [1,2], André Chanzy[1]*, Guillaume Pouget[1], Flamain Fabrice[1] and Dominique Courault[1]

1 1114 UMR INRAE-Avignon University EMMAH, Domaine St. Paul, 84914, Avignon, France
2 Agronomy Department, Faculty of Agriculture, Shabu-Lafia Campus, Nasarawa State University Keffi, Nigeria
* Correspondence: andre.chanzy@inrae.fr

Abstract: Conventional methods of crop mapping need ground truth information to train the classifier. Thanks to the frequent acquisition allowed by recent satellite missions (Sentinel 2), we can identify temporal patterns that depend on both phenology and crop management. Some of these patterns are specific to a given crop and thus can be used to map it. Thus, we can substitute ground truth information used in conventional methods with agronomic knowledge. This approach was applied to identify irrigated permanent grasslands (IPG) in the Crau area (Southern France) which play a crucial role in groundwater recharge. The grassland is managed by making three mows during the May-October period which leads to a specific temporal pattern of leaf area index (LAI). The mowing detection algorithm was designed using the temporal LAI signal derived from Sentinel 2 observations. The algorithm includes some filtering to remove noise in the signal that might lead to false mowing detection. A pixel is considered a grassland if the number of detected mows is greater than 1. A data set covering five years (2016-2020) was used. The detection mowing number was done at the pixel level and then results are aggregated at the plot level. An evaluation data set including 780 plots was used to assess the performances of the classification. We obtained a Kappa index ranging between 0.94 and 0.99 according to the year. These results were better than other supervised classification methods that include training data sets. The analysis of land-use changes shows that misclassified plots concern grasslands managed less intensively with strong intra-parcel heterogeneity due to irrigation defects or year-round grazing. Time series analysis, therefore, allows us to understand different management practices. Real land-use change in use can be observed, but long time series are needed to confirm the change and remove ambiguities with heterogeneous grasslands.

Keywords: irrigation; remote sensing; Sentinel-2; grasslands; leaf area index; land use classification

Citation: Abubakar, M. A.; Chanzy, A.; Pouget, G.; Flamain, F.; Courault, D. Detection of Irrigated Permanent Grasslands with Sentinel-2 Based on Temporal Patterns of the Leaf Area Index (LAI). Remote Sens. 2022, 14, 3056. https://doi.org/10.3390/ rs14133056

Academic Editor:

Thomas Alexandridis, Christos Chalkias, Konstantinos X. Soulis, Dionissios Kalivas and Emmanouil Psomiadis

Received date: 18 May 2022
Accepted date: 22 June 2022
Published date: 25 June 2022

1. Introduction

According to the United Nations [1], water is a scarce resource thus, its justifiable and judicious use must remain a crucial and fundamental target for sustainable developments across the globe, especially in a world with a constantly increasing populace that directly or indirectly depends on this scarce resource for sustaining their activity and food production system. Undoubtedly agriculture remains an obvious focal point in water management, as the main water user [2], with irrigation accounting at world-scale about 70% of the global freshwater withdrawals [3]. The effect of global changes is anticipated to heighten the issue of water shortage and irrigation needs [4]. Thus, attention is needed on appraisals related to irrigation activities to bolster water resource management, maximize water productivity, and boost agricultural water sustainability [5]. To match water needs and resources, better planning is needed for irrigation activities [6]. One of the key solutions to good irrigation planning is the provision of extensively detailed spatial delineations of croplands under irrigation [7] and the description of irrigation systems and strategies that may lead to various water needs across the year [8]. There is therefore a challenge to detect not only the irrigated areas but also the associated production systems.

The classification of irrigated areas is widely discussed in the literature [8]. While the use of medium-resolution satellites has allowed the establishment of methodological bases applicable to regional scales, there is a renewed interest in these methods with the Sentinel satellites, which offer both good temporal repeatability (3-5 days) and good spatial resolution (10m), which is particularly relevant for crop monitoring. Classification methods for irrigated surfaces are generally based on radar data giving temporal series of surface moisture, data in the optical domain with monitoring of vegetation dynamics, and meteorological data. The use of optical data to separate irrigated and non-irrigated areas is based on the green cover dynamic, which displays a higher level when additional water is brought to the crop. Indices based on meteorological data enhance the quality of the classification. In general, these indices are linked to climatic water stress, which allows for a better characterization of irrigation periods [9, 10, 11]. In addition to the meteorological data, thermal infrared observations enable the implementation of a surface energy balance model to infer the evaporative fraction that is found as a relevant classifier [12] complementary to vegetation indices.

Supervised classification is the most common approach with the implementation of different methods such as decision trees, random forest, support vector machine (SVM), or neural networks for the most frequently cited. The classifiers are in general based on the remotely sensed quantities and/or the derived indices combining several measurements as spectral indices in the optical domain or the radar polarization ratio. It is difficult to report on the obtained accuracy in general terms, since the pedoclimatic conditions, the spatial domain, and the type of irrigated and non-irrigated crops differ considerably from one study to another. For instance, the kappa index ranges between 0.36 [9] and 0.9 [13]. In recent years many studies have been based on Sentinel satellite observations [8] using either Sentinel 1, 2, or both. The combined use of radar Sentinel-1 and optical Sentinel-2 has shown a moderate improvement in classifications [5, 13, 14, 13] when compared to methods based on Sentinel-2 only. However, supervised classification has some limitations, such as the need to collect training data or to deal with missing data. The latter can be an important issue in the optical

domain with the clouds. Therefore, when working over large spatial domains, the selection of cloud-free images can considerably reduce the time series.

An alternative is to use temporal characteristics of the remotely sensed quantities. For instance, in [10], a classification of the temporal characteristics of the vegetation signal such as the maximum and the range of variation of the vegetation index is proposed. For an 18-year period, the training can be limited to a wet and dry year, while an excellent overall accuracy was obtained (>0.95). The authors of [5] showed that it is possible to separate irrigation systems between crops and orchards based on the variability of the radar signal and the temporal autocorrelation length of this signal. Several studies [6, 10, 15, 11] show that consideration of agronomic traits related to phenology and cropping interventions can provide relevant information to characterize irrigated systems. In a broader context it is found that agronomic features can be extracted from multitemporal remote sensing data [16] and applied to crop mapping for instance with canola [17] and potatoes [18] with an improved accuracy in comparison to classical supervised classification methods. These encouraging results led us to take profit of the short revisit time of Sentinel 2 satellites to map Irrigated Permanent Grasslands (IPG) using a temporal approach based on the detection of agronomic traits. In the study site (the Crau area in South-East France), IPG are irrigated using flooding techniques, which has a strong impact on the regional water budget by consuming a very large amount of water (about 20000 m^3/ha/year [19]) but also provides important externalities such as the groundwater recharge. IPG is an interesting case as it provides very clear agronomic traits with several mowing events across the year that can be used for the classification.

The characterisation of grasslands has already been the subject of several studies. The authors of [20] showed that with a limited number of SPOT images (3 in the study) one can separate mown grasslands from grazed grasslands with a kappa=0.82. In this study, it was also found that LAI is the best indicator to make such a distinction. More recently the authors of [21] classify grassland use intensity with 5 rapid eyes images based on the variability of the temporal signal. A similar approach was followed by [22] who used a series of 14 Landsat dates to distinguish 6 classes of grassland reflecting different management strategies. These results announce the potential of Sentinel-2, which was used to detect mowing events [23, 24, 25, 26, 27]. All the proposed methods are based on frequent temporal sampling of vegetation index and local minimum detection. The proposed approaches differ in the methods for filtering the vegetation indices time series and the algorithm for detecting local minima associated with mowing. The quality of the results depends on the scale of the work, with overall accuracies of about 70-80% for studies covering large regional territories [27,24) and better than 90% for smaller territories [26]. The difficulties mentioned by these studies concern the variability of management methods, such as the quantities of grass removed during mowing, spatial heterogeneities (e.g. presence of trees), and acquisition dates that are not always optimal for identifying mowing events. The use of radar series that are not impacted by cloud covers is an alternative exploited in [28,29]. However, the rate of detection errors remains significant due to errors that are inherent to the measured quantities and its interaction with other factors as the plant water content. The combination of optical and radar images was implemented in [25]. The authors used a deep learning algorithm and showed that combining radar quantities (coherence and backscattering coefficient) and NDVI is the best option with an F1-score obtained at a regional scale of 0.88. It should be noted that these characterisations are done on known grassland areas and are not used for the classification of grassland areas. The originality of the present study was then to explore the capabilities of mowing event detection to map IPG and non-irrigated grassland (NIG).

The goal of the study was to develop a classification method to map IPG in South-East France. The approach was developed in the context of the Crau area in Southern France in the

Mediterranean. IPG are both an emblematic crop of the areas and plays an important role in the superficial aquifer water budget [(Merot et al., 2008a)]. In this paper, we develop a mowing event algorithm able to minimise false mowing event detection and account for temporal sampling of Sentinel-2 data that may present missing observation dates during mowing periods. The classification performance was compared to the traditional classification method made directly on vegetation indices time series and the THEIA product, which is an operational product implemented over France.

2. Materials and Methods

2.1. The study site

The Crau area (Fig. 1) is located at 43°38 N, 5°00 E (5 m a.s.l), near the Rhône delta in Southern France, which covers a surface area of 540 to 600 km^2. The climate of the Crau area is Mediterranean with an average annual rainfall of 600 mm (non-uniform) and a potential evapotranspiration of 1100 mm. Mean air temperature of about 7-8°C (in winter) and 24°C (in summer) [23,30,31]. The Crau area is characterised by native shallow soils of about 60-80 cm with 90% stones consequently rendering its water retention very low. Soils irrigated using flooding techniques present a loamy surface soil layer thanks to sediments transported via irrigation water with a layer depth that can reach 60 cm depending on the length of the irrigation period [23]. IPG are the most predominant irrigated crops in the Crau area [19, 23] with a coverage of about 13000 ha (23%) as depicted in Fig.1 (the dark green plots). The irrigation practice of permanent grasslands in the Crau area is more than 4 centuries old which can be dated back to the 16th century [30]. The common practice mostly remains the same which involves the use of gravity (flood) for irrigation, in areas specifically dedicated to hay production and the rearing of sheep. The water used for flooding irrigation contributes to more than 75% of the groundwater table. This ground water table is used for irrigation of intensive orchard and market garden productions, domestic and industrial purposes to roughly 280,000 people around the southern part of the area [23,30]. Duration for irrigation in a year extends to about seven months [19] from March to September. IPG management is regulated by the selling label *"foin de Crau"* the first COP (Certified Origin Product) in France leading to standardize management with three or four grass mowings from May 1st to the end of October and sheep grazing in winter. In general grass fields are irrigated optimally to cover the water needs but, in some places, and some years the access to water might be critical thus leading to reduce grass productivity and skipping a mowing operation. Some farmers do not follow the label rules, for example when they breed animals all year round, which leads to a different spatial and temporal dynamics of the vegetation cover than the one obtained with the recommended cultivation practices, which are dominant on the territory. The grass fields are in general homogeneous but heterogeneities in vegetation cover were found at the field boarder or within the field when surface levelling is not satisfactory generating heterogeneities in the water supply. Therefore, if a dominant grass development temporal pattern is expected and then used to identify grassland areas, the mentioned variation can interfere with the classification process.

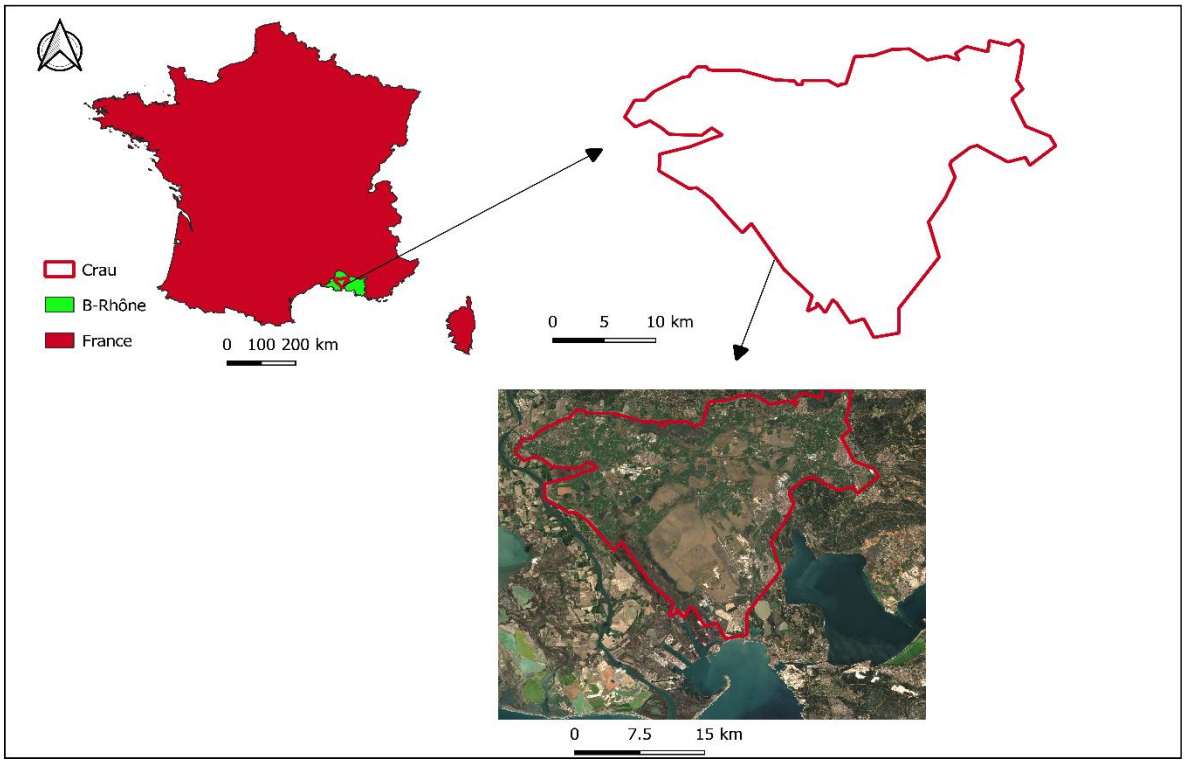

Figure 1. Study site location.

2.2. Data used

2.2.1. Field survey

A field survey was done to identify crop type and irrigation over a total of 809 plots (all plots were greater than 1 ha) by a visit done during the 2016-2020 period. During the visit, surveyed plots were identified, and observed crops were reported in the plot map established over the whole area. Irrigated permanent grasslands (IPG) consisted of 391 plots and Not Irrigated Grasslands (NIG) comprise 418 plots. In addition, aerial photographs were used to check management features such as soil levelling, land-use change, or grazing. For that purpose, we used Google Earth images acquired during the 2015-2021 period together with the IGN (the French National Geography Institute) 2020 flight campaign. Plot boundaries were drawn in 2012 throughout the Crau area leading to 18058 polygons. The map was initiated with the cadastre, which we then corrected manually to delimit homogeneous spatial entities in terms of their use hereafter referred to as plot. The resulting SIG layer was then used to aggregate classification results produced at pixel scale over plot's polygons.

2.2.2. Satellite data

Time series of Sentinel-2 of level 2A optical images were used for this study, which were collected from both Sentinel-2A and Sentinel-2B for all dates from 2016 to 2020. We used the images distributed by the French land data open-source service center (https://www. theia-land.fr/), which also proposed cloud masks that were used to remove pixels affected by clouds. The number of remaining dates during the considered period (March 15th to October 30th) is given in Table 1. As Sentinel 2B satellite was operational during 2017 we got less date in 2016 and 2017. At the pixel level, the number of available dates varied due to the occurrence of clouds, which was not homogeneous within the studied area.

Table 1. Statistics on the number of days available over the period from 15 April to 30 October after removing the dates impacted by clouds. The filtering is carried out at the pixel level and the statistics have been calculated on all the pixels of the Crau area.

Year	Average	maximum	minimum
2016	26	31	20
2017	43	49	37
2018	52	61	44
2019	54	59	48
2020	49	56	42

The BVNET algorithm using bands 3, 4, and 8 was used. The algorithm calculates biophysical canopy variables such as the Leaf Area Index (LAI). Due to its robustness, especially on homogeneous canopies such as grasslands, the algorithm has been integrated into the S2 toolbox developed by the European Space Agency. It is based on a neural network trained on simulated spectral reflectance using a radiative transfer model [32]. Temporal profiles of LAI were then established for every 10-meter pixel.

2.3. Developed irrigated permanent grassland detection algorithm.

The specificity of irrigated grasslands is that they present several mowing-vegetation growth cycles during the year. To detect a grassland, we can also rely on the level of LAI, which is generally high (LAI > 4) when the vegetation is well developed, and the growth rate after a cut which is specific to grassland. For example, in the study area, it takes 30 to 50 days after a mow to return to a vegetation development comparable to that before the mow. Although these characteristics specific to irrigated grassland should make it relatively easy to identify them with a temporal sampling such as that offered by the Sentinel-2 mission, we were confronted in the time series with LAI variations linked to atmospheric corrections that may generate temporal patterns of LAI leading to confusion with grassland mowing events. In addition, the presence of clouds during the mowing periods reduced the time sampling of the LAI and prevents a clear detection of a mowing event.

As in [23, 24, 26, 27], the detection algorithms of mowing events developed in the study are based on a sharp reduction in vegetation amount followed by a significant vegetation development during the following 45 days. To monitor the development of vegetation, we used the LAI estimated from Sentinel 2. If this quantity has not been used in previous mowing event detection studies that rely on NDVI or NDII [23, 24, 27, 26], the main reason for this choice comes from the nature of the quantity, which is a characteristic of plant cover and can therefore be directly linked to agronomic knowledge and crop model outputs. This is important for the design of algorithms characterising agronomic traits, their parameterisation, and their generalisation to include prior information from agronomic knowledge. Moreover, it has been shown that LAI is more sensitive to variations in well-developed vegetation while conventional vegetation indices tend to saturate more easily [29]. The disadvantage is that the computed LAI is more sensitive to atmospheric corrections as we no longer have the normalization of measurements made on classical vegetation indices such as the NDVI. Moreover, on some surface types, the LAI inversion algorithm may fail. For example, we found very high and variable LAI values on greenhouses with a non-negligible risk of confusion with grasslands.

To detect an irrigated grassland, we made the following main assumptions:

- There are at least 2 mowing events during the May to October period. If most of the irrigated grassland is managed with 3 or 4 mowing events, this threshold makes it possible to consider less intensively managed grasslands or to allow for the possibility

of missing a mowing event due to an unfavourable time series with a long cloudy period during the mowing period. Such a situation can happen even in the Mediterranean area despite the high revisit frequency of the sentinel-2 satellites.

- A mowing event is characterized by a local minimum with significant variations in LAI over 45 days before and after this minimum. The period of 45 days after the minimum reflects the growth time of the grassland after mowing. The period of 45 days before may seem long since a mowing induces an immediate drop in the amount of vegetation. However, we found that some mowings were delayed and then the grassland began to senesce, resulting in a decrease in green leaf area as captured by the LAI estimate. A shift of 10 to 20 days in the maximum LAI before mowing can thus be observed. In addition, gaps in LAI time series may lead to the maximum being sought over a somewhat longer period.

To implement these assumptions, we propose a five steps algorithm as summarized in Figure 2

Step 1: we first flagged the LAI time series by considering that the maximum LAI must be greater than *tlaimin* and lower than *tlaimax*. *tlaimin* threshold reflects the fact that irrigated grassland leads to strong vegetation development while *tlaimax* is dedicated to eliminating surface type on which the LAI computation fails leading to unrealistic high values.

Step 2: To eliminate local minimum due to short-term LAI variations as induced by poor atmospheric corrections, different smoothing procedures were presented in [24, 26, 33]. In this work, we used the smooth spline algorithm in R [34], which is efficient and flexible. The algorithm involved a degree of freedom parameter (*df*) controlling the smoothing process. The minimum was then detected on the smoothed LAI time series that might be slightly delayed in comparison to the date of the corresponding minimum in the observed LAI time series.

Step 3: Some remaining anomalies in the LAI time series that might impact the LAI variations computation will be corrected. When the LAI is too small, i.e. lower than *tlailow* or when the difference between the observed LAI and the smoothed LAI is greater than *difmax*, the observed LAI is substituted by the corresponding smoothed LAI value.

Step 4: Every detected minimum in step 2 is validated according to different criteria. First, the date of the observed minimum (*tmin*) is searched in the observed LAI time series within a time window around the minimum detected on the smoothed series. This time window ranges from *dtb1* days before and *dta1* days after the date of the minimum detected in step 2. The time *tmin* must fall within the considered period starting at *dbeg* and ending at *dend*, being in our case May 1st and October 15th, respectively. Then the value of the minimum was analysed. We consider that the minimum LAI must be lower than a threshold, this threshold being adapted according to the LAI sampling date before and after the minimum date. Indeed, if the LAI is sampled loosely around the minimum, the truncation effect of the time series may result in a minimum value that is larger than the true minimum, as the vegetation may have started to grow at the time of the measurement. The threshold is therefore set according to the following relationship:

tminlai= tminlai0 when dt<dtmin0
tminlai=tminlai1 when dt> dtmin1

$$tminlai = tminlai0 + {}^{dt}/_{(dtmin1 - dtmin0)} \cdot (tminlai1 - tminlai0) \quad (1)$$

with *dt* being the time interval between the first acquisition date before and after *tmin*. If the minimum is validated (*LAI(tmin)<tminlai*), the last test was done on the LAI variations before (within the [*tmin-dtb – tmin*] period and after (within the [*tmin– tmin+dta*] period) that must be greater than *threshlai*. The period before the minimum is reduced when the LAI sampling is

tightened. If the measurement period of the *nbb* observations before the minimum is shorter than *dtb* then this period is used to calculate the LAI variation.

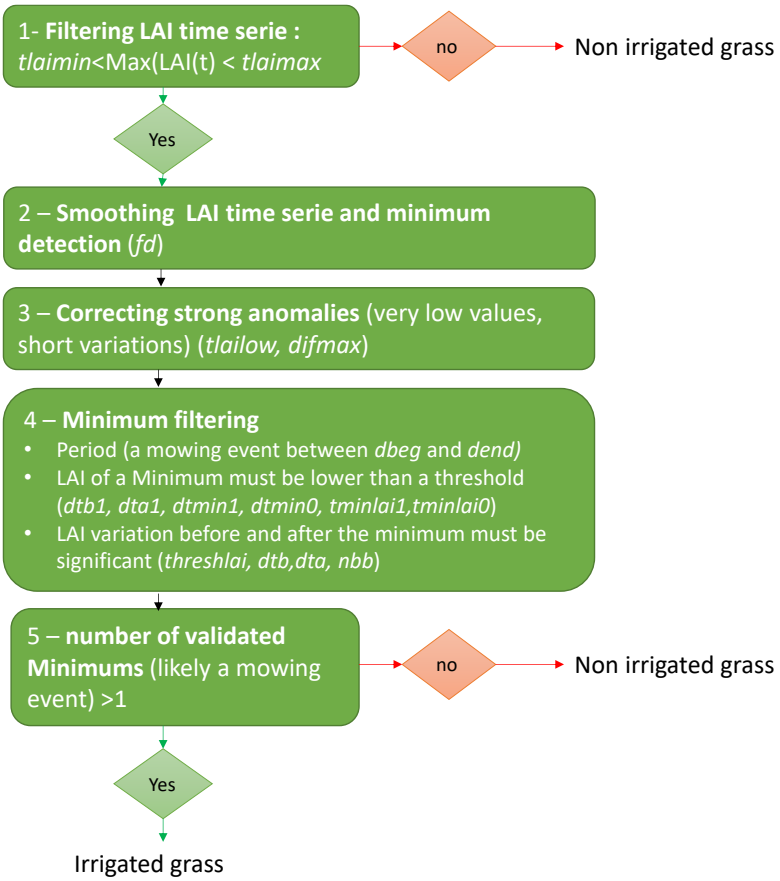

Figure 2. Five steps of the developed irrigated grassland algorithm at the pixel level.

Step 5: The number of validated minimums, considered as mowing events, is established and used to apply the irrigated grassland filter being a minimum of two events.

The algorithm is applied at the pixel level. However, due to plot heterogeneity or border effect, an aggregation was done within the plot boundary after applying a buffer of 20 m to provide a classification at the plot level. A plot was then declared as irrigated grassland when a majority of pixels were classified as irrigated grassland, the majority being qualified by a percentage of the pixels that has to be determined (*pixperc*).

The detection algorithm involved 16 parameters that are summarized in Table 2. As the number of parameters was large we prescribed some of them to values consistent with our agronomical knowledge while the other parameters were calibrated.

Table 2. List of parameters and value retained to implement the developed method.

Parameters	Definitions	Range of values used when calibrated	Final value
fd	degree of freedom of the smoothing algorithm	5, 10, 15, 17	10
tlaimax	LAI threshold. a pixel is declared being not a grassland when the maximum of LAI time series is greater than *tlaimax*	10, 10.5, 11, 11.5	10.5

tlaimin	LAI threshold. A pixel is declared not being a grassland when the maximum of the LAI time series is lower than tlaimin	4.0, 4.1, 4.2, 4.3, 4.4, 4.5	4.2
threshlai	LAI variation threshold before and after the detected minimum	0.5, 1.0, 1.5, 2.0, 2.5	1.5
dta1	Period to search for the true minimum after the smoothed minimum		15
dtb1	Period to search for the true minimum before the smoothed minimum		25
tlailow	LAI threshold to characterize unrealistic low LAI value		0.4
nbb	Number of points to consider in searching the maximum before a cut	2,4,6,8	4
dtmin1	Minimum time interval between observations bracketting the minimum leading to selecting the largest tminlai (tminlai1)		25
dtmin0	maximum time interval between observations bracketting the minimum leading to selecting the smallest tminlai (tminlai0)		10
tminlai1	largest LAI threshold to validate a minimum LAI (when time sampling is sparse)		2.5
tminlai0	smallest LAI threshold to validate a minimum LAI (when time sampling is frequent)		2
dta	Period length after a minimum to characterize LAI variation		45
dtb	Period length before a minimum to characterize LAI variation		45
difmax	The difference between the observed and the smoothed LAI above which the LAI is corrected.		2.6
Pixperc	The minimum rate of pixels detected as irrigated grass in a plot to classify it as an irrigated grass plot	50,70,90	90

2.4. Calibration and Evaluation

The calibration procedure targeted the best parameters to be used for the separation of IPG from NIG. The calibration was done considering 29 vignettes surrounding a known IPG plot. In each vignette, we determined 6 polygons, 3 being inside the grassland plot and three being outside (Figure 3) corresponding to surfaces that might be orchards, vineyards, field crops, market gardens, dry grasslands... Each polygon is considered as a single entity on which metrics describing the mowing event number distribution are computed.

The cost function used for calibration was the percentage of well-classified polygons i.e. that having a majority of pixels with at least 2 mowing events for the IPG polygons and lower than 2 for the NIG polygons. A database covering the 2016-2020 period was generated, considering that every year provides a set of data to compute the cost function.

Two phases are considered in the calibration. First, based on agronomic knowledge and/or visual analysis of LAI time series, we set *dta* and *dtb* to 45 days, *dta1 to 15* days, *dtb1 to 25* days, and *dbeg* and *dend* set to May 1st and October 15th, respectively. Then *fd*, *tlaimax*, *tlaimin*, *threslai*, and *pixperc* were calibrated using a manual fitting considering the range of values given in Table 2. In that first calibration phase, the LAI anomaly correction (step 3) and the filtering tests on the minimum value (step 4) involving the other parameters were not activated.

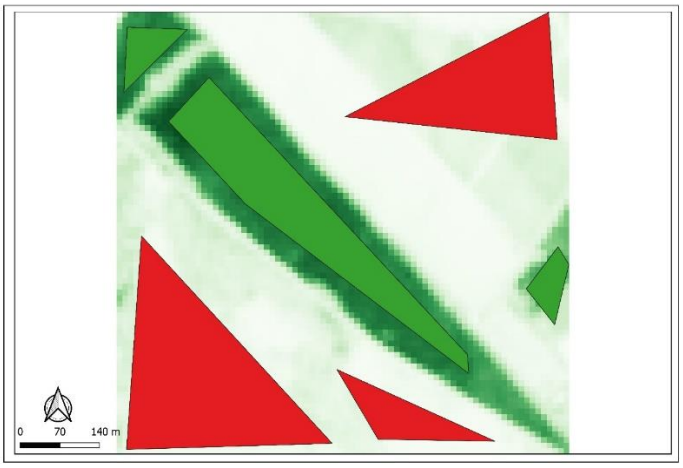

Figure 3. Green polygons symbolise IPG while red polygons symbolise NIG.

Then, in a second phase, some refinements were added to the minimum detection algorithm *dtlimlai0, dtlimlai1, dtmin0, dtmin1, and tlailow* were prescribed to 15, 25, 10, 25, 2, 2.5, and 0.4, respectively, based on the visual analysis of LAI time series that led to an error in the first phase. The other parameters (*difmax, nbb*) were calibrated.

The evaluation was made at the plot level on 780 plots not used for the calibration with 362 IPG plots and 418 NIG plots, which in detail their break down goes as 162 orchards; 100 vineyards; 99 greenhouses; 20 dry grass; 33 field crops, and 4 lawns.

2.5. Accuracy assessment

Accuracy assessment remains an important aspect of mapping projects utilizing remotely sensed information [35]. The different classifications made in the study were evaluated using the overall accuracy (OA), the producer's accuracy (PA), and Cohen's Kappa index (K), all quantities being derived from the confusion matrix having the following terms: TG (well-classified irrigated grassland plots), FG (plot classified as irrigated grassland while not an irrigated grassland), TNG (well classified not irrigated grassland plots), FNG (irrigated grassland plot classified as not irrigated grassland).

$$Overall\ accuracy = \frac{\mathrm{TG+TNG}}{TG+FG+TNG+FNG} \cdot 100 \qquad 2$$

Producer's accuracy corresponds to the error due to omission (exclusion). From the perspective of the land use map maker, it indicates how accurate is the map: for a given class, how many plots among the reference plots in the map were tagged accurately. It is defined for the IPG as ;

$$Producer's\ accuracy = \frac{\mathrm{TG}}{\mathrm{TG+FNG}} \cdot 100 \qquad 3$$

The Cohen's Kappa index (K) characterizes the map agreement with the ground truth after removing the chance factor. It is an indication of the adding value of the classification method, which is defined as ;

$$K = \frac{\text{overall accuracy} - \text{chance agreement}}{1 - \text{chance agreement}} \quad (4)$$

where chance agreement is the probability of having a good classification by chance, which is defined by

$$\text{chance agreement} = \frac{(TG+FG)\cdot(TG+FNG)+(FNG+TNG)\cdot(FG+TNG)}{(TG+FG+FNG+TNG)^2}$$

2.6. Benchmark

Different existing classification methods based on Sentinel 2 data were considered to assess the adding value of the new proposed method described above. First, we made a supervised classification based on the Support Vector Machine (SVM) method, which is rather common and powerful for discriminating two classes. The classification was carried out on cloud-free LAI images taken over the whole year. Due to the proximity of the coast, we have large cloudiness heterogeneities. To maximise the number of images, the Crau area was divided into 4 zones (A, B, C, and D) and for each zone, we selected the images according to the following two criteria: 1) the whole zone is cloud-free as well as 2) for the training polygons (Figure 3). As a consequence, the number of images used for the classification varied between 12 and 25 in 2016, 13 and 33 in 2017, and 24 and 38 in 2018 according to the zones. The training dataset is similar to that used for the developed algorithm by taking randomly three pixels in every polygon described in the 2.5 section. The training was done for each year with the cloud-free images selected for each of the 4 zones. The classification was then applied to each zone and aggregated over the Crau area to produce a binary image (IPG/NIG) per year.

We also consider the THEIA land use map as a benchmark since it is implemented yearly over the whole national territory (https://www.theia-land.fr/ceslist/ces-occupation-des-sols/). It is a supervised classification [36] based on random forest classification using all Sentinel-2 dates and the VIS and NIR bands and as auxiliary information the topography, the urban map, the Corinne Land Cover map, and the RPG ('Registre Parcellaire Graphique) data which gathers farmer's annual declarations to get subsidies from the European Union. Seventeen classes were identified with one dedicated to grasslands. In our study, the detection of one class, the grassland class, among the others was evaluated. The produced maps were given at the scale of Sentinel 2 10-meter pixels.

The evaluation of the two benchmark classifications was done on the evaluation plots described in section 2.5. Therefore, each evaluation plot is classified according to the majority class (>50% of the pixels in the plot).

3. Results

3.1. Calibration

The most important parameter is the smoothing parameter *(df)* whose effect is clearly illustrated in Figures 4-6. The goal of the smoothing is to remove signal oscillations that are not linked to mowing events (Figure 4). We observed that most of these undesirable oscillations correspond to short-term variations. Therefore, the smoothing should be strong enough to remove them (i.e. $df < 15$) but should not be too strong as some mowing events might be missed (i.e. $df = 5$). The calibration led to $df = 10$, which corresponds to an intermediate case in Figure 5. When applying the minimum detection on the smoothed LAI time series, we identified 3 events that are consistent with the mowing calendar (Figure 6). The rate of misclassified plots was about 13% after phase 1 (Table 3). The main source of error comes from the detection of NIG as IPG (9%) as shown in Figure 7.

Table 3. Calibration performance after the first and second phases on the calibration data set. TG represents well-classified irrigated grassland polygons), FG, polygons classified as irrigated grassland while not an irrigated grassland, TNG, well classified not irrigated grassland polygons and FNG; irrigated grassland polygons classified as not irrigated grassland.

Calibration phases	Total plots	TG	TNG	FG	FNG
First calibration phase	748	372	281	69	26
Second calibration phase	748	416	304	25	3

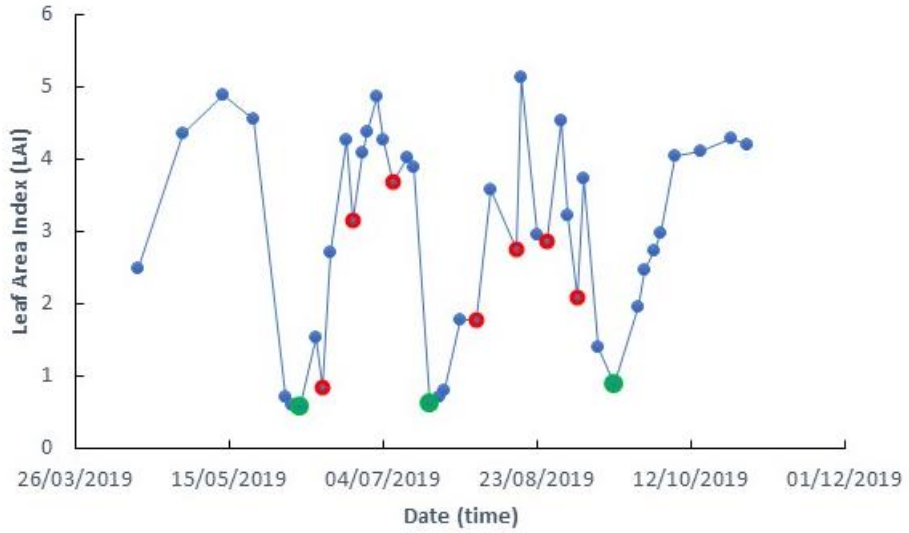

Figure 4. Observed LAI time series of an IPG pixel before smoothing, red dots correspond to LAI minimums that are not linked to mowing events. Green dots are LAI minimum linked to mowing event.

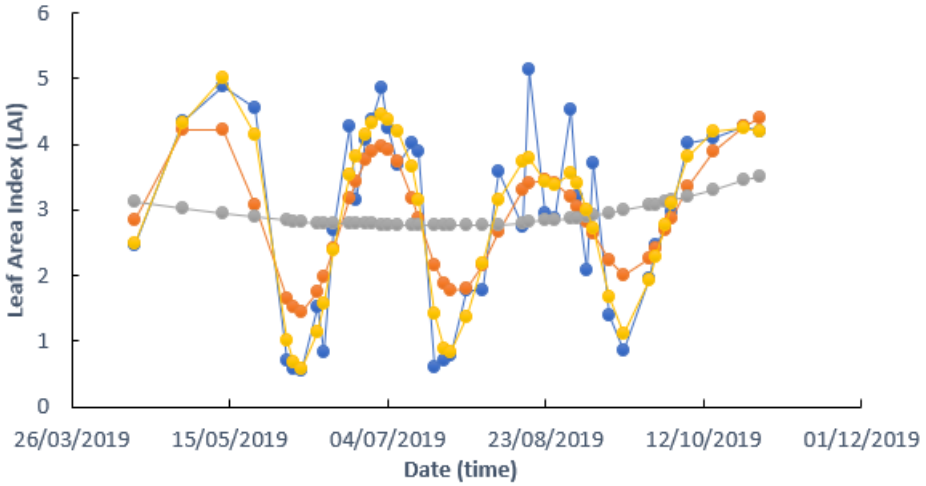

Figure 5. Effect of degrees of freedom (*df*) of the smoothed algorithms on LAI times series of an IPG pixel. In blue the observed LAI, in grey, orange and yellow the smooth LAI times series with *df* equal 5, 10 and 15, respectively.

In the presented case in Figure 7, the smoothing was not appropriate and some strong LAI oscillations were still present in the smoothed signal; thus, triggering the identification of false mowing events. However, the LAI values corresponding to the detected minimum were high and larger than what is expected with freshly mowed grass. An additional test on the LAI values at the detected minimum is a way to resolve the ambiguity displayed in Figure 7. The

analysis of such errors led to defining the series of tests and data manipulation as described in section 2.3 in steps 3 and 4, which parameters were characterized in phase 2. After this phase, we reduced the misclassified plots rate to less than 4%, with still a greater probability to miss a NIG than an IPG (Table 3). The final values of the parameters of the algorithm are reported in Table 2.

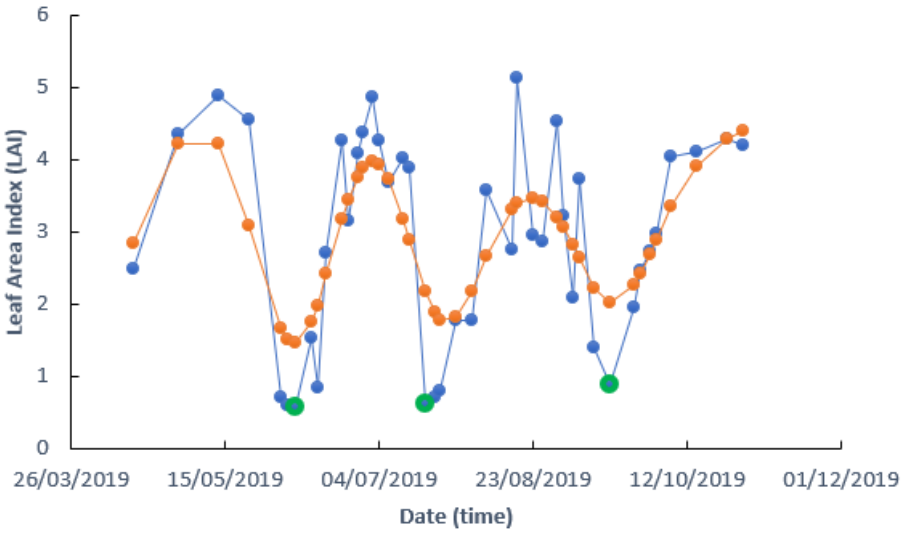

Figure 6. Observed LAI time series (blue) and smoothed LAI time series (orange) of an IPG pixel. Green dots correspond to minimum LAI detected on the smoothed LAI time series.

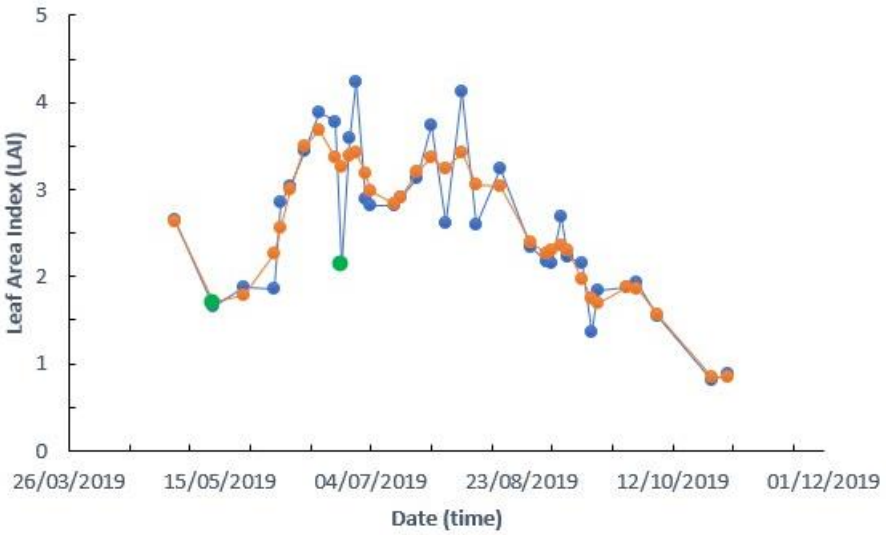

Figure 7. Observed (blue) and smoothed (orange) LAI time series of a NIG pixel detected as an IPG. The green dots correspond to the detected mowing events using the developed algorithm after the first phase of calibration.

To illustrate the results of the algorithm, we selected an area covering two grassland plots surrounded by NIG area. The results obtained in 2019 are displayed in Figure 8 where letters represent the exact location of the pixel time series A, B, and C displayed in Figures 6, 9, and 10, respectively. There is a clear difference in grass management with four mowing events in the northern plot and three in the southern (Figure 8) as illustrated in Figures 6 and

10. If the plots are mostly homogeneous, some areas with less mowing events can be seen at the plot boarder, in the middle corresponding to a ditch bringing the water, and, in some patches. The case of point A (Figure 9) indicates that the missed last mowing event is explained by low grass growth at the end of the season. The difference between the minimum and the maximum after harvest was below 1.5 (*threshlai* < 1.5) reflecting less productive area that might be induced by soil properties or the quality of the irrigation with heterogeneities induced by poor soil levelling.

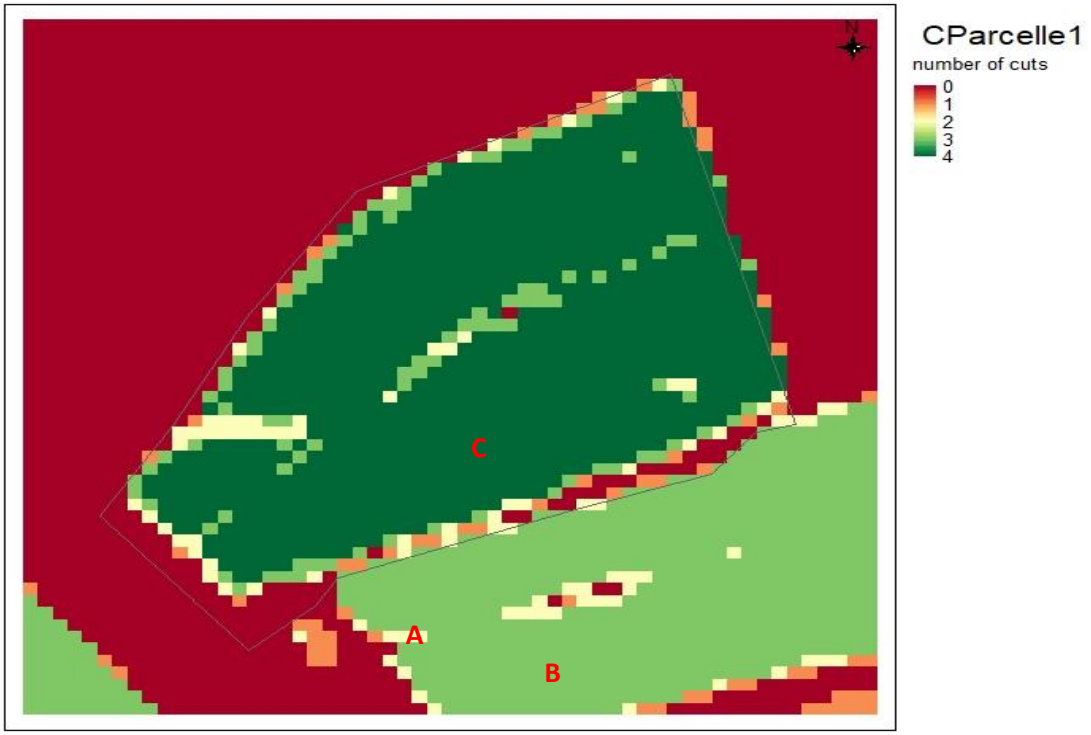

Figure 8. Results obtained after the second phase of calibration in 2019 showing locations of Fig. 6, 9, and 10.

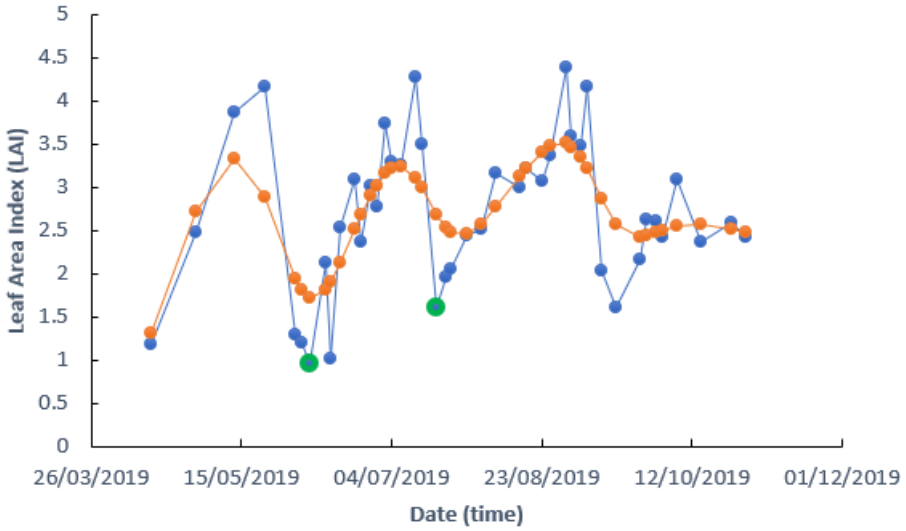

Figure 9. Observed signal (blue) and smoothed (orange) LAI time series of an IPG pixel showing two mowing events (green dots).

3.2 Evaluation

Results obtained on the evaluation data set are given in Table 4. Excellent results were obtained with an OA greater than 97% and a Kappa index between 0.94 and 0.99. The producer accuracy is equal to 100% for the NIG class, meaning that a parcel declared as a NIG is always NIG. This shows that the additional filtering can handle situations like the one shown in Figure 7. The producer's accuracies of the IPG class are a little less good, which means that some IPG plots are not detected. We will come back to this point in the discussion. There is also a year effect that appears clearly. For example, 2020 was the worst year, while the best results were obtained in 2018. The 2018 year is the wettest year during the summer, which might limit the irrigation pressure and therefore allowed good production throughout the cycle. In 2020 there was gap of 20 days in the measurements, which did not allow for the detection of the maximum grass development between the second and the third mowing events, leading to miss both of them.

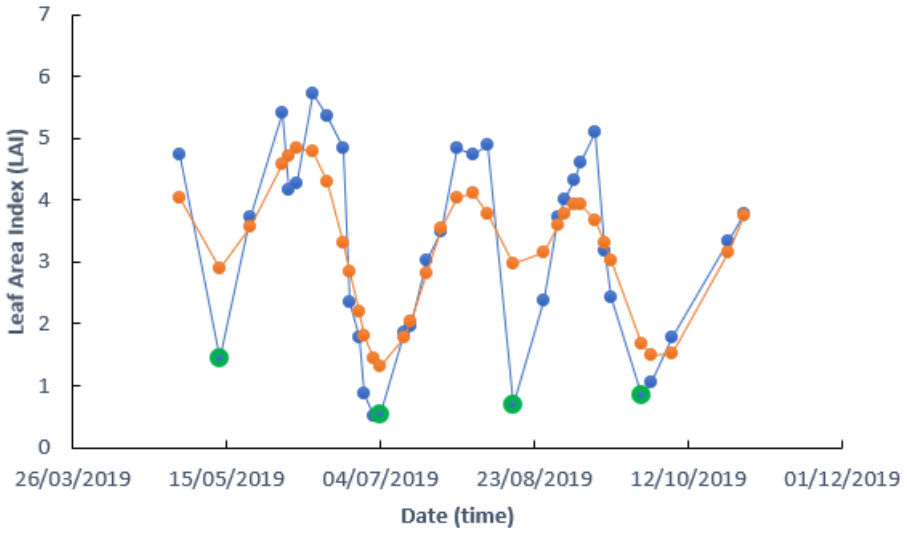

Figure 10. Observed (blue) and smoothed (orange) LAI time series of an IPG pixel showing four mowing events (green dots).

Table 4. Summary of all the classification performances conducted in the Crau area.

Year	Overall accuracy	Producer's accuracy (IPG)	Producer's accuracy (NIG)	Kappa indice
Developed Classification Leaf Area Index (Sentinel-2) + proposed algorithm				
2016	97.7	95.2	100.0	0.96
2017	99.1	98.3	100.0	0.98
2018	99.7	99.4	100.0	0.99
2019	98.8	97.5	100.0	0.98
2020	96.9	93.8	99.7	0.94
THEIA Classification Satellite image + Land use data +Supervised classification				
2016	97.2	95.5	98.7	0.95
2017	98.6	96.9	100.0	0.97

2018	98.4	97.8	98.9	0.97
Classification via Support Vector Machine (SVM)				
Satellite images + supervised classification using SVM method				
2016	67.2	72.6	68.4	0.51
2017	71	78.3	79.1	0.63
2018	73.3	81.3	76.2	0.58

These good results have to be tempered by the fact that IPGs are likely a class easy to detect as shown by the good results depicted in Table 4 with the THEIA classification approaches. However, our results are clearly better than those obtained with the SVM method, which means that algorithms based on artificial intelligence cannot necessarily capture the agronomic traits as used in our method. Although slightly better, our results are comparable to those of THEIA, which relies on a rich spatialized ground truth with the administrative census and Corinne Land Cover data.

4. Discussion

The proposed method was applied to the whole territory of the Crau area having 18058 plots with an illustration given in Figure 11 for the year 2018, showing all plots of IPG (in green) and NIG (in red). We do not have any reference on the whole territory and we can therefore only make relative analyses. This was done by addressing the following two questions: i) what is the impact of classifying land use at plot scale compared to a pixel scale approach? ii) what is the evolution of irrigated areas between years and can it be linked to changes in land use? Finally, we discussed the novelty of the approach and its generalisation.

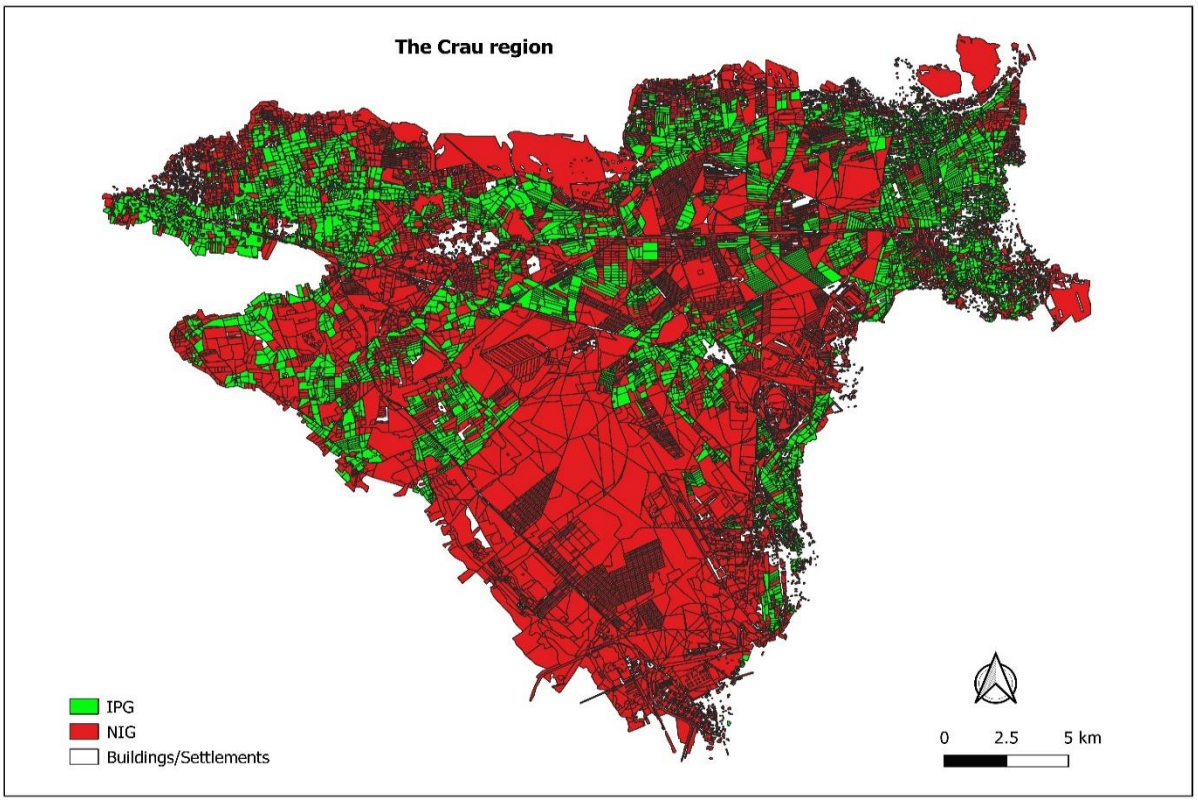

Figure 11. Land use map using the developed algorithm in 2018.

4.1. Impact of plot aggregation in the classification process

One of the constraints of the method applied in this work is that the land-use class is determined at the scale of a plot. We have seen in Figure 8 that the edges of the plot, the irrigation ditches within the plot, and certain less productive areas could lead to a lower number of mows and thus induce a misclassification of the pixel. It is also possible to have isolated pixels located in NIG areas that present several mowing-like events. Working at the plot level reduces the risk of error since the land-use class is based on a majority of pixels. However, a plot map with their boundaries is not always available, especially when large areas are considered. Furthermore, the plot map may contain errors generating errors in the areas counted or misclassification of an IPG plot when it includes a significant part (>10% in our case) of an area that is not an IPG. For inventory purposes, we can imagine applying the developed classification method at the pixel level rather than at the plot level. To see the impact of such a choice we compared the total surface over the Crau area obtained using either a pixel-based approach by counting the pixels classified in each class or a plot-based approach where we summed the surface of the plots per class.

The pixels of the study site (the Crau) were taken from an extraction polygon that is as close as possible to the considered area being the aggregation of plots. As this area sometimes presents a bit complex boundary (Figure 10), the extracted polygon was drawn inside the area explaining the small differences in the total areas of the pixel-based and plot-base counting (Table 5). The percentages of IPG based on the plot-based approach ranged from 25-26% and 74-75% for NIG while for the pixel-based approach, the percentages of IPG ranged from 22-25% and 75-78% for the NIG. The underestimation obtained with the pixel-based approach, likely due to the plot boarder effect, remained however moderate.

Table 5. Total surfaces obtained for IPG and NIG classes using the developed classification algorithm obtained with a plot aggregation or a pixel-based approaches.

	Plot-based approach		
	IPG	**NIG**	**Total plots**
2016	13318 ha	40264 ha	53581 ha
2017	13717 ha	39864 ha	53581 ha
2018	13839 ha	39742 ha	53581 ha
2019	13994 ha	39587 ha	53581 ha
2020	13850 ha	39731 ha	53581 ha
	Pixel-based approach		
	IPG	**NIG**	**Total pixels**
2016	11480 ha	40520 ha	52000ha
2017	11770 ha	40230 ha	52000 ha
2018	12345 ha	39655 ha	52000 ha
2019	11561 ha	40439 ha	52000 ha
2020	12758 ha	39242 ha	52000 ha

4.2. Ability to detect land-use changes

The proposed method implemented across the five years (2016-2020) gave us an overview of the consistency of the results from one year to another. Results are displayed in Table 6 by considering plots where the classification remains stable over the five years (i.e GGGGG and NNNNN classes), plots that met one change that can be attributed to a land-use change, and plot having several changes reflecting problems in their classification. In 91% of

the cases, perfect stability was observed. The analysis was made on plots presenting one change with spatial illustrations depicted in Figure 12. The figure shows that changes are spread over the area with plots of different sizes. The causes of the change were identified by analysing the high-resolution images acquired during the considered period. From these images, we can identify the following key features clearly:

LUC: land-use change, most of them being IPG converted in urban areas, orchards or abandoned and vice versa

EXPL: some plots have been levelled and resown, the algorithm can fail to classify such plots as IPG, especially during the first year after leveling because there is relatively very low vegetation growth.

MGT: Some plots are very heterogeneous likely due to permanent grazing or irrigation problems such as the insufficient flow of irrigation water or a lack of levelling preventing a homogeneous water supply.

In the other cases, hereafter labelled as ERR, there were no clear features that could explain the classification change during the considered period.

Table 6. Composition of land-use change classes. (The Land-use type sequence corresponds to the five-year succession G and N corresponding to the IPG and NIG classes, respectively).

Case ID	Land-use type	Sources of variations	Number of plots >1 ha
Consistent classification through the 5 years			
1	G G G G G		3156
2	N N N N N		6623
Plots presenting one land-use change through the 5 years			
3	G G G G N	MGT (60); ERR (15)	75
4	G G G N N	MGT (34); LUC (15); EXPL (10)	59
5	G G N N N	MGT(40); LUC (40); EXPL (20);	100
6	G N N N N	MGT (21); EXPL (6); LUC (10)	37
7	N G G G G	MGT (139); EXPL (14); ERR (32)	185
8	N N G G G	MGT (27); LUC (7); EXPL(11); ERR (5)	50
9	N N N G G	MGT (20); ERR (5); LUC(6)	31
10	N N N N G	MGT (47); LUC (20); EXPL (3)	70
Plots presenting ≥ 2 land-use changes through the 5 years			
11	G N G N G	MGT(65); EXPL (25); ERR (10)	100
12	All plots		331

G=grassland; N=non-grassland.

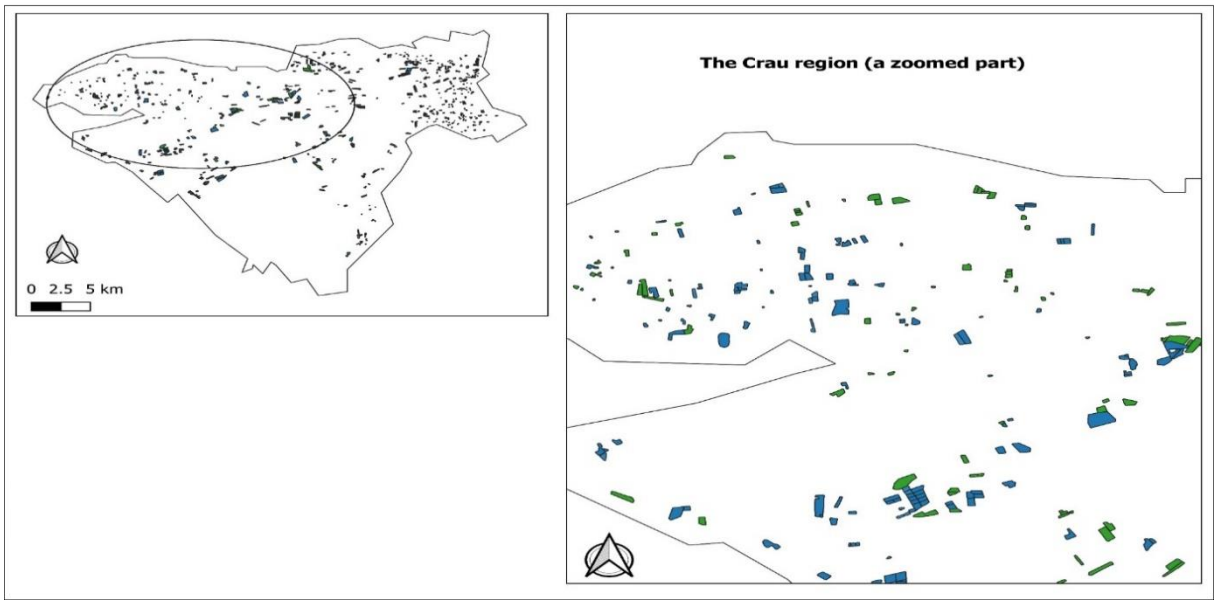

Figure 12. Landuse change map 2016-2020 showing changes from IPG to NIG (green) and NIG to IPG (blue) with a zoomed part.

Analysis of the data in Table 6 shows that over the 5 years, 607 (6%) plots presented one change in classification while 331 (3%) plots had at least two changes. The analysis of the high-resolution images on plots with time series presenting at least one change shows that when a plot is detected as an IPG it is always an IPG. On the 707 plots controlled, only one case corresponding to a young grassed orchard generated an error. This confirms the reliability of the algorithm when an IPG is detected as shown in table 4 with a producer accuracy close to 100%. Among plots with at least one year classified as IPG (class Id 1, 3-11 in Table 6), 19% have discontinuous NIG-IPG series over the 5 years. These plots are mostly related to heterogeneity problems (MGT) (in 66% of the cases) while in 27% of the cases, a real change in use (LUC) or a plot levelling (EXPL) was observed. If we consider the cases where the change is confirmed over the last 2 or 3 years (Case ID 4,5,8,9), the cumulative rate of LUC and EXPL features increased to 50%.

This leads us to conclude that the use of long series (5 years) allows us to characterise the IPGs even when they present strong heterogeneities linked to irrigation defects or grazing during the summer period. The occurrence of IPG detection could be a marker of grassland management and might be used as information to refine the description of grassland systems. Detection of real land-use change needs confirmation of the change over several years (> 3 years), which requires time series longer than 5 years to reduce the ambiguity between actual land-use change and classification errors induced by grassland management.

4.3 Novel aspects and generalization

Our study shows that a classification based on temporal signal with agronomic trait detection offers much better results than a supervised classification such as the use of the SVM method. This superiority is probably exacerbated with the detection of intensively farmed grasslands. Indeed, with grasslands, there is no strong seasonality in vegetation variation. Vegetation cycles are numerous and asynchronous between IPG plots making the identification of a specific grassland pattern in the data series across the whole Crau area difficult by a simple supervised classification algorithm like SVM. This comparison is

somewhat contradicted by the very good results obtained by THEIA, which also used a supervised random forest classification. However, the a priori knowledge on the territory integrated in the classification can have a very important weight in the obtained performances and it would be interesting to analyse the impact of remotely sensed classifiers on the results. If classification approaches based on agronomic traits detection are efficient, they remain specific to a given class of land use and are not adapted to simultaneously identify a large number of classes as could be done by usual classification methods. Thus, a complementarity between methods might be foreseen, approaches based on the temporal signal being dedicated to answering some specific questions requiring a good accuracy on a given land use class as for IPG in the Crau area.

The advantage of our method is that it does not require supervised learning even if some calibration was required on a few plots. The question is then to establish to which extent our approach is generic and implementable in other contexts. First, we found that a single set of parameters was suitable for the five years. Analysis of the classification errors has shown that classification errors come more from ground problems (plot heterogeneity, management variability) and the timing of the LAI time series than the detection algorithms itself. Thus, we can reasonably support the idea that calibrated algorithms can be applied to any year. The implementation of the development method to other territories needs to be examined more carefully. Most of the parameters (10 over 16) were prescribed either from agronomic knowledge (*dta1, dtb1, dta, dtb, tminlai0, tminlai1, dtmin0, dtmin1, tlailow*) or on visual analysis on some problematic LAI time series (*difmax*). We think that these parameters can be adapted to other contexts. As far as the calibrated parameters are concerned, they have to be considered individually. *nbb* and *fd* are related to the temporal frequency of the images. It is conceivable that in a cloudier context, they may have to be revisited. *threshlai* and *tlaimin* are related to the temporal dynamics of the LAI of grasslands, which is influenced by the plot management and the soil and climate conditions. But with a good knowledge of the grasslands of the targeted territory, it should be possible to give an estimation for both parameters. This was the case in our study with *tlaimin* whose values were explored over a narrow range (from 4.0 to 4.5). The filtering of outliers with *tlaimax* seems to us to have a generic scope while the *pixperc* parameter could be the most impacted by new contexts with different intra-plot heterogeneities. In conclusion, we think that adaptations of the parameters based on the knowledge of the territorial characteristics of the grasslands should allow good accuracy. A calibration will undoubtedly be necessary to obtain the precision levels obtained in our study but this must be done only once for all years.

Several algorithms, comparable to the one above, have recently been published [23, 24, 26, 27]. While the approaches used are similar, the solutions for filtering the signal from atmospheric remaining effects and detecting drops in the time series of vegetation indices are very different. It is however difficult to compare our results with those of these studies since in our work we are interested in the identification of grasslands whereas in the other studies, it is the number of mowing events that is sought. In all cases, the timing of the time series and the diversity of the grasslands due to their management or heterogeneity lead to detection errors. In spite of the good scores obtained in our classifications, we had mowing detection errors which did not necessarily led to a classification error, since the observation of two events is sufficient to classify the IPG even though they are mowed three or four times a year. We can also point out that the complexity of the mowing detection algorithms is largely due to anomalies in the temporal series of the vegetation index. This could be simplified if the data

were better filtered upstream and there is no doubt that this will be possible in the future. In this sense the approach in [27] to improve cloud masks is interesting.

5. Conclusions

A new algorithm for the identification of Irrigated Permanent Grass (IPG) was developed in this study. It is based on the detection of agronomic traits thanks to the possibility offered by the Sentinel 2 mission to provide frequent images of the vegetation development. In our area located in the Mediterranean about 40 images per year can be exploited during the period of interest (mid-April to October ending). IPGs were classified by detecting mowing events assuming that a pixel is an IPG when at least two mowing events were detected. The developed classification method offers very good results, better than that obtained when using supervised classification as SVM or land use product as the THEIA product covering the French territory. The method presents the advantage of not depending on training samples, even if some calibration was necessary to fix some thresholds and deal with the remote sensing signal noise. We believe that calibration effort will likely be lower when addressing IPG detection in other geographical contexts. Moreover, once established the algorithm can be applied directly to another year.

Despite the good performance of the developed algorithm, it is faced with some constraints that lead to failure to detect mowing activities. For instance, when there is relatively very low biomass or a heterogeneous plot, the developed algorithm tends to fail by missing some mowing events. This can be seen as a weakness, but our analysis has shown that the IPG class covers several management modalities. Depending on the objectives, such a weakness can be a strength to characterize different production systems. In addition, the detection of mowing should make it possible to understand the technical itineraries and to provide information to inform the farming practice heterogeneities over large territory to implement crop models. Real changes in use can be observed, but long time series are needed to confirm the change and remove ambiguities with heterogeneous grasslands.

In general, one can question the relevance of relying on agronomic traits specific to certain types of land use to map them. In this work, we have relied on a clear, specific, and somewhat caricatural trait and this has allowed excellent results. The results in the literature are not necessarily as precise, probably due to less clear specific features that can lead to ambiguities. We believe, for example, that the separation of vineyards and orchards, which is important to map different irrigation strategies, may be more difficult to characterize. Moreover, it was found that the method requires frequent acquisition to catch the events of interest. For locations with frequent cloud cover, combining optic and radar images can be an option to overcome the lack of optical data.

Acknowledgments

This work was funded by the Petroleum Technology Development Fund (PTDF) under the Federal Ministry of Petroleum, Nigeria, in collaboration with INRAE-EMMAH Avignon as part of a PhD research program.

The authors would like to thank the reviewers for helping us improve the quality of this research work, all suggestions and observations were taken into consideration and highly appreciated.

Conflicts of Interest: The authors declare no conflict of interest.

References

(1) *International Decade for Action on Water for Sustainable Development, **2016**, 2018-2028*. https://www.un.org/en/events/waterdecade/background.shtml (accessed 2022-04-14).

(2) Wriedt, G.; Van der Velde, M.; Aloe, A.; Bouraoui, F. Estimating Irrigation Water Requirements in Europe. *Journal of Hydrology* **2009**, *373* (3), 527–544. https://doi.org/10.1016/j.jhydrol.2009.05.018.

(3) Wada, Y.; Wisser, D.; Eisner, S.; Flörke, M.; Gerten, D.; Haddeland, I.; Hanasaki, N.; Masaki, Y.; Portmann, F. T.; Stacke, T.; Tessler, Z.; Schewe, J. Multimodel Projections and Uncertainties of Irrigation Water Demand under Climate Change. *Geophysical Research Letters* **2013**, *40* (17), 4626–4632. https://doi.org/10.1002/grl.50686.

(4) Marras, P. A.; Lima, D. C. A.; Soares, P. M. M.; Cardoso, R. M.; Medas, D.; Dore, E.; De Giudici, G. Future Precipitation in a Mediterranean Island and Streamflow Changes for a Small Basin Using EURO-CORDEX Regional Climate Simulations and the SWAT Model. *Journal of Hydrology* **2021**, *603*, 127025. https://doi.org/10.1016/j.jhydrol.2021.127025.

(5) Bazzi, H.; Baghdadi, N.; Ienco, D.; El Hajj, M.; Zribi, M.; Belhouchette, H.; Jose Escorihuela, M.; Demarez, V. Mapping Irrigated Areas Using Sentinel-1 Time Series in Catalonia, Spain. *Remote Sens.* **2019**, *11* (15), 1836. https://doi.org/10.3390/rs11151836.

(6) Gao, Q.; Zribi, M.; Escorihuela, M.; Baghdadi, N.; Segui, P. Irrigation Mapping Using Sentinel-1 Time Series at Field Scale. *Remote Sensing* **2018**, *10* (9), 1495. https://doi.org/10.3390/rs10091495.

(7) Ambika, A. K.; Wardlow, B.; Mishra, V. Remotely Sensed High Resolution Irrigated Area Mapping in India for 2000 to 2015. *Sci. Data* **2016**, *3*, 160118. https://doi.org/10.1038/sdata.2016.118.

(8) Massari, C.; Modanesi, S.; Dari, J.; Gruber, A.; De Lannoy, G. J. M.; Girotto, M.; Quintana-Segui, P.; Le Page, M.; Jarlan, L.; Zribi, M.; Ouaadi, N.; Vreugdenhil, M.; Zappa, L.; Dorigo, W.; Wagner, W.; Brombacher, J.; Pelgrum, H.; Jaquot, P.; Freeman, V.; Volden, E.; Prieto, D. F.; Tarpanelli, A.; Barbetta, S.; Brocca, L. A Review of Irrigation Information Retrievals from Space and Their Utility for Users. *Remote Sens.* **2021**, *13* (20), 4112. https://doi.org/10.3390/rs13204112.

(9) Ozdogan, M.; Gutman, G. A New Methodology to Map Irrigated Areas Using Multi-Temporal MODIS and Ancillary Data: An Application Example in the Continental US. *Remote Sensing of Environment* **2008**, *112* (9), 3520–3537. https://doi.org/10.1016/j.rse.2008.04.010.

(10) Deines, J. M.; Kendall, A. D.; Hyndman, D. W. Annual Irrigation Dynamics in the US Northern High Plains Derived from Landsat Satellite Data. *Geophys. Res. Lett.* **2017**, *44* (18), 9350–9360. https://doi.org/10.1002/2017GL074071.

(11) Maselli, F.; Battista, P.; Chiesi, M.; Rapi, B.; Angeli, L.; Fibbi, L.; Magno, R.; Gozzini, B. Use of Sentinel-2 MSI Data to Monitor Crop Irrigation in Mediterranean Areas. *International Journal of Applied Earth Observation and Geoinformation* **2020**, *93*, 102216. https://doi.org/10.1016/j.jag.2020.102216.

(12) Pun, M.; Mutiibwa, D.; Li, R. Land Use Classification: A Surface Energy Balance and Vegetation Index Application to Map and Monitor Irrigated Lands. *Remote Sensing* **2017**, *9* (12), 1256. https://doi.org/10.3390/rs9121256.

(13) Demarez, V.; Helen, F.; Marais-Sicre, C.; Baup, F. In-Season Mapping of Irrigated Crops Using Landsat 8 and Sentinel-1 Time Series. *Remote Sens.* **2019**, *11* (2), 118. https://doi.org/10.3390/rs11020118.

(14) Pageot, Y.; Baup, F.; Inglada, J.; Baghdadi, N.; Demarez, V. Detection of Irrigated and Rainfed Crops in Temperate Areas Using Sentinel-1 and Sentinel-2 Time Series. *Remote Sens.* **2020**, *12* (18), 3044. https://doi.org/10.3390/rs12183044.

(15) Julien, Y.; Sobrino, J. A.; Jiménez-Muñoz, J.-C. Land Use Classification from Multitemporal Landsat Imagery Using the Yearly Land Cover Dynamics (YLCD) Method. *International Journal*

of Applied Earth Observation and Geoinformation **2011**, *13* (5), 711–720. https://doi.org/10.1016/j.jag.2011.05.008.

(16) Karantzalos, K.; Karmas, A.; Tzotsos, A. Monitoring Crop Growth and Key Agronomic Parameters through Multitemporal Observations and Time Series Analysis from Remote Sensing Big Data. *Advances in Animal Biosciences* **2017**, *8* (2), 394–399. https://doi.org/10.1017/S2040470017001261.

(17) Ashourloo, D.; Shahrabi, H. S.; Azadbakht, M.; Aghighi, H.; Nematollahi, H.; Alimohammadi, A.; Matkan, A. A. Automatic Canola Mapping Using Time Series of Sentinel 2 Images. *ISPRS Journal of Photogrammetry and Remote Sensing* **2019**, *156*, 63–76. https://doi.org/10.1016/j.isprsjprs.2019.08.007.

(18) Ashourloo, D.; Shahrabi, H. S.; Azadbakht, M.; Rad, A. M.; Aghighi, H.; Radiom, S. A Novel Method for Automatic Potato Mapping Using Time Series of Sentinel-2 Images. *Computers and Electronics in Agriculture* **2020**, *175*, 105583. https://doi.org/10.1016/j.compag.2020.105583.

(19) Merot, A.; Bergez, J.-E.; Capillon, A.; Wery, J. Analysing Farming Practices to Develop a Numerical, Operational Model of Farmers' Decision-Making Processes: An Irrigated Hay Cropping System in France. *Agricultural Systems* **2008**, *98* (2), 108–118. https://doi.org/10.1016/j.agsy.2008.05.001.

(20) Dusseux, P.; Vertes, F.; Corpetti, T.; Corgne, S.; Hubert-Moy, L. Agricultural Practices in Grasslands Detected by Spatial Remote Sensing. *Environ. Monit. Assess.* **2014**, *186* (12), 8249–8265. https://doi.org/10.1007/s10661-014-4001-5.

(21) Gómez Giménez, M.; de Jong, R.; Della Peruta, R.; Keller, A.; Schaepman, M. E. Determination of Grassland Use Intensity Based on Multi-Temporal Remote Sensing Data and Ecological Indicators. *Remote Sensing of Environment* **2017**, *198*, 126–139. https://doi.org/10.1016/j.rse.2017.06.003.

(22) Stumpf, F.; Schneider, M. K.; Keller, A.; Mayr, A.; Rentschler, T.; Meuli, R. G.; Schaepman, M.; Liebisch, F. Spatial Monitoring of Grassland Management Using Multi-Temporal Satellite Imagery. *Ecol. Indic.* **2020**, *113*, 106201. https://doi.org/10.1016/j.ecolind.2020.106201.

(23) Courault, D.; Hadria, R.; Ruget, F.; Olioso, A.; Duchemin, B.; Hagolle, O.; Dedieu, G. Combined Use of FORMOSAT-2 Images with a Crop Model for Biomass and Water Monitoring of Permanent Grassland in Mediterranean Region. *Hydrology and Earth System Sciences* **2010**, *14* (9), 1731–1744. https://doi.org/10.5194/hess-14-1731-2010.

(24) Schwieder, M.; Wesemeyer, M.; Frantz, D.; Pfoch, K.; Erasmi, S.; Pickert, J.; Nendel, C.; Hostert, P. Mapping Grassland Mowing Events across Germany Based on Combined Sentinel-2 and Landsat 8 Time Series. *Remote Sensing of Environment* **2022**, *269*, 112795. https://doi.org/10.1016/j.rse.2021.112795.

(25) Lobert, F.; Holtgrave, A.-K.; Schwieder, M.; Pause, M.; Vogt, J.; Gocht, A.; Erasmi, S. Mowing Event Detection in Permanent Grasslands: Systematic Evaluation of Input Features from Sentinel-1, Sentinel-2, and Landsat 8 Time Series. *Remote Sens. Environ.* **2021**, *267*, 112751. https://doi.org/10.1016/j.rse.2021.112751.

(26) Andreatta, D.; Gianelle, D.; Scotton, M.; Vescovo, L.; Dalponte, M. Detection of Grassland Mowing Frequency Using Time Series of Vegetation Indices from Sentinel-2 Imagery. *GIScience & Remote Sensing* **2022**, *59* (1), 481–500. https://doi.org/10.1080/15481603.2022.2036055.

(27) Kolecka, N.; Ginzler, C.; Pazur, R.; Price, B.; Verburg, P. H. Regional Scale Mapping of Grassland Mowing Frequency with Sentinel-2 Time Series. *Remote Sens.* **2018**, *10* (8), 1221. https://doi.org/10.3390/rs10081221.

(28) Taravat, A.; Wagner, M.; Oppelt, N. Automatic Grassland Cutting Status Detection in the Context of Spatiotemporal Sentinel-1 Imagery Analysis and Artificial Neural Networks. *Remote Sensing* **2019**, *11* (6), 711. https://doi.org/10.3390/rs11060711.

(29) De Vroey, M.; Radoux, J.; Defourny, P. Grassland Mowing Detection Using Sentinel-1 Time Series: Potential and Limitations. *Remote Sens.* **2021**, *13* (3), 348. https://doi.org/10.3390/rs13030348.

(30) Séraphin, P.; Vallet-Coulomb, C.; Gonçalvès, J. Partitioning Groundwater Recharge between Rainfall Infiltration and Irrigation Return Flow Using Stable Isotopes: The Crau Aquifer. *Journal of Hydrology* **2016**, *542*, 241–253. https://doi.org/10.1016/j.jhydrol.2016.09.005.

(31) Trolard, F.; Bourrié, G.; Baillieux, A.; Buis, S.; Chanzy, A.; Clastre, P.; Closet, J.-F.; Courault, D.; Dangeard, M.-L.; Di Virgilio, N.; Dussouilliez, P.; Fleury, J.; Gasc, J.; Géniaux, G.; Jouan, R.; Keller, C.; Lecharpentier, P.; Lecroart, J.; Napoleone, C.; Mohammed, G.; Olioso, A.; Reynders, S.; Rossi, F.; Tennant, M.; de Vicente Lopez, J. The PRECOS Framework: Measuring the Impacts of the Global Changes on Soils, Water, Agriculture on Territories to Better Anticipate the Future. *Journal of Environmental Management* **2016**, *181*, 590–601. https://doi.org/10.1016/j.jenvman.2016.07.002.

(32) Weiss, M.; Baret, F.; Leroy, M.; Hautecoeur, O.; Bacour, C.; Prevot, L.; Bruguier, N. Validation of Neural Net Techniques to Estimate Canopy Biophysical Variables from Remote Sensing Data. *Agronomie* **2002**, *22* (6), 547–553. https://doi.org/10.1051/agro:2002036.

(33) Tian, J.; Zhu, X.; Chen, J.; Wang, C.; Shen, M.; Yang, W.; Tan, X.; Xu, S.; Li, Z. Improving the Accuracy of Spring Phenology Detection by Optimally Smoothing Satellite Vegetation Index Time Series Based on Local Cloud Frequency. *ISPRS Journal of Photogrammetry and Remote Sensing* **2021**, *180*, 29–44. https://doi.org/10.1016/j.isprsjprs.2021.08.003.

(34) Hastie, T. J, and Tibshirani R. J. *Generalized additive models*. Chapman and Hall/CRC, **1990**, ISBN 978-0-412-34390-2.

(35) Congalton, R. G. Accuracy Assessment and Validation of Remotely Sensed and Other Spatial Information. *International Journal of Wildland Fire* **2001**, *10* (3–4), 321–328. https://doi.org/10.1071/WF01031.

(36) Inglada, J.; Vincent, A.; Arias, M.; Tardy, B.; Morin, D.; Rodes, I. Operational High Resolution Land Cover Map Production at the Country Scale Using Satellite Image Time Series. *Remote Sens.* **2017**, *9* (1), 95. https://doi.org/10.3390/rs9010095.

Chapter 4

Delineation of orchard, vineyard, and olive trees based on phenology metrics derived from time series of Sentinel-2

4.1 Intention note

Water management is a critical issue in areas under irrigation. To supervise plant water needs across vast terrains, an interesting tool is remote sensing which can provide useful information on land cover and crop development (Tucker, 1979).

Irrigated perennial woody fruit trees are among the major water users in Southern France and there is a need to accurately identify these crop types. However, the delineation of irrigated woody fruit trees remains difficult because of their structural heterogeneity. At the regional scale, a large spatial variability is observed due to different management practices (inter-row with grass or bare soil, different irrigation techniques…)The limitation of mapping orchards from remote sensing is also due to the difficulties in separating different fruit trees or species (Usha and Singh, 2013). Approaches based on the analysis of specific temporal patterns generated from satellite image time series (SITS) appear as interesting methods to classify heterogeneous crops (Masialeti et al., 2010; Odenweller and Johnson, 1984; Pena et al., 2017; M.A. Peña and Brenning, 2015).

Some key phenological traits such as the start of the season (start of greenness), length of the season (peak of greenness), end of the season (senescence), etc. can be identified when exploiting multi-temporal time series to aid in accurate delineations. This work has used a classification based on phenology metrics (PMs) derived from the Sentinel-2 time series to separate orchards, vineyards, and olive trees. A large dataset from the ground survey is used as a reference to calibrate and validate the method. The method was applied on two different sites in South-Eastern France. Overall accuracies ranged from 89-96% and Kappa of 0.86-0.95 (2016-2021), respectively. This method gave higher performances than standard supervised classifications based on the use of a learning data set with random forest algorithms.

Résumé

La télédétection est un outil largement utilisé pour cartographier les cultures. De nombreuses études sont basées sur des méthodes de classifications supervisées qui requièrent des bases de données de référence qui sont parfois coûteuses à acquérir sur le terrain. L'identification des couverts tels que les vignes, vergers et oliviers reste toujours un challenge car l'hétérogénéité de ces cultures conduit à un signal spectral et temporel complexe à analyser. Par ailleurs ces cultures présentent une grande variabilité de pratiques agricoles (inter-rang enherbé ou non, différents types d'irrigation…) ce qui conduit à des signaux radiométriques mélangeant les contributions de la canopée et du sol. Des approches basées sur l'analyse de séries temporelles présentent l'avantage de limiter l'acquisition de données de références pour cartographier les

cultures. Ce chapitre porte sur le développement d'une méthode de classification basée sur des grandeurs phénologiques (PM) dérivées de la série temporelle Sentinel-2 pour distinguer les vignes, vergers et oliviers. La méthode a été appliquée sur deux sites agricoles différents dans le Sud-Est- de la France, la Crau et le bassin de l'Ouvèze. Les PM ont été calculées en ajustant un modèle logistique double sur les profils temporels des indices de végétation. Les PM générés ont ensuite été introduits dans un algorithme de classification de type random forest (forêt aléatoire (RF)). En comparant différents indices de végétation, les résultats ont montré que l'indice de surface foliaire (LAI) avait le score le plus élevé pour distinguer les vergers des vignes. Pour délimiter la classe des oliviers, L'usage d'un autre indice basé sur le ratio des bandes verte et proche infrarouge (GCVI) indice de végétation de la chlorophylle verte (s'est plus avéré plus performant pour identifier les classes visées. Les précisions globales obtenues varient de 89 à 96 % avec des valeurs pour l'indice Kappa de 0,86-0,95 (2016-2021), respectivement. Ces précisions sont nettement supérieures aux précisions obtenues lorsque l'on applique une classification de type RF en considérant toutes les valeurs de LAI (Kappa compris entre 0,3 et 0,52). Ces résultats montrent l'intérêt d'utiliser les traits phénologiques plutôt que les séries temporelles brutes des données de télédétection. La méthode peut être bien reproduite chaque année sans requérir de données supplémentaires.

Mots-clés : classification des cultures ligneuses ; Sentinel-2 ; phénologie des cultures ; olivier ; verger ; vignobles ; Méditerranée.

4.2 Graphical Abstract

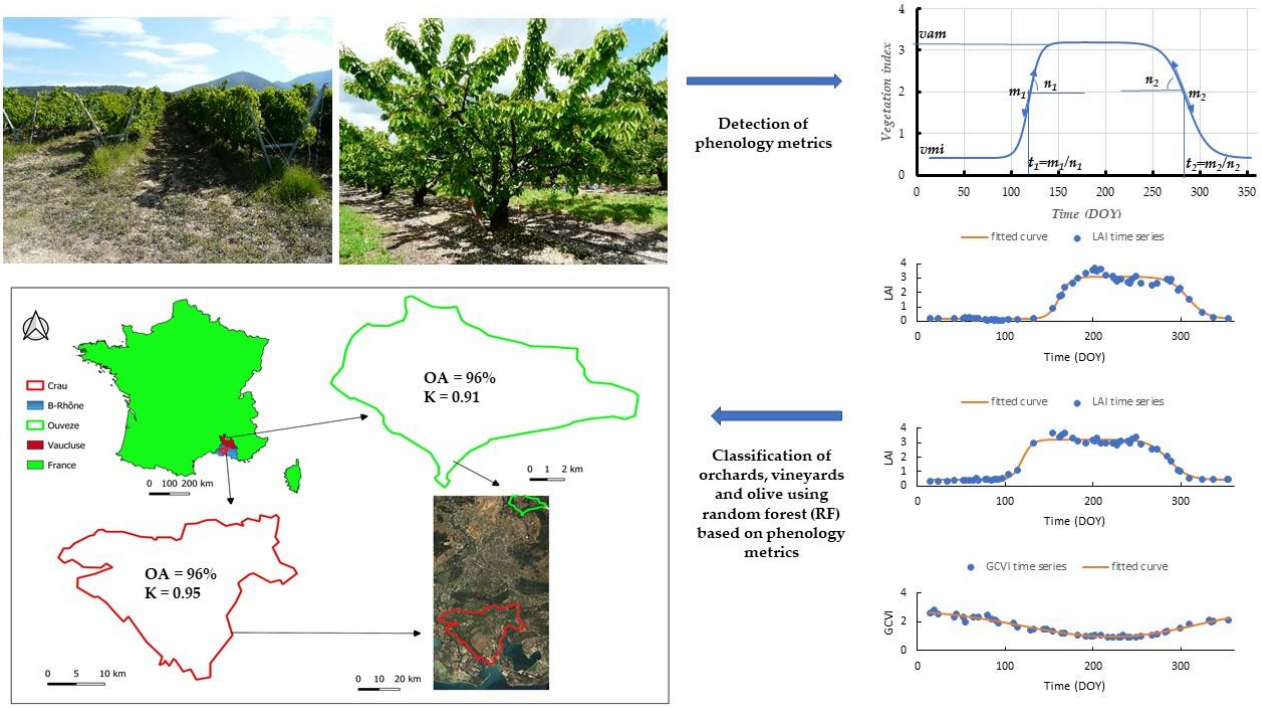

Delineation of Orchard, Vineyard, and Olive Trees Based on Phenology Metrics derived from Time-Series of Sentinel-2

Mukhtar Adamu Abubakar [1,2], André Chanzy [1,*], Fabrice Flamain, Guillaume Pouget, and Dominique Courault[1]

[1] 1114 UMR INRAE-Avignon University EMMAH, Domaine St. Paul, 84914, Avignon, France; mukhtar.abubakar@inrae.fr (M.A.A); fabrice.flamain@inrae.fr (F.F); guillaume.pouget@inrae.fr (G.P); domonique.courault@inrae.fr (D.C)

[2] Agronomy Department, Faculty of Agriculture, Shabu-Lafia Campus, Nasarawa State University, Keffi 961101, Nigeria. dattijoh@nsuk.edu.ng (M.A.A)

Affiliation 1; mukhtar.abubakar@inrae.fr
[2] Affiliation 2; dattijoh@nsuk.edu.ng
* Correspondence: andre.chanzy@inrae.fr

Citation: Abubakar, M.A.; Chanzy, A.; Flamain, F.; Pouget, G.; Courault, D. Delineation of Orchard, Vineyard, and Olive Trees Based on Phenology Metrics Derived from Time Series of Sentinel-2. Remote Sens. 2023, 15, 2420. https://doi.org/10.3390/rs15092420.

Academic Editor: Jinyang Du, Lingmei Jiang, Tianjie Zhao, Shengli Wu and Kebiao Mao

Received date: 27 March 2023
Revised date: 2 May 2023
Accepted date: 3 May 2023
Published date: 5 May 2023

Abstract: This study aimed to propose an accurate, and cost-effective analytical approach for the delineation of fruit trees of orchards, vineyards, and olives in Southern France considering two locations. A classification based on phenology metrics (PM) derived from the Sentinel-2 time series was developed to perform the classification. The PM were computed by fitting a double logistic model on temporal profiles of vegetation indices to delineate orchard and vineyard classes. The generated PM were introduced in a random forest (RF) algorithm for classification. The method was tested on different vegetation indices, the best results being obtained with the leaf area index. To delineate the olive class, the temporal features of the green chlorophyll vegetation index were found to be the most appropriate. Obtained overall accuracies ranged from 89-96% and Kappa of 0.86-0.95 (2016-2021), respectively. These accuracies are much better than applying the RF algorithm on the LAI times series, which led to a Kappa ranging between 0.3 and 0.52 and demonstrates the interest of using phenological traits rather than the raw time series of the remote sensing data. The method can be well reproduced from one year to another. This is an interesting feature to reduce the burden of collecting ground truth information. If the method is generic it needs to be calibrated in given areas as soon as a phenology shift is expected.

Keywords: woody crop classification; Sentinel-2; random forest; crop phenology; olive, orchard, vineyards; Mediterranean.

1. Introduction

Among the several hazards of climate change and global warming on natural resources, the most significant threat is its implication on the accessible availability of freshwater. Unequivocally, the agricultural sector is the highest consumer of water universally with irrigation accounting for about 70% of freshwater withdrawals [1–3]. Thus, supervision of irrigation activities is crucial to buttress the execution of water management policies and to improve water use productivity [4,5]. Supervision of irrigation activities not only encompasses spatial assessments of areas under irrigation but also irrigation strategies [4–7], which differ between crop systems [8]. Therefore, mapping the different irrigated crops is an important issue in water management, particularly in the Mediterranean region which is sensitive to variations in agricultural activities and land use due to its exposure to excessive climatic threats [9]. Irrigation patterns and water quantity depend on crop type and associated irrigation methods for instance flooding irrigation applied to grassland, which mobilizes a great quantity of water while drip irrigation applied in horticultural production leads to frequent water supplies but with much less water. If numerous works address irrigated crop delineation less attention has been paid to the delineation of perennial woody crops such as fruit trees of orchards, vineyards, and olive groves that are common in the Mediterranean.

Crop classification from remote sensing data is a field that has been widely studied for decades and is gaining interest with new satellite missions such as the Sentinel missions that have considerably improved temporal resolution and spectral richness. Progress in the identification of grasslands and field crops is undeniable [9–11]. On the other hand, the case of woody perennial crops such as fruit orchards, vineyards, or olive groves might pose more problems and progress is still possible. The difficulty comes mainly from the fact that these covers have a great diversity of development because of the age of the plantation, their density, the mode of management such as pruning, and the confusion that there can be with other plant covers (non-irrigated meadows, wetlands...).

Concerning woody crops, high-resolution Landsat TM images were used to identify crop classes (olive and citrus) in Marrakech, Morocco using the temporal profile of normalized difference vegetation index (NDVI) simply by setting a threshold of maximum and minimum values of the NDVI across the season [12] leading to an overall accuracy (OA) of 83%. Peña et al. [13] classified fruit trees by comparing Landsat 8 image times series considering the full band, the normalized difference water index (NDWI), and the normalized difference vegetation index (NDVI). The best results were obtained using the full spectral information, in particular with visible and SWIRS bands (OA = 94%). while the NDVI led to the worst results. They tested the interest of dates and highlighted that the beginning (greenness) and end (senescence) of the growing cycle were the most significant phases for the separation. They obtained an OA of 94% with four dates. The interest in image acquisition during the greenness period was confirmed in [14]. In this study, it was demonstrated that up to seven types of orchards can be classified by considering all Landsat 8 spectral bands as well as a combination of bands. Recently tree fruits crop type mapping was conducted in Egypt by examining

various temporal windows, spectral approaches, and several combination methods between S1 (Sentinel-1) and S2 (Sentinel-2) data inserted into RF [15]. Good accuracy was found with S2 alone while improvement was found by combining the textural S1 information with the spectral S2 observations, which led to an OA of 96%. In [16] a classification was done to delineate apple orchards, vineyards, and annual crops in Iran. Phenology was used to select the optimal dates. By combining S1, Landsat 8 images, and the digital elevation model, an OA of 89% was obtained. Another recent study was conducted in Juybar, Iran where an automatic approach to map citrus orchards was implemented using S1 and S2 and the ALOS digital surface model (DSM) [17]. Without training and by considering a very large number of images (148), textural, and spectral features, it was possible to separate citrus and non-citrus surfaces with an OA of 99.7%. The approach is a very favorable case with evergreen trees (citrus), which presents a contrast with the other surfaces. These studies have shown that good results can be obtained with perennial woody crop mapping. The quality of the results obtained came from the number of images used, the choice of the dates considered, and the complementarity between spectral indices in the optical domain and textural indices derived from SAR images. The quality of the classifications also came from the specificity of the signatures of the various covers. In this respect, the phenology makes it possible to target the dates of observation to be considered in particular during the phases of greenness and senescence. In past studies, phenology is not used directly as a classification criterion but more to determine optimal dates. The use of phenological traits may present advantages in the exploitation of time series by the fact that they are relatively independent of the dates of acquisition. This can be interesting in a situation where partial cloud cover is frequent in the temperate zone, and can disturb the homogeneity of the time series from one point to another in the area to be mapped. This can considerably disturb the learning algorithms.

Conventional crop phenology also termed ground phenology (GP) [18] is the particular re-occurring events of crop life traits like budburst, leaf development, senescence, flowering, and maturity [19], which is laborious to collect, time-consuming and expensive as well [18,20]. These GP observations correlate to key particular plant physiological activities that govern natural resource uptake by plants. Despite GP remaining objective and precise, its characterization over a wide-scale area remains a challenge [21]. Satellite remote sensing is capable of offering time series on vegetation development with a short revisit period, which can serve as a source of data to monitor vegetation phenology at a local and regional scale with proxies termed land surface phenology (LSP) [22]. Phenology metrics (PM) obtained from the analysis of vegetation indices time series were often used to characterize the LSP [23–25]. In the past, most of the studies related to crop phenology were done using medium-resolution sensors (MODIS, AVHRR) allowing frequent acquisition over the whole globe [18]. The spatiotemporal resolution was enhanced by combining those medium-resolution sensors, with high-resolution (LANDSAT) [26,27]. Most research on LSP carried out using information from these satellite sensors is faced with a drawback of mixed pixels and thus, restricted in their implementation across complex or fragmented terrains [28]. Such a drawback can be now overcome by using S2, which allows accurate supervision of crop changes [29]. PM are linked to the variation of the seasonal pattern in cropland surfaces derived from satellite observations [30]. The most common patterns are the start of the season (SOS), the peak of the growing season (POS), the end of the season corresponding to the senescence (EOS), and the length of

the season (LOS) [30,31]. In other terms, in a growing year season, the major phases of phenology controlling the spectral patterns of vegetation are (i) the date of photosynthetic commencement (green-up), (ii) the date of maximum plant green leaf (maturity), (iii) the date of decline in photosynthetic activities (senescence) [32]. The mentioned PM are normally computed from the common normalized difference vegetation index (NDVI) or other popular indices for instance [31,33]. But despite that, the NDVI method can bring some drawbacks, like restricted sensitivity to vegetation photosynthetic dynamics [34] while biophysical variables like LAI (leaf area index) can improve the PM, particularly for farmlands. The use of phenology as a classifier for crop mapping has been applied in many studies. In [35] PM (SOS, EOS, LOS, and the peak integral reflecting the photosynthetic activity) were derived from MODIS NDVI time series using the TIMESAT algorithm [36] and used to characterize different agricultural systems (fallow, rainfed crop, irrigated crop and irrigated perennial). It was shown that the PM were able to monitor agricultural system evolution across two decades 2000-2019 with an OA ranging from 93% and 97%. In that case, irrigated perennials were evergreen orchards (citrus) which makes the distinction with annual crops easier. According to [37], they developed a phenology-based approach to delineate wheat and barley by identifying the heading date using temporal feature of the different S2 bands. Good results were obtained (OA of 76%) across three sites in Iran, and the USA (North California and Idaho). These studies, among others, have shown that the PM can be used as a classifier to map crops. The quality of the results depends very much on the specificity of the temporal signatures of the different crops to be identified and the diversity of plant cover that can be found in a given class. Moreover, the added value of using PM rather than time series of spectral and/or vegetation index data was not yet demonstrated.

The objective of this study is to characterize the main classes of perennial woody crops, namely fruit orchards (OC), vineyards (VY), and olive groves (OL), which are cropping systems with different irrigation strategies. Within these classes, there is a great diversity of situations marked by the type of cover, pruning practices, or soil management in the inter-row. To address this diversity of situations we intend to rely on phenological traits to identify the crops studied in this work. Such approaches have proven to be successful in the identification of annual crops and we assumed that such approaches could be interesting for perennial woody crops. Indeed, we believe that if the diversity of the characteristics of a type crop due to their management and their ages can lead to variable remote sensing signatures, these crops share the same phenological traits. The study is carried out on two sites about 100 km apart but with different climatic conditions and plant cover other than the desired perennial woody crops. The challenge will be to evaluate the performance of classifications carried out with PM, to analyze their added value in comparison with approaches based on the time series of vegetation index, and to establish the genericity of a classification model from one year to another or from one site to another.

2. Materials and Methods

2.1 Study sites

The study was conducted across two different locations in South-East France namely the Ouveze-Ventoux and the Crau area (Figure 1). These study sites are representative of the Mediterranean with a strong diversity of cropping systems including fruit orchards (cherries plums, peaches apricots), olives, and vineyards.

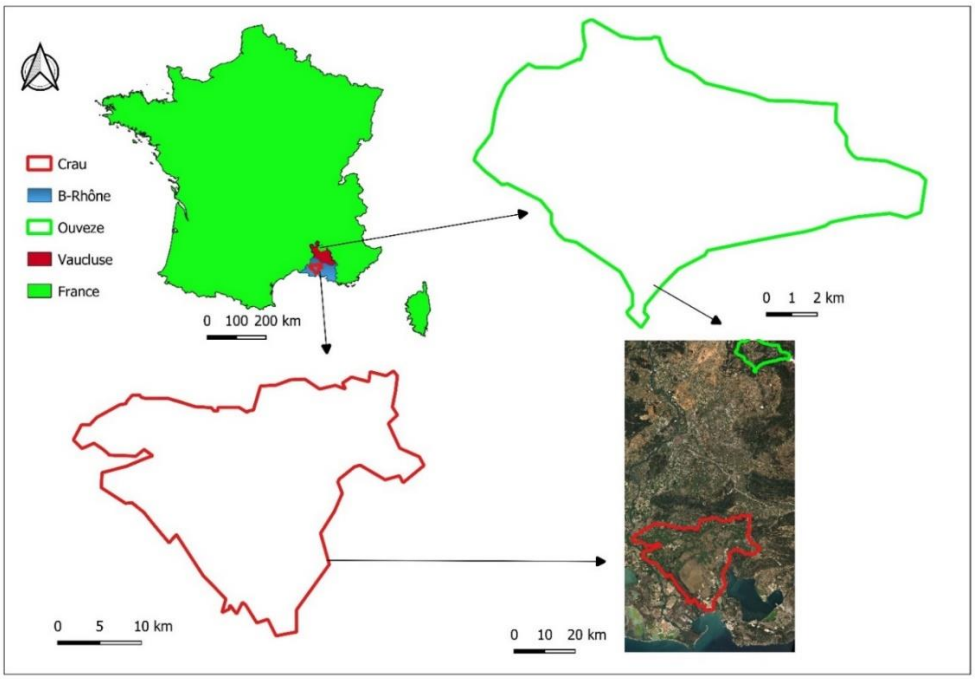

Figure 1. Map of France depicting the two selected study sites (Ouveze-Ventoux and Crau).

The Ouveze-Ventoux is located at 44° 10' N and 5° 16' E (with the lowest and highest elevation of 230 and 630 m a.s.l) in the South France of the Provence region with a surface area of 59 km^2 and forest and semi-natural environments inhabiting about 57.7% [38], associated to specific bioclimatic and geomorphological surroundings. It has the typical Mediterranean climate identified by cold and moist winters and dry and hot summers. Annual precipitation is about 750 mm per year, annual mean temperature of 12.6°C; The number of plots on Ouveze-Ventoux is about 3500 of which OC occupied about 40% (1413), and VY occupied about 34% (1186) of the cultivated area.

The Crau is positioned between 43° 38' N and 5 °00' E (5m a.s.l) close to the Rhône delta in South Eastern France with a surface area of 600 km^2 and a typical Mediterranean climate [10]. The annual average rainfall is 600 mm (non-uniform). Potential evapotranspiration of 1100 mm and mean air temperature of 14.8 °C [9,39,40]. The soils are shallow ranging from 60-80 cm having 90% stones making water retention capacity to be very low. Soils irrigated via flooding methods have a loamy surface soil layer from the constantly deposited sediments leading to a layer depth of about 60 cm depending on the length of the irrigation period [9]. The water used for flooding irrigation contributes to more than 75% of the groundwater table which is used for irrigation of intensive orchards and market garden productions, domestic and industrial purposes to about 280,000 people around the southern part of the area [39,40]. The number of plots in Crau is about 17980 of which OC occupied about 11% (2050), VY occupied about 4% (790) and OL occupied about 5% (1050) of the cultivated area.

2.2. Ground truth information

The collection of ground truth data was conducted in the two study areas during the 2016-2021 period. Plot boundaries were drawn in both sites, starting from the cadastral survey and the RPG (*Régistre Parcellaire Graphique*), which is used for subsidy allocation to farmers. The boundaries were fine-tuned using an aerial picture to isolate homogeneously managed

surfaces. The whole area was therefore segmented with 17980 and 3501 plots in the Crau and Ouveze-Ventoux areas, respectively (but 16680 and 1601 plots were used in this study due to the exclusion of 20 meters from each plot boundary to avoid the effect of mixed pixels at the plot border). A subset of the controlled plot was surveyed and identified, and crop types were taken into note during field visits. In the Ouveze-Ventoux study area, a total of 234 plots (Figure 2) were identified as OC, and other classes (DC), which encompasses field crops, dry grasslands, and greenhouses. In the Crau study area, a total of 243 (out of 18058) plots were selected of which are OC, (35), (60), and DC (60) encompassing greenhouse, dry grass, forest, field crop, irrigated grassland, and wetland. Aerial photographs from IGN (the French national mapping service) and Google Earth images collected during the 2016 to 2021 period were used to understand anomalies found in vegetation time series derived from satellite, principally to assess surface heterogeneity and change in management between field visits. The number of plots in each class is given in Table 1. Fields were split into two groups dedicated to the training and the validation. As there are very few numbers of olive plots, the OL class was not considered in the Ouveze Ventoux site.

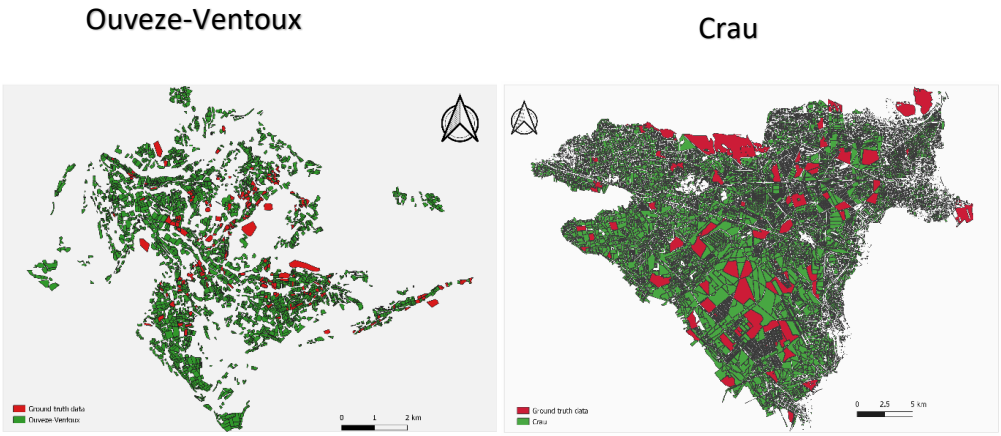

Figure 2. Map of the two study areas displaying locations of the selected ground truth plot.

Table 1. Ground truth information of the two study sites used for model calibration and validation during 2016-2021.

Ouveze Ventoux site		Crau site	
Land use	**Ground data (number of plots)**	**Land use**	**Ground data (number of plots)**
OC	60	OC	88
VY	100	VY	35
OL	-	OL	60
DC	74	DC	60

2.3 Satellite data

In our study, time-series of Sentinel-2 (S2) optical images were utilized and were obtained from both Sentinel-2A and Sentinel-2B of all dates in a given year within the 2016-2021 period considering the visible (B2, B3, and B4), the near-infrared (B8 and mid-infrared (B11 our B12) bands. We utilized the open-source service center to obtain images

(https://www.theia-land.fr/, accessed on 17 May 2022), it offers cloud treatments (cloud mask) to eliminate pixels influenced by clouds (images with > 30% cloud cover), and for this obvious reason, the number of images utilized vary across study sites and years. Since Sentinel-2B satellites were functional in the time of 2017, lesser dates were obtained from the 2016-2017 year. The number of cloud-free images (with <30% cloud cover and subsequently masked) used for each year across the two study sites is reported in Table 2. An additional cloud filtering was added when creating the time series for each plot. The dates for which there was at least one pixel in the considered plot impacted by clouds were removed. This led, for a given site, to have time series with different dates from one plot to another.

Table 2. Number of cloud-free available images across the two study sites used for the classification

S/N	Year	Ouveze-Ventoux	Crau
1	2016	39	43
2	2017	45	49
3	2018	52	55
4	2019	51	56
5	2020	49	52
6	2021	50	51

2.4 Vegetation indices and biophysical variables.

To begin with, various vegetation indices and biophysical variables were utilized for spectral-temporal analysis which was subdivided into those highlighting greenness like the popular normalized difference vegetation index (NDVI), enhanced vegetation index (EVI), green chlorophyll vegetation index (GCVI) to those highlighting moisture like normalized difference moisture index (NDMI), land surface water index (LSWI), and finally on biophysical variables like leaf area index (LAI), fraction vegetation cover (FCOVER) and the fraction of absorbed photosynthetically active radiation (FAPAR) as summarized in Table 3. The biophysical variables used in this study were computed with the BVNET algorithm by utilizing the B2, B3, B4, and B8 bands. The algorithm is robust and has been fused into the S2 toolbox developed by the European Space Agency, it operates on the principles of neural network calibrated (trained) on simulated spectral reflectance utilizing a radiative transfer model [41] and time series of LAI implemented across every 10-m spatial resolution. In each plot polygon across the two study sites, a buffer of 20 meters was removed to avoid the impact of mixed pixels at the plot boundary. The plot mean was computed by averaging the vegetation indices of all pixels in a given buffered polygon using the zonal statistics function in R [("Zonal statistics in R | GeoProfesja," 2016)] which was the values taken for the land classification.

Table 3. List of tested vegetation indices and biophysical variables

Full name	Index	Formula	Reference
Canopy greenness-related vegetation indices			
Normalized Difference Vegetation Index	NDVI	$\frac{NIR - RED}{NIR + RED}$	[(Rouse Jr et al., 1973)]
Green Normalized Difference Vegetation Index	GNDVI	$\frac{NIR - GREEN}{NIR + GREEN}$	[(Gitelson et al., 1996)]
Enhanced Vegetation Index	EVI	$2.5 * \frac{NIR - RED}{NIR + C1 * RED - C2 * BLUE + L}$	[(Huete et al., 2002)]
Transformed Soil Adjusted Vegetation Index	TSAVI	$a * \frac{NIR - a * RED - b}{RED + a * (RED + a(NIR - b) + c * (1 + a^2)}$	[(Baret et al., 1989)]
Atmospherically Resistant Vegetation Index	ARVI	$\frac{NIR - (RED - 1 * (BLUE - RED))}{NIR + (RED - 1 * (BLUE - RED))}$	[(Kaufman and Tanre, 1992)]
Green Chlorophyll Vegetation Index	GCVI	$\frac{NIR}{GREEN} - 1$	[(Gitelson et al., 2006)]
Water-related vegetation indices			
Normalized Difference Moisture Index	NDMI	$\frac{NIR - SWIR12}{NIR + SWIR12}$	[(Gao, 1995)]
Land Surface Water Index	LSWI	$\frac{NIR - SWIR1}{NIR + SWIR1}$	[(Xiao et al., 2005)]
Biophysical variables			
Leaf Area Index	LAI		[(Weiss et al., 2002)]
Fraction Vegetation Cover	FCOVER		[(Weiss et al., 2002)]
Fraction of Absorbed Photosynthetically Active Radiation	FAPAR		[(Weiss et al., 2002)]

2.5 Time series Metric derivation for classification

In our study, vegetation indices time series were fitted to an analytical model that represents the development of plants in relation to their phenology and uses the parameters of such relationships (PM) as a classifier used in the land classification. This is a significant variation from conventional classifiers which target directly vegetation indices or diffusion of surface reflectance. The double sigmoid fitting function is shown in Equation 1 [51,52] fitted to the raw vegetation index time series using a non-linear least square method (nls function in R).

$$V(t) = vmin + vamp\left(\frac{1}{1+e^{m1-n1t}} - \frac{1}{1+e^{m2-n2t}}\right) \quad (1)$$

Where V(t) stands for a given vegetation index at time t, *vmin,* and *vamp* are minimum (background greenness) and amplitude parameters of one year respectively, m_1, n_1, m_2, *and* n_2 are parameters controlling the curve shape (Figure 3). Some critical points are important to highlight as $t_1 = m_1/n_1$, which is the inflection point within the growth period while $t_2 = m_2/n_2$ corresponds to the inflection point at the end of the season during the leave senescence phase.

Quantities t_1 and t_2 can be used as proxies of the start of the season (SOS) and end of the season (EOS), respectively [53]. Parameters n_1 and n_2 reflect the slope at the inflection points, t_1, and t_2.

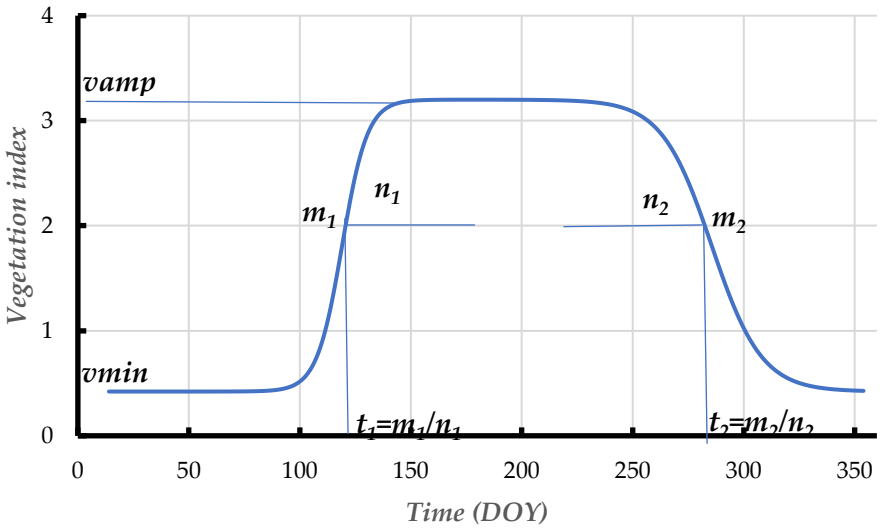

Figure 3. Double logistic fitting showing SOS and EOS.

With deciduous trees and annual crops, t_1 occurs when leaves are growing while t_2 corresponds to leave senescence. It is expected that parameters involved in equation 1 or their derivatives are specific to a given crop and thus can be used in calibration schemes. Furthermore, since t_1 is strained by the whole structure of the phenology, it is rarely impacted by noise while t_2 is more undetermined for trees since defoliation is slow which relies on water accessibility and conditions of weather [54]. The PM used in this study includes all these parameters (v_{amp}, v_{min}, m_1, n_1, m_2, n_2, t_1, t_2) plus the residual standard deviation (*std*) characterizing the difference between the fitted curves and the data. Some fitting examples are given in Figure 4. It shows that whatever the temporal dynamic of the vegetation, Equation 1 can be calibrated. However, when the curve does not follow the expected double logistic shape, as with a mowed grassland (Figure 4a) the *std* is high and the phenology timing given by *t1* and *t2* (*t1*=200 and *t2*=330) is significantly different in the presented case from that of an orchard or a vineyard. We expected that those parameters might be considered by the classification algorithm and thus would lead to the field classified as DC.

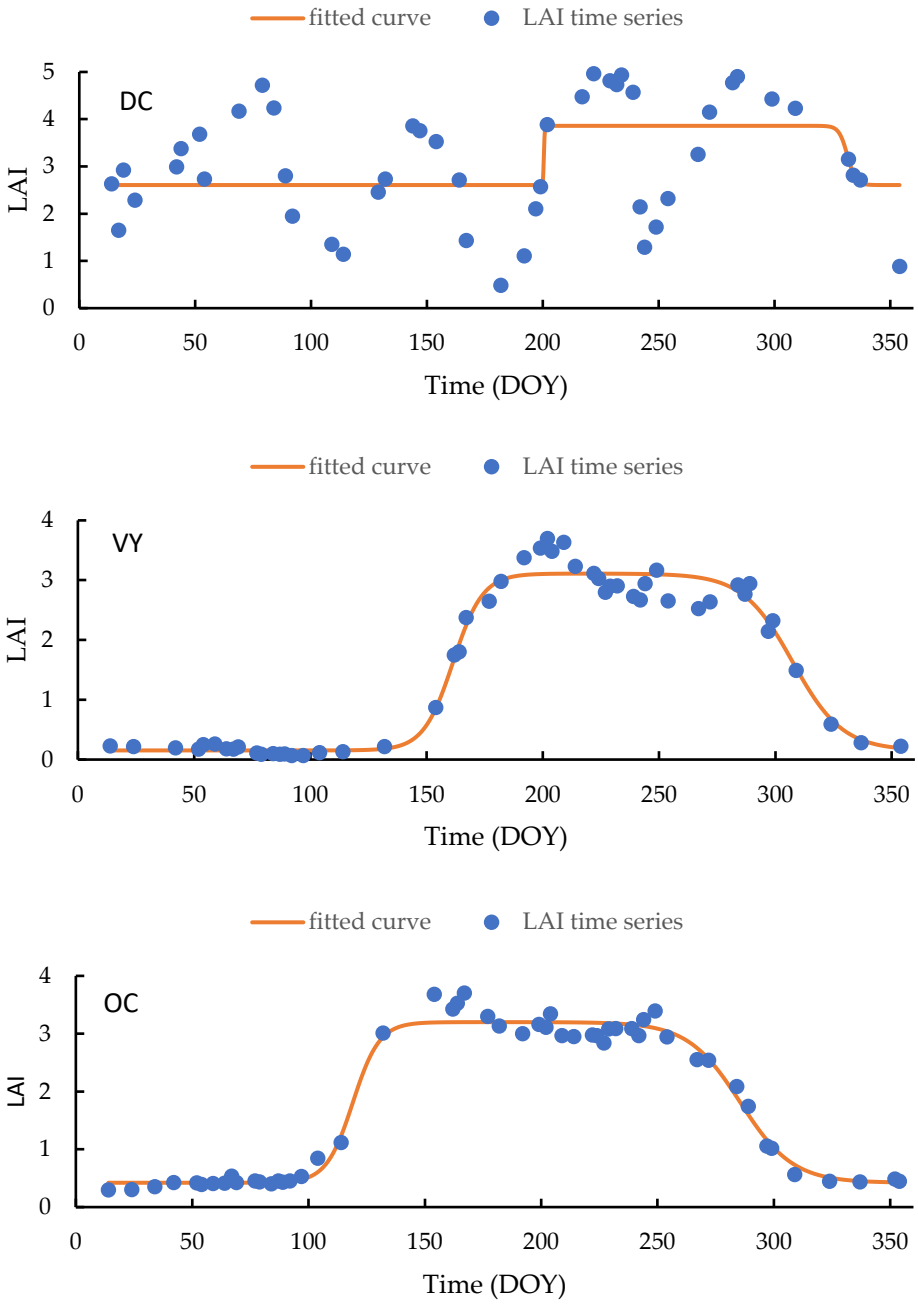

Figure 4. DC class with the fitted curve (a), VY class with the fitted curve (b), and OC class with the fitted curve (c).

2.6 Classification method

Land use classification was made using a machine learning (ML) approach. Among the ML approaches, random forest (RF) is often used for land use classification. The approach is based on decision trees that can handle a lot of variables [55,56] which was the case in this study [56]. The RF method is a non-parametric ML approach that displays good results when compared to the conventional parametric approaches [37]. We optimized the performance of the RF model by tunning (automatically done) on two significant parameters namely *mtry*

(indicates the number of predictors tested at each tree node) and *ntree* (displays the number of decision trees runs at each iteration), the accuracy of the classification was enhanced by tunning on the number of *ntree* (after starting with the default value of 500 trees) using hyperparameter tuning for each year and each site, the justification for such tunning according to the site is that each year has its specific features thus, we adopted the value that leads to the best performance of the classifier. Finally, the model output is decided by the number of a majority of votes by the classifier ensembles.

Regarding remote sensing and land surface phenology mapping, the RF classifier remains an effective approach [35] thus, for classification accuracy assessments ground truth information was equally split into two batches for each class namely calibration (50% proportional distribution from each class in the target population) and evaluation (50% from each crop class) datasets utilizing a spatial cross-validation method from the CAST package in R [57]. The aforementioned spatial cross-validation aid ensures the selected ground truth data of a similar field will be apportioned either in the calibration or evaluation dataset to keep away from over-fitting. Accuracy evaluations were done by the confusion matrix which gives the number of plots well classified on the diagonal and the number of erroneous detections between classes outside the diagonal with predicted class in column and actual class in line [58]. Accuracy metrics for the classification results include overall accuracy (OA), Kohen's Kappa which removes the chance factor, user's accuracy (UA), and producers' accuracy (PA). These metrics were computed directly from classification routines or using the CARET package in R [58] when the classification was done with different steps.

3. Results

3.1 Analysis of temporal profile for orchard, vineyard, and olive trees to derive phenology metrics

In both areas, OC and VY trees are deciduous and therefore exhibit a similar temporal pattern that is characterized by a maximum plateau in the summer. However, despite the close resemblance in the temporal patterns, there are still some significant features that can be used to separate them. For instance, OC trees mostly have SOS during 60-80 DOY and 100-120 DOY time intervals in the Crau and Ouveze-Ventoux areas, respectively. With VY, such intervals are delayed by about 30 days in both areas (Figure 4). Moreover, the growth rate with vineyards is more gradual. The differences between the areas are explained by the type of orchards and the climate, the Ouveze area being located more to the North with higher altitudes and thus lower temperature, which induces delays in phenology. The level of the plateau is variable. It depends on the age and density of the stands. However, in general, the values obtained in summer by the VY remain lower than those of the OC, except for the irrigated VY dedicated to table grapes. The LAI variations in mid-season can be variable according to the inter-row management and pruning practices. For a given field, the temporal features remain rather stable between years meaning that the classification algorithms might be applied over different years.

OL groves are observable in the Crau. The fact of having evergreen leaves leads to a very different temporal signature in comparison to that of OC and VY with variations rather governed by the soil cover. For the other surfaces (DC class), there is a great diversity of temporal signatures. For many of them, very different evolutions are observed (market gardening, irrigated meadows, dry meadows) from the previous cases, while ambiguities could appear with some surfaces such as wetlands which also show a seasonality comparable to OC plots.

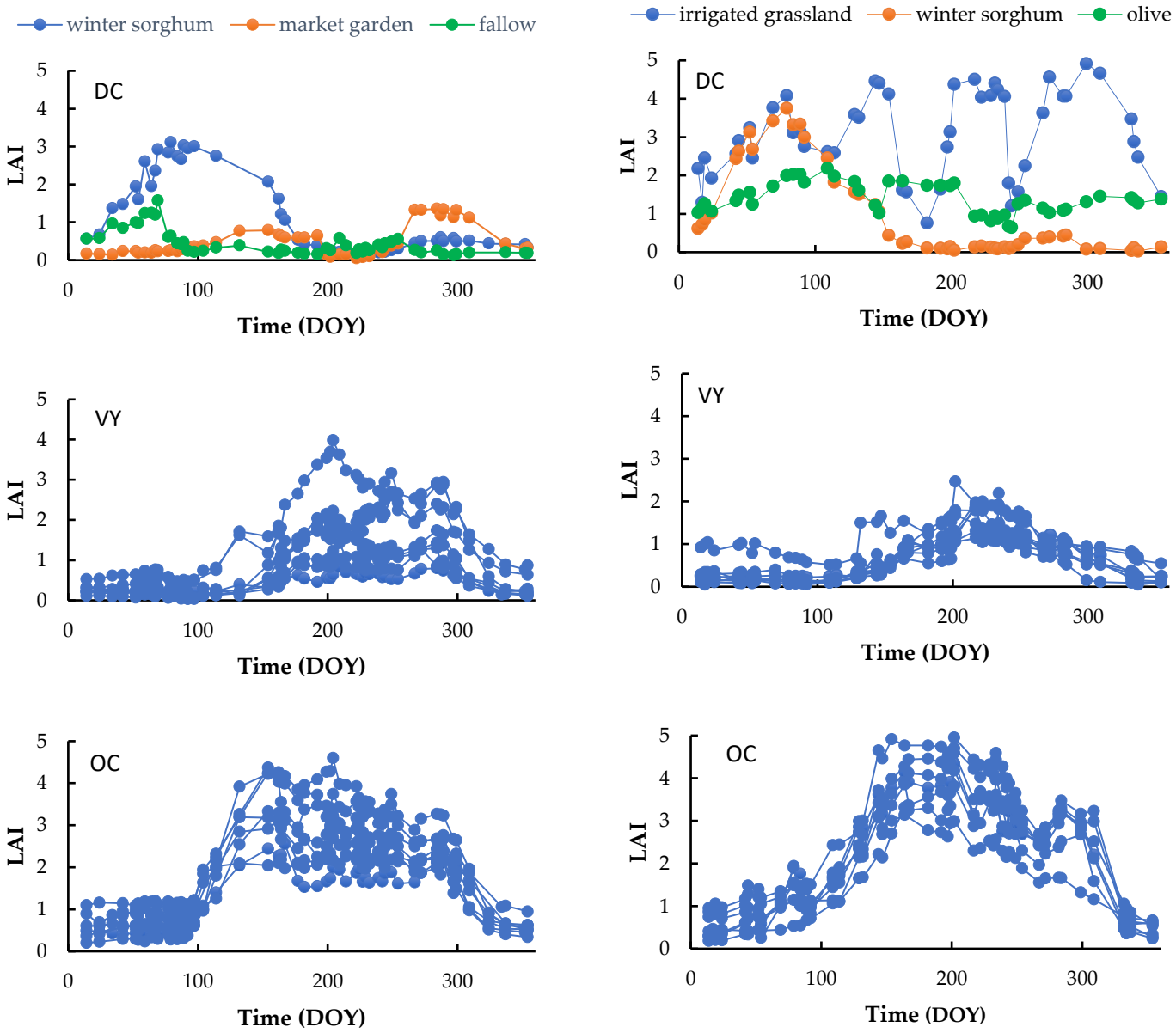

Figure 5. Temporal profile of DC (a), VY (b), OC (c) in Ouveze-Ventoux and temporal profile of DC (d), VY (e), and OC (f) in the Crau site.

3.2 Selection of indices and biophysical variables using the proposed method.

Different vegetation indices related to canopy greenness, water, and, biophysical variables were analyzed to make the selection of the best indices and biophysical variables for the year 2021 in the Ouveze-Ventoux site. For all indices and biophysical variables, we fitted the double logistic model to infer the PM. These PM together with statistical parameters qualifying the quality of the fit (*std*) were used as input in the RF algorithm to separate three classes: OC, VY, and DC. If all the considered variables representing vegetation development led to comparable results, the best results were obtained with LAI (Table 4). Moreover, using such a quantity is an advantage since it is directly comparable to field observations which facilitates its interpretation and thus the establishment of thresholds that could be useful to conduct the classification [10]. Additionally, a further comparison was conducted from 2020 to 2018 (years with larger data acquisitions dates when both Sentinel 2 satellites were operated)

among the best two performing vegetation indices (NDVI and TSAVI) and LAI. This is to ensure that the LAI remains a good choice across the years. This was the case with a K ranging between 0.85 and 0.88 when using the LAI while the kappa ranged between 0.72 and 0.79 with the NDVI and between 0.68 and 0.74 with the TSAVI.

Table 4. Classification performance of different vegetation indices and biophysical variables in Ouveze-Ventoux for 2021.

Vegetation indices	**OA (%)**	**K**
NDVI	82	0.71
GNDVI	80	0.70
EVI	82	0.75
TSAVI	87	0.85
ARVI	81	0.77
GCVI	73	0.70
NDMI	82	0.71
LSWI	80	0.77
Biophysical variables	**OA (%)**	**K**
LAI	92	0.89
FAPAR	90	0.88
FCOVER	87	0.85

3.3 Accuracy assessments

3.3.1 Delineation of orchards and vineyards in Ouveze-Ventoux site.

The classification in the Ouveze-Ventoux site was done by considering three classes namely OC, VY, and DC. The classification was made using the PM derived from the LAI temporal profiles (Table 5). Misclassified fields mainly came from confusion between VY and DC. In about half of the cases, the confusion came from young stands having a low vegetative development and thus a canopy signal which was not very clear as displayed in Figure 6. Therefore, we merged young stands, presenting a maximum LAI lower than 0.5 to the DC class and replay the classification. By applying such a threshold, the classification accuracy was slightly improved (Table 6). The producer's accuracy is revealing errors due to commission with OC class being the best with a producer's accuracy of 0.96. To test the classification over time, the classification was done each year from 2016 to 2021 with results summarized in Table 7. The performance of the classification was slightly affected in 2017 and 2016 and the probable explanation for this might be ascribed to fewer acquisitions of S2 images since only one of the Sentinel 2 constellations was operated.

Table 5. Confusion matrix for OC and VY classification using PM of LAI in 2021 (subscript a and p correspond to actual and predicted class, respectively)

	DC_p	**OC_p**	**VY_p**	**Total**	**User's accuracy**
DC_a	35	0	2	37	0.94
OC_a	1	29	0	30	0.96
VY_a	5	1	44	50	0.88
Total	41	30	46	117	
Producers's accuracy	0.86	0.96	0.96		
OA = 0.92 ; K = 0.89					

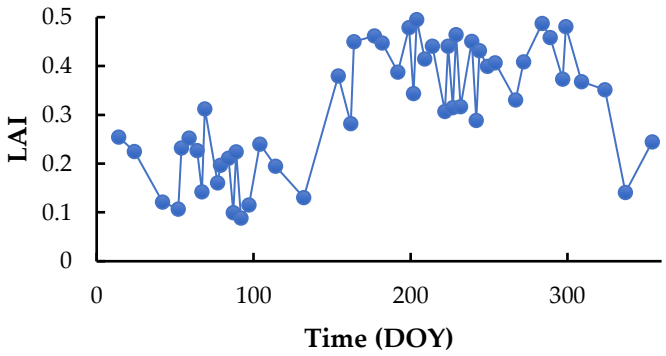

Figure 6. Temporal profile of a young VY misclassified as DC in Ouveze-Ventoux.

Table 6. Confusion matrix for OC and VY classification using PM from LAI 2021 time series and applying a LAI= 0.5 for OC and VY classes (subscript a and p corresponds to actual and predicted class, respectively)

	DC_p	OC_p	VY_p	Total	User's accuracy
DC_a	37	0	2	39	0.95
OC_a	0	30	0	30	1.00
VY_a	1	1	46	48	0.97
Total	38	31	48	117	
Producers's accuracy	0.95	0.96	0.95		
OA = 0.96 ; K = 0.91					

Table 7. Results of OC and VY classification in Ouveze-Ventoux from 2016-201 based on PM derived from LAI time series and applying LAI = 0.5 thresholds for OC and VY classes

Year	Site	Accuracy assessments	
		OA (%)	Kappa
2016	Ouveze-Ventoux	89	0.86
2017		90	0.89
2018		91	0.90
2019		94	0.92
2020		95	0.93
2021		96	0.91

The classification was then applied to all fields large enough to have at least one pixel after applying a buffer of 20 meters on the plot boundary. The field distribution confirms the importance of OC and VY in the Ouveze-Ventoux area as shown in Figure 7 below.

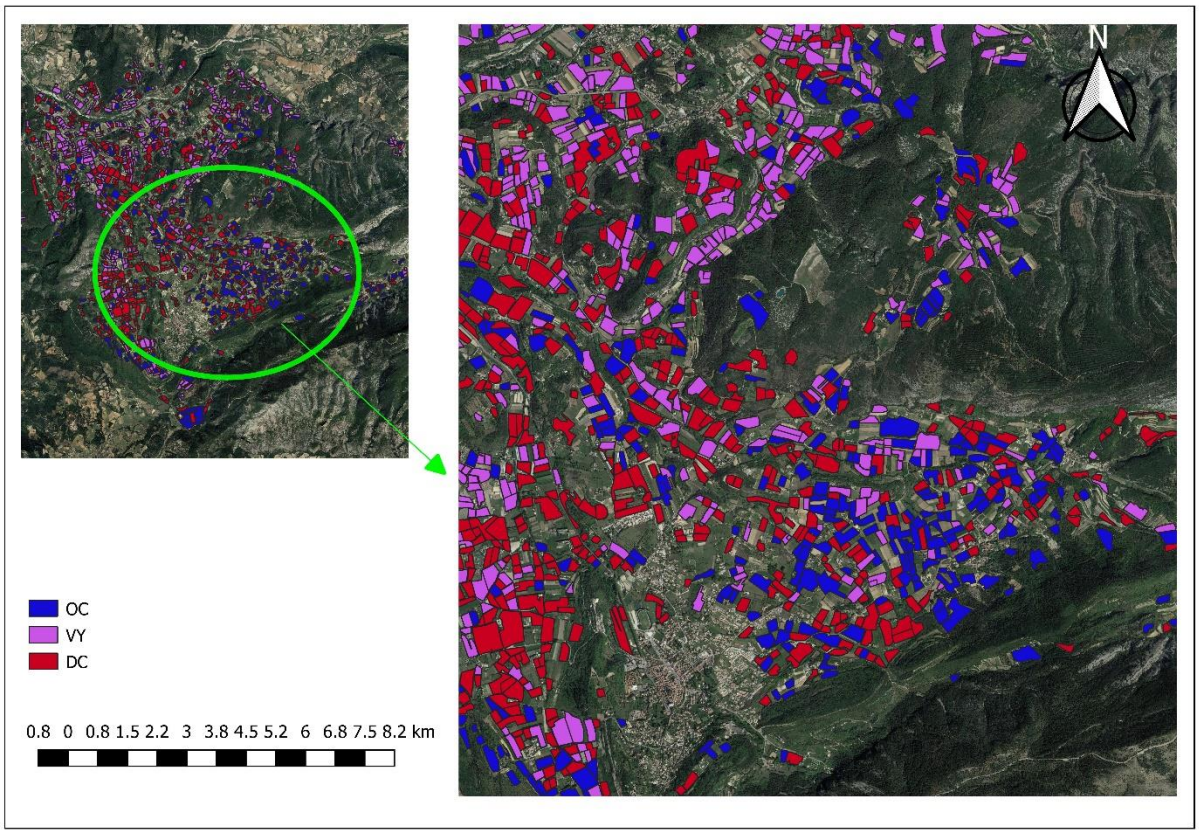

Figure 7. Spatial distribution of OC, VY, and DC classes in the Ouveze-Ventoux site for the year 2021.

3.3.2 Delineation of orchards, vineyards, and olives in the Crau site.

On the Crau site, we find the three classes mapped on the Ouveze-ventoux site (VY, OC, and DC) to which an OL class has been added because of the high representation of olive groves. It is also worth noting the high diversity of the DC class with market gardening, steppe areas, wetlands, and field crops. First, we begin by conducting the classification considering the four classes (DC, OC, OL, VY). Results displayed in Table 8 exhibit rather weak results with particular difficulties in delineating DC and OL classes. We decided to perform the classifications in two steps. In the first step, we gathered both OL and DC in a single DC class. Then, in a second step, we delineated DC and OL. Results of the first step are reported in Table 9 showing a significant improvement with a Kappa rising from 0.69 to 0.91. Remarkably, results were also strongly improved for the VY class with user accuracy increasing from 0.28 to 0.61. Note that the OC class was very well characterized in spite of a large diversity of tree types and varieties. As for the Ouveze-Ventoux site, an analysis of the misclassified fields showed again the difficulties in identifying the phenology in juvenile tree stands. A LAI threshold was therefore applied to the OC and VY by considering that all plots having a maximum LAI lower than 1 belong to the DC class. The quality of the classification continues to improve (Kappa = 0.95) but at the cost of not identifying young orchards and vineyards (Table 10).

Table 8. Confusion matrix for OC, VY, OL, and DC classification based on PM from 2021 time series (subscript a and p correspond to actual and predicted class, respectively)

	DC_p	OC_p	OL_p	VY_p	Total	User's accuracy
DC_a	19	0	11	0	30	0.63
OC_a	0	42	0	2	44	0.95
OL_a	10	0	20	0	30	0.67
VY_a	11	2	0	5	18	0.28
Total	40	44	31	7	122	
Producers's accuracy	0.50	0.95	0.65	0.71		
OA = 0.70 ; K = 0.69						

Table 9. Confusion matrix for OC and VY classification based on PM from 2021 LAI time series and after gathering OC and DC in common DC class (subscript a and p correspond to actual and predicted class, respectively)

	DC_p	OC_p	VY_p	Total	User's accuracy
DC_a	60	0	0	60	1.00
OC_a	0	44	0	44	1.00
VY_a	6	1	11	18	0.61
Total	66	45	11	122	
Producers's accuracy	0.91	0.98	1.00		
OA = 0.94 ; K = 0.91					

Table 10. Same as Table 9 with an additional threshold of LAI=1 for OC and VY classes of LAI in 2021 (subscript a and p correspond to actual and predicted class, respectively)

	DC_p	OC_p	VY_p	Total	User's accuracy
DC_a	62	0	0	62	1.00
OC_a	0	44	0	44	1.00
VY_a	3	1	12	16	0.75
Total	65	45	12	122	
Producers's accuracy	0.95	0.98	1.00		
OA = 0.97 ; K = 0.95					

In step 2, we distinguished the olive trees (OL) in class DC. It is necessary to identify in the time series discriminating features of the olive trees, which could then be used as classifiers. In Figure 8, we show the time series of a sample of OL plots and plots identified as DC. We conducted this comparison for two variables, the LAI used in the previous classification and the GCVI, which leads to a typical signature of olive trees with a systematic decrease of the signal in the summer period compared to earlier and later periods in the year. This signature is typical of the OC class. In order to appreciate the generality of this behavior we represented in a diagram (Figure 9) the average value of the vegetation index (VI) at the beginning of the year (between DOY 1 in 100) in abscissa and the average value in the middle of the year (between DOY 150 and 250) in ordinates. When the vegetation of the OL trees is well developed, there is a systematic decrease of the GCVI, which is all the stronger as the GCVI is high. It is also interesting to note that the area of the diagram of points covered by OC plots is specific with little coverage of DC plots, whose dispersion in the diagram reflects the diversity of vegetation cover encountered in this class. Similar results are obtained with LAI

(Figure 9a) but with less specificity of olive plots and a less clear relationship between the difference in LAI over the two periods and the development of olive trees as shown by the scatter of the OC points. Concerning the behaviour of the GCVI with the OL trees, the reasons for the reflectance ratio in the NIR and green band cannot be explained by the seasonality of the grass cover under the canopy. Indeed, the impact of the herbaceous cover should decrease with tree cover, which is contrary to what we observe. The reason could come from the orientation of the leaves and their spectral properties, which could be influenced by heat and summer water stress.

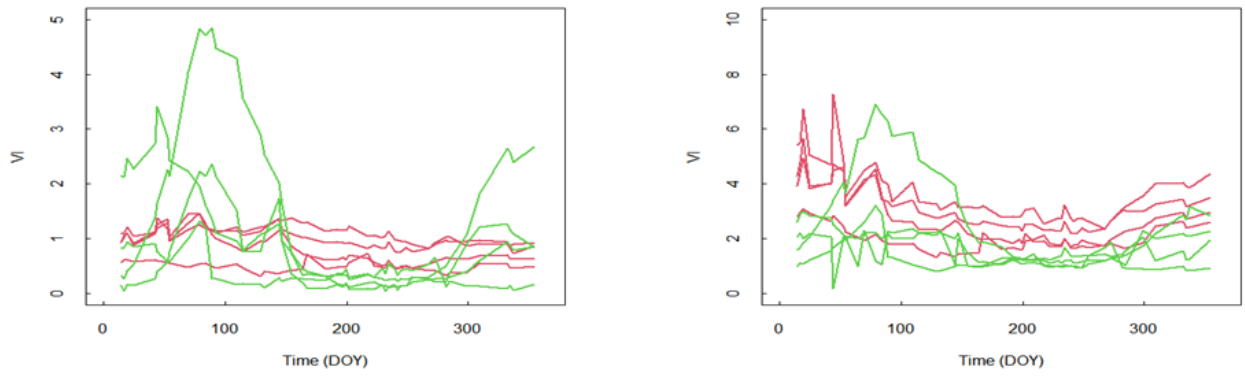

a) b)

Figure 8: Vegetation indice time series observed on OL plots (red) and DC (green). In a) the vegetation indices is the LAI, in b) the vegetation indices are GCVI.

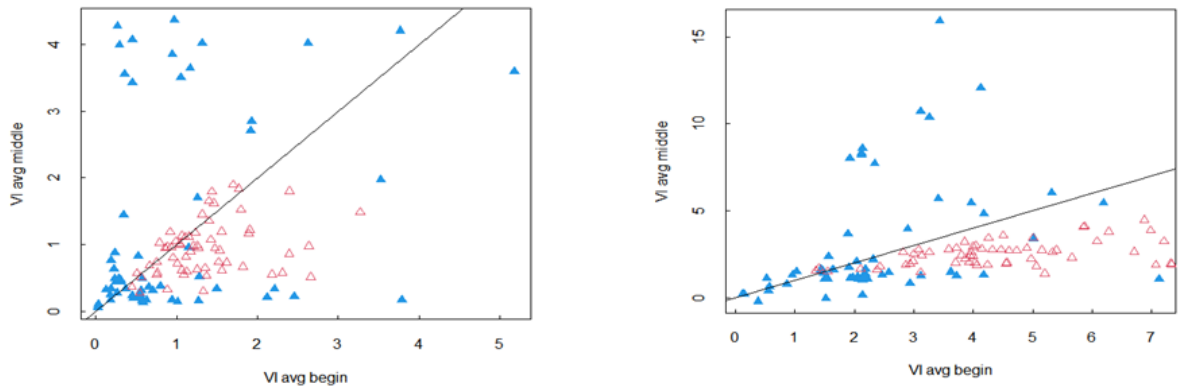

a) b)

Figure 9: Average vegetation indices during the summer period (DOY 150-250) as a function of the average vegetation indices at the beginning of the year (DOY 1-100) for olive plots (red triangle) and end DC plots (blue triangle). In a) the vegetation indices are the LAI and in b) the vegetation indices are GCVI.

To carry out the classification, we calculated characteristics for each of the periods, namely the beginning of the year from DOY=1 to DOY=100 and the middle of the year from DOY=150 to DOY=250. The following characteristics were considered: the mean, the standard deviation, the slope, and the origin of the linear regression between the vegetation indices and time as well as the corresponding correlation coefficient. The classification was done with the RF method using the 12 variables thus obtained (6 per period) as classifiers. The results are given in Table 11 when using the GCVI as the vegetation indices.

Table 11. Confusion matrix for DC and OL classification based on a temporal feature from 2021 GCVI time series (subscript a and p correspond to actual and predicted class, respectively)

	DC_p	OL_p	**Total**	**User's accuracy**
DC_a	25	5	30	0.87
OL_a	1	29	30	0.97
Total	26	34	60	
Producers's accuracy	0.96	0.88		
OA = 0.91 ; K = 0.82				

When using LAI instead of the GCVI results were degraded with an OA=0.82 and a Kappa=0.70. In the misclassified plots analysis, it can be seen that the DC plots classified as OL correspond to mowed grasslands or more or less dense forests. Concerning the grasslands, it is easy to identify them because, on the periods used to calculate the characteristics of the signal, we have a strong variability of the GCVI. As far as the forests are concerned, they do not generally show the summer decrease of the GCVI. These features could not be identified by the calibration of the classification model, but can easily be considered by doing a post-processing. Thus, we propose to classify as DC the plots classified as OL when 1) the sum of the standard deviations of the signal obtained on each period is higher than 2, which never happens with OL trees, or 2) when the GCVI is higher than 3 and the average increases between period 1 and 2 contrary to the behaviour of OL trees. Applying this post-processing we obtain an OA = 0.97 and a K= 0.94 (Table 12).

Table 12. Results of OL classification in Crau from 2016-201 using GCV

Year	**Site**	**Accuracy assessments**	
		OA (%)	**Kappa**
2016	Crau	90	0.86
2017		90	0.88
2018		95	0.93
2019		93	0.92
2020		94	0.91
2021		97	0.94

The final classification obtained after chaining step 1 and step 2 are displayed in Table 13, VY class being the most difficult to determine. The good results were maintained across the years (Table 14) with, however, some degradation for 2016 and 2017 years, during fewer S2 data were available. One can note little loss in accuracy in 2018, 2019, and 2020. This might

be the result of the final thresholding that is specific to 2021. However, they always remain better than the results obtained when no thresholds were applied.

Table 13. Confusion matrix of DC, OC, OL, and, VY classification in Crau for 2021.

	DC_p	OC_p	OL_p	VY_p	Total	User's accuracy
DC_a	31	0	1	0	32	0.97
OC_a	0	44	0	0	44	1.00
OL_a	1	0	29	0	30	0.97
VY_a	3	1	0	12	16	0.75
Total	35	45	30	12	122	
Producers's accuracy	0.89	0.98	0.97	1.00		
			OA = 0.96 ; K = 0.95			

Table 14. Results of OC, VY, OL global classification accuracy in Crau from 2016-201.

Year	Site	Accuracy assessments	
		OA (%)	Kappa
2016	Crau	89	0.87
2017		90	0.87
2018		92	0.90
2019		94	0.91
2020		93	0.91
2021		96	0.95

3.4 Feature importance ranking

Feature importance process in the RF algorithm involves building a classification and regression tree to create OOB (out-of-bag) sample data. According to the OOB data, the RF algorithm can confirm the significant (importance) role of the input data and generate each feature's important score which is displayed as MDA (mean decrease accuracy). The principle is to convert a feature's value to a random number compute its influence on the model's precision and quantify the parameter's importance according to the MDA value generated from several computations. When the value is higher, the importance variable too becomes higher [59]. Both in Ouveze-Ventoux and Crau t_1 and v_{amp} are the two most significant feature variables showing the importance of the start of the season and the amplitude of variation of the LAI signal. On the contrary, the EOS as reflected by t2 had a lower impact on the classification.

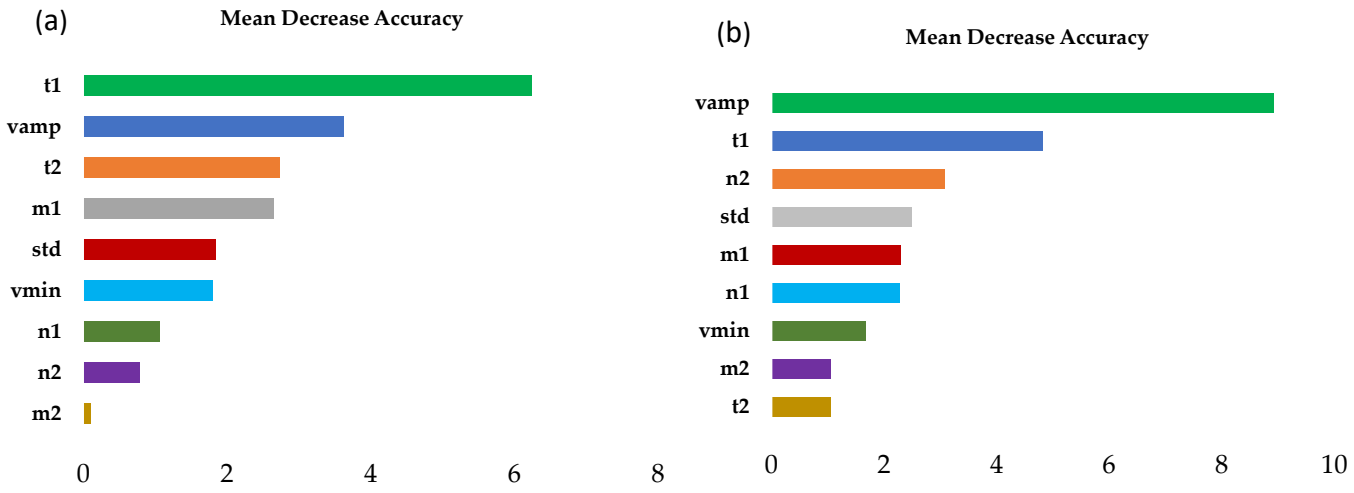

Figure 10. Feature importance ranking (mean decrease accuracy) for Ouveze-Ventoux (a) and Crau (b)

4. Discussion

4.1 Benchmark and novelty of the proposed classification approach

One of the reasons behind the scarcity of RS-based maps delineating fruit trees could be ascribed to the difficulty of differentiating several tree crop classes spectrally and temporarily to generate precise maps. For instance, the use of NDVI temporal profile of fruit trees such as grapes, mangoes, and bananas displayed no clear distinction between the different fruit tree types [60]. The novelty in our approach was to apply the classification on plant phenological traits rather than using a temporal series of images. If we obtained good results it is necessary to assess the adding value of our approach compared to existing approaches. Two benchmarks were considered:

- A classification made directly on the times series of LAI without interpreting the phenology in time series. This was done using the RF method. In the Crau area, we did not consider the last step separating olive orchards from other surfaces, and focused on the first step which considers the following three classes only: OC, VY, and DC.
- The THEIA land use map is yearly implemented across the entire French national territory (https://www.theia-land.fr/ceslist/ces-occupationdes-sols/, accessed on 17 May 2022). It uses RF-supervised classification on all S2 dates (VIS and NIR bands) with other supplementary data like urban maps, topography, Corine Land Cover map, and *'Registre Parcellaire Graphique'* (RPG) that collect yearly farmer's declarations on subsidy collection from the European Union (EU). The number of identified classes was seventeen of which OC (tagged as 221 and 14 in 2017 and 2018 respectively) and VY (tagged as 222 and 15 in 2017 and 2018 respectively) are inclusive and in our study, the detection of orchards and vineyards were assessed. The maps were prepared at 10 m pixels of S2 and aggregated at the field level to be comparable with the results of our study.

The accuracies of the classification made on temporal series of LAI images were far below that obtained with our method with an OA ranging from 41 to 60 and a Kappa ranging from 0.31 to 0.52 across the two study sites from the 2016-2021 (Table. 15) while we obtained Kappa larger than 0.80. Results from 2016-2017 had the worst performance and this might be because S2 had data acquisition limited to S2A. The difficulty of classifying directly on LAI images can be explained by the very strong diversity of situations, in particular in the DC class that might hamper the possibility to capture specific features of the crop of interest. Better results were found with the THEIA product (Table 16) which involves much more information layers that better constrained the classification. However, the use of our method led to a significant improvement.

Table 15. Classification performance of the raw spectral satellite images (LAI) across the two study sites for OC and VY using RF classifier.

Year	Site	OA (%)	K
2016	Ouveze-Ventoux	43	0.30
2017		47	0.32
2018		55	0.41
2019		51	0.49
2020		55	0.51
2021		52	0.50
2016	Crau	41	0.32
2017		45	0.31
2018		49	0.41
2019		55	0.52
2020		60	0.51
2021		58	0.49

Table 16. THEIA classification performance across the two study sites for OC and VY using RF classifier and other supplementary data.

Year	Site	OA (%)	Kappa
2016	Ouveze-Ventoux	73	0.70
2017		77	0.72
2018		75	0.71
2019		78	0.75
2020		75	0.71
2021		72	0.69
2016	Crau	76	0.73
2017		75	0.69
2018		79	0.75
2019		75	0.72
2020		73	0.68
2021		78	0.75

4.2 Training sample size and generality of the proposed approach across years and sites.

Former studies highlighted that large data samples bolster RF classification accuracy. while in some situations, larger data samples might lower the RF classification accuracy depending on the dataset quality. In our study, we obtained good accuracy using a small training data set of 117 (out of 1601 in Ouveze-Ventoux) and 122 (out of 16680 in Crau) This corroborates the conclusions of Nguyen et al. [27] and Colditz [61] who found that datasets consisting of 0.15% to 0.35% of the study sites are sufficient to attain a precise land cover delineations. As a rule of thumb, studies related to land use/land cover should operate with restricted data because of the excessive price of organizing field data. Therefore, to reduce the ground truth collection burden, we can imagine applying the RF model determined for a given year to the other years. This idea is supported by the results displayed in Figure 11 which have shown that the main temporal patterns of the LAI times series are rather stable from one year to another. Therefore, we have applied the RF model established in 2021 to the PM computed for 2016, 2017, 2018, 2019, and 2020 LAI time series. The results of the classifications thus made

are given in Table 17. The results revealed that PM used for the training of the model is robust irrespective of the different years however with slightly lower accuracies with an average loss of 8% (max 14%) in OA and 0.10 (max 0.16) in kappa. Results obtained in the Crau are found to be a bit better, while the smallest time series in 2016 and less extent 2017 did not have a strong impact on the classification performance. In all cases, the accuracy remains much better than that obtained when the classification was made directly on the LAI time series and comparable to the THEIA classification.

Table 17. Classification performance using PM for classifying orchards and vineyards applying the predicted model of 2021 across years and sites.

Accuracy Assessment					
		Calibrated RF model		2021 model across years	
Year	**Site**	**OA**	**Kappa**	**OA**	**Kappa**
2016	Ouveze-Ventoux	89	0.86	81	0.72
2017		90	0.89	83	0.76
2018		91	0.90	82	0.79
2019		94	0.92	83	0.81
2020		95	0.93	86	0.85
2016	Crau	89	0.87	83	0.79
2017		90	0.87	82	0.78
2018		92	0.90	85	0.80
2019		94	0.91	87	0.83
2020		93	0.91	86	0.80
	Calibrated RF model			**2021 model across sites**	
2021	Ouveze Ventoux	96	0.91	71	0.65
2021	Crau	89	0.87	60	0.51

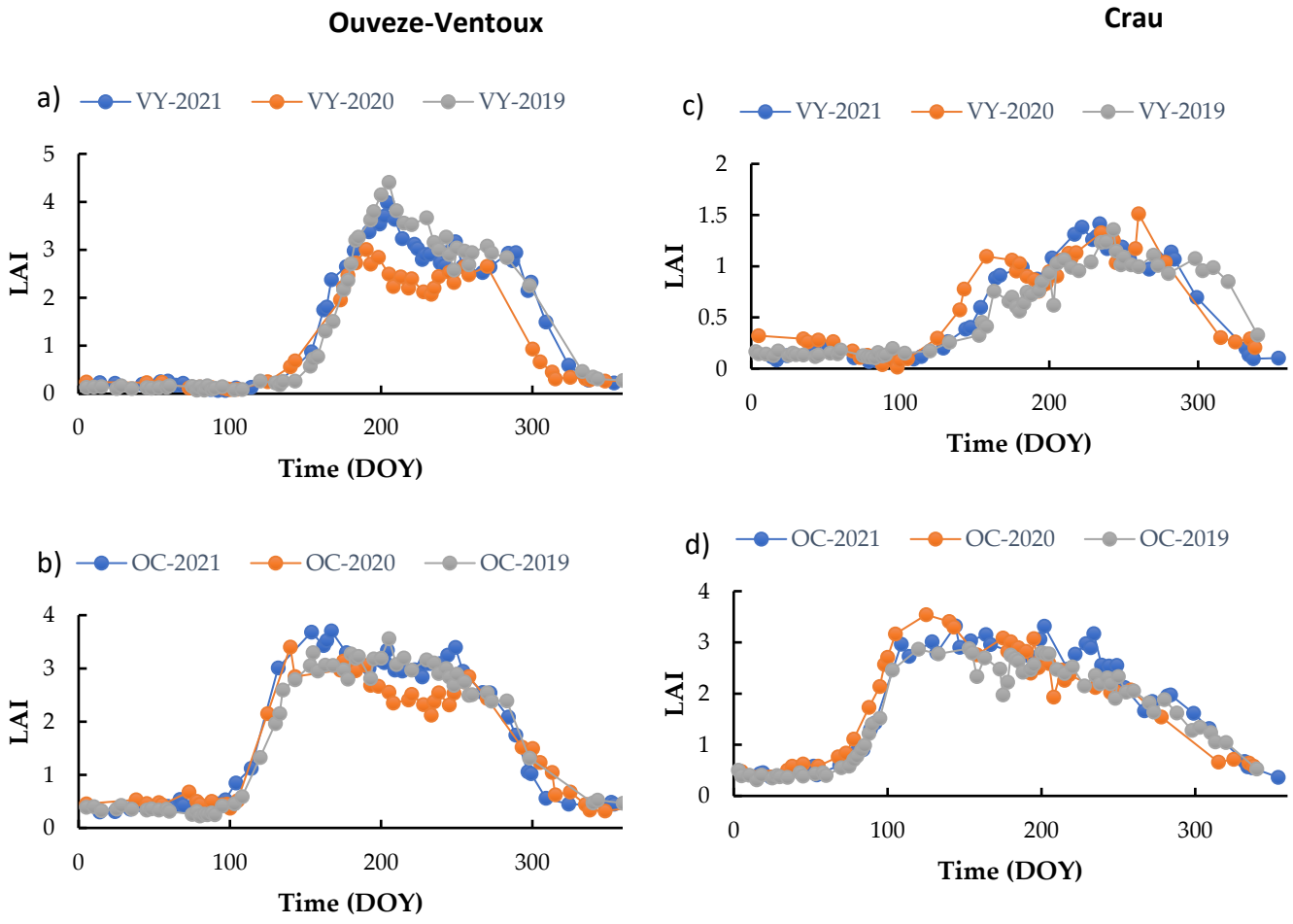

Figure 11. Temporal profile of OC and VY in Ouveze-Ventoux (a and b) and Crau (c and d) study areas from 2019 to 2021.

The same exercise was done to make comparisons across sites (i.e the model of 2021 established in the Ouveze-Ventoux site to be used for Crau and vice versa). In this exercise, the performance of the model was affected (Table 17). This further corroborates the fact that each model generated is strictly adapted to a given location, the climatic and geographical variations and diversity in crop management practices across the two sites might be responsible for the decline in results performances since the model was adapted to a different location (based on their PM).

4.3 Limitations and prospects of the proposed classification approach

Despite the novelty and good performance of our proposed approach, we are faced with quite some drawbacks which are to be highlighted in this section. One of the obvious drawbacks is the inability of the approach to successfully classify young OC and VY. In general, the canopy size of young fruit trees (OC and VY) is very scanty (low) and consequently creates room for misclassification since our approach is based on the temporal dynamics of the LAI. One of the main reasons is the contribution of inter-row vegetation, which can be dominant in young stands. As a result, we can end up with a LAI signal that is no longer dominated by the plant of interest. In Figure 12, we see that the SOS is earlier with the VY plot than with the OC plot, which is contrary to the expected result. Such drawbacks are minimized by considering only OC and VY plots with sufficient development, which led us to put thresholds in our reference dataset by assimilating several young OC and VY to the DC class. To obtain an optimal result this thresholding depends on the considered area, which is probably the reflection of different cultural practices for the management of the inter-row. The determination of these thresholds is a real limitation of the method. There is therefore a strong stake to work on the separation of the contributions coming from the inter-row vegetation and the canopy of the stand of interest. A finer analysis of the spectral signature and/or a finer analysis of the temporal dynamics could contribute to a better separation of these two components and thus work on the specific signal of the crop of interest.

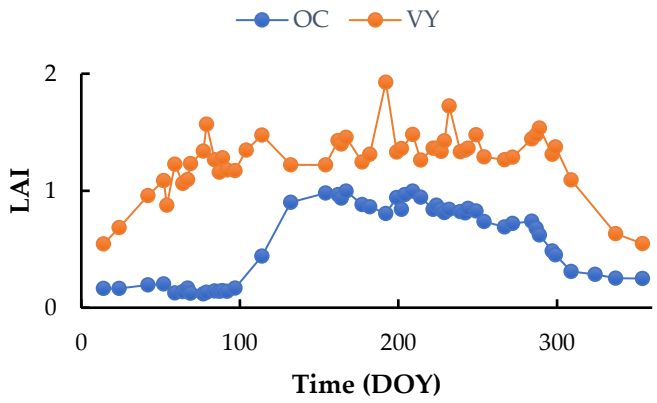

Figure 12. Temporal pattern of a young OC field and a temporal pattern of a young VY.

Another instance is the inability of the approach to accurately classify heterogeneous plots. The trees are sparse due to age differences, creating so many sources of interference most especially from soil background among others. This creates sources for interferences with the

main canopy of the heterogenous orchard or vineyard fields since only the mean of all the total pixels in a given farm plot is utilized thereby creating a different form of the temporal pattern away from that of the fruit trees of interest. Such deviations from the main temporal patterns of fields used for training the model consequently lead to degraded fits by the model and lead to misclassifications when making predictions to the global extent.

Despite the highlighted drawbacks mentioned above, the prospect of PM-based delineations is encouraging for many reasons. Our analysis of data showed that we can separate three (3) crucial fruit tree types (OC, VY, and OL). PM-based classifiers were used only as input classifiers to the RF model thus the approach can be extended to profit from some spectral bands and some particular vegetation indices like enhanced bloom index (EBI) [62]) capable of separating the individual orchard (like cherry, plum, apricot, peach, nectarine, etc.) and vineyard (table and wine) classes. Despite our work using S2, we might be faced with issues of data missing (gap) in some areas due to the presence of the cloud affecting the capacity of inferring accurate PM and thus affecting the classification accuracy. Future satellite systems with better spatial and temporal resolutions can be merged with S2 or even synergy between optical and synthetic aperture radar (SAR) can be exploited.

5.0 Conclusions

Fruit tree delineations have been a difficult topic in crop delineation using remote sensing information. S2 has offered an encouraging avenue to build a classification strategy based on crop phenology and the temporal features of canopy development. Therefore, our study proposed a novel method to identify deciduous and evergreen fruit trees like OC, VY, and OL, by using a time series of LAI (for OC and VY) and GCVI (for OL) derived from S2 data to infer PM as classifiers used by an RF algorithm. The method has been developed and implemented on two areas (Ouveze-Ventoux and Crau areas) located in the south-east of France, separated by a hundred kilometers. The main differences are the climate with cooler and wetter climate in the Ouveze-Ventoux area and the composition of the DC class which is strongly different between sites. The obtained performances led to an overall accuracy ranging between 0.89 and 0.96 and a Kappa index ranging between 0.87 and 0.95. This is far better than the results we can obtain by applying the RF method on LAI time series (the same used to infer the phenology metrics) and significantly better than the THEIA classification which is an operational tool implemented over the France territory using multiple sources of ground information. Moreover, as the method is independent of the satellite acquisition dates, we can apply a RF classification model obtained from one year to the other years while keeping a reasonable accuracy.

While this study shows the value of using phenology and leaf development parameters to identify perennial woody crops, the use of phenology may have some limitations. It is shown that the differences in phenology induced by climate do not allow the use of a calibrated RF model from one site to another. The proposed generic approach must therefore be calibrated on each study area as soon as a temporal shift in phenology is expected. Moreover, in the case of mixed cover composed of plants with different temporal dynamics, it may be difficult to capture the phenology of the plant of interest. This is the case in this study with young plantations having an inter-row with grass. Mixing the signals from the tree canopy with those from the inter-row does not allow the identification of the phenological traits of the trees. To overcome such limitations additional information as that provided by textural

analysis of remote sensing images might be an interesting avenue to improve the results. From that perspective, the use of satellites with different resolutions can be envisaged.

Author Contributions: Conceptualization, M.A.A., and A.C.; Data curation, M.A.A., F.F., and G.P.; formal analysis, M.A.A.; Methodology, M.A.A., A.C., and G.P.; Software, G.P.; Supervision A.C. and D.C.; writing-original draft, M.A.A. and A.C.; writing-review and editing, M.A.A., A.C. and D.C. All authors have read and agreed to the published version of the manuscript.

Funding: This work was funded by the Petroleum Technology Development Fund (PTDF) under the Federal Ministry of Petroleum, Nigeria, in collaboration with INRAE-EMMAH Avignon as part of a PhD research program.

Data Availability Statement: Sentinel 2 data are available at the following hyperlink: https://www.theia-land.fr/, accessed on 17 May 2022. THEIA classification data can be found at the following hyperlink: https://www.theia-land.fr/ceslist/ces-occupation-des-sols/, accessed on 17 May 2022. Inglada, Jordi, Vincent, Arthur, & Thierion, Vincent. (2018). Theia OSO Land Cover Map 2018 [Data set]. Zenodo. https://doi.org/10.5281/zenodo.3613415 (accessed on 17 May 2022). plot boundary map and evaluation data over the CRAU and OUVEZE-VENTOUX are available on request from the corresponding author.

Conflicts of Interest: We are not aware of any conflict of interest linked to this publication, and there is no significant financial aid for this work that could have influenced its outcome.

Reference

(1) Kummu, M.; Guillaume, J. H. A.; de Moel, H.; Eisner, S.; Floerke, M.; Porkka, M.; Siebert, S.; Veldkamp, T. I. E.; Ward, P. J. The World's Road to Water Scarcity: Shortage and Stress in the 20th Century and Pathways towards Sustainability. *Sci Rep* **2016**, *6*, 38495. https://doi.org/10.1038/srep38495.

(2) Wada, Y.; Wisser, D.; Eisner, S.; Flörke, M.; Gerten, D.; Haddeland, I.; Hanasaki, N.; Masaki, Y.; Portmann, F. T.; Stacke, T.; Tessler, Z.; Schewe, J. Multimodel Projections and Uncertainties of Irrigation Water Demand under Climate Change. *Geophysical Research Letters* **2013**, *40* (17), 4626–4632. https://doi.org/10.1002/grl.50686.

(3) Richardson, K. J.; Lewis, K. H.; Krishnamurthy, P. K.; Kent, C.; Wiltshire, A. J.; Hanlon, H. M. Food Security Outcomes under a Changing Climate: Impacts of Mitigation and Adaptation on Vulnerability to Food Insecurity. *Clim. Change* **2018**, *147* (1–2), 327–341. https://doi.org/10.1007/s10584-018-2137-y.

(4) Bazzi, H.; Baghdadi, N.; Ienco, D.; El Hajj, M.; Zribi, M.; Belhouchette, H.; Jose Escorihuela, M.; Demarez, V. Mapping Irrigated Areas Using Sentinel-1 Time Series in Catalonia, Spain. *Remote Sens.* **2019**, *11* (15), 1836. https://doi.org/10.3390/rs11151836.

(5) Ozdogan, M.; Gutman, G. A New Methodology to Map Irrigated Areas Using Multi-Temporal MODIS and Ancillary Data: An Application Example in the Continental US. *Remote Sensing of Environment* **2008**, *112* (9), 3520–3537. https://doi.org/10.1016/j.rse.2008.04.010.

(6) Xie, Y.; Lark, T. J. Mapping Annual Irrigation from Landsat Imagery and Environmental Variables across the Conterminous United States. *Remote Sens. Environ.* **2021**, *260*, 112445. https://doi.org/10.1016/j.rse.2021.112445.

(7) Bazzi, H.; Baghdadi, N.; Amin, G.; Fayad, I.; Zribi, M.; Demarez, V.; Belhouchette, H. An Operational Framework for Mapping Irrigated Areas at Plot Scale Using Sentinel-1 and Sentinel-2 Data. *Remote Sensing* **2021**, *13* (13), 2584. https://doi.org/10.3390/rs13132584.

(8) Massari, C.; Modanesi, S.; Dari, J.; Gruber, A.; De Lannoy, G. J. M.; Girotto, M.; Quintana-Segui, P.; Le Page, M.; Jarlan, L.; Zribi, M.; Ouaadi, N.; Vreugdenhil, M.; Zappa, L.; Dorigo, W.; Wagner, W.; Brombacher, J.; Pelgrum, H.; Jaquot, P.; Freeman, V.; Volden, E.; Prieto, D. F.; Tarpanelli, A.; Barbetta, S.; Brocca, L. A Review of Irrigation Information Retrievals from

Space and Their Utility for Users. *Remote Sens.* **2021**, *13* (20), 4112. https://doi.org/10.3390/rs13204112.

(9) Courault, D.; Hadria, R.; Ruget, F.; Olioso, A.; Duchemin, B.; Hagolle, O.; Dedieu, G. Combined Use of FORMOSAT-2 Images with a Crop Model for Biomass and Water Monitoring of Permanent Grassland in Mediterranean Region. *Hydrology and Earth System Sciences* **2010**, *14* (9), 1731–1744. https://doi.org/10.5194/hess-14-1731-2010.

(10) Abubakar, M.; Chanzy, A.; Pouget, G.; Flamain, F.; Courault, D. Detection of Irrigated Permanent Grasslands with Sentinel-2 Based on Temporal Patterns of the Leaf Area Index (LAI). **2022**. https://doi.org/10.20944/preprints202205.0273.v1.

(11) Courault, D.; Bsaibes, A.; Kpemlie, E.; Hadria, R.; Hagolle, O.; Marloie, O.; Hanocq, J.-F.; Olioso, A.; Bertrand, N.; Desfonds, V. Assessing the Potentialities of FORMOSAT-2 Data for Water and Crop Monitoring at Small Regional Scale in South-Eastern France. *Sensors* **2008**, *8* (5), 3460–3481. https://doi.org/10.3390/s8053460.

(12) Simonneaux, V.; Duchemin, B.; Helson, D.; Er-Raki, S.; Olioso, A.; Chehbouni, A. G. The Use of High-Resolution Image Time Series for Crop Classification and Evapotranspiration Estimate over an Irrigated Area in Central Morocco. *Int. J. Remote Sens.* **2008**, *29* (1), 95–116. https://doi.org/10.1080/01431160701250390.

(13) Pena, M. A.; Liao, R.; Brenning, A. Using Spectrotemporal Indices to Improve the Fruit-Tree Crop Classification Accuracy. *ISPRS-J. Photogramm. Remote Sens.* **2017**, *128*, 158–169. https://doi.org/10.1016/j.isprsjprs.2017.03.019.

(14) Peña, M. A.; Brenning, A. Assessing Fruit-Tree Crop Classification from Landsat-8 Time Series for the Maipo Valley, Chile. *Remote Sensing of Environment* **2015**, *171*, 234–244. https://doi.org/10.1016/j.rse.2015.10.029.

(15) Nabil, M.; Farg, E.; Arafat, S. M.; Aboelghar, M.; Afify, N. M.; Elsharkawy, M. M. Tree-Fruits Crop Type Mapping from Sentinel-1 and Sentinel-2 Data Integration in Egypt?S New Delta Project. *Remote Sens. Appl.-Soc. Environ.* **2022**, *27*, 100776. https://doi.org/10.1016/j.rsase.2022.100776.

(16) Kordi, F.; Yousefi, H. Crop Classification Based on Phenology Information by Using Time Series of Optical and Synthetic-Aperture Radar Images. *Remote Sens. Appl.-Soc. Environ.* **2022**, *27*, 100812. https://doi.org/10.1016/j.rsase.2022.100812.

(17) Toosi, A.; Javan, F. D.; Samadzadegan, F.; Mehravar, S.; Kurban, A.; Azadi, H. Citrus Orchard Mapping in Juybar, Iran: Analysis of NDVI Time Series and Feature Fusion of Multi-Source Satellite Imageries. *Ecol. Inform.* **2022**, *70*, 101733. https://doi.org/10.1016/j.ecoinf.2022.101733.

(18) Misra, G.; Cawkwell, F.; Wingler, A. Status of Phenological Research Using Sentinel-2 Data: A Review. *Remote Sens.* **2020**, *12* (17), 2760. https://doi.org/10.3390/rs12172760.

(19) Zeng, L.; Wardlow, B. D.; Xiang, D.; Hu, S.; Li, D. A Review of Vegetation Phenological Metrics Extraction Using Time-Series, Multispectral Satellite Data. *Remote Sens. Environ.* **2020**, *237*, 111511. https://doi.org/10.1016/j.rse.2019.111511.

(20) Zheng, Y.; Wu, B.; Zhang, M.; Zeng, H. Crop Phenology Detection Using High Spatio-Temporal Resolution Data Fused from SPOT5 and MODIS Products. *Sensors* **2016**, *16* (12), 2099. https://doi.org/10.3390/s16122099.

(21) Garrity, S. R.; Bohrer, G.; Maurer, K. D.; Mueller, K. L.; Vogel, C. S.; Curtis, P. S. A Comparison of Multiple Phenology Data Sources for Estimating Seasonal Transitions in Deciduous Forest Carbon Exchange. *Agric. For. Meteorol.* **2011**, *151* (12), 1741–1752. https://doi.org/10.1016/j.agrformet.2011.07.008.

(22) Brown, M. E.; de Beurs, K. M.; Marshall, M. Global Phenological Response to Climate Change in Crop Areas Using Satellite Remote Sensing of Vegetation, Humidity and Temperature over 26 Years. *Remote Sens. Environ.* **2012**, *126*, 174–183. https://doi.org/10.1016/j.rse.2012.08.009.

(23) Salinero-Delgado, M.; Estévez, J.; Pipia, L.; Belda, S.; Berger, K.; Paredes Gómez, V.; Verrelst, J. Monitoring Cropland Phenology on Google Earth Engine Using Gaussian Process Regression. *Remote Sensing* **2022**, *14* (1), 146. https://doi.org/10.3390/rs14010146.

(24) Hanes, J. M.; Liang, L.; Morisette, J. T. Land Surface Phenology. In *Biophysical applications of satellite remote sensing*; Springer, 2014; pp 99–125.

(25) Henebry, G. M.; Beurs, K. M. de. Remote Sensing of Land Surface Phenology: A Prospectus. In *Phenology: An integrative environmental science*; Springer, 2013; pp 385–411.

(26) Frantz, D.; Stellmes, M.; Roeder, A.; Udelhoven, T.; Mader, S.; Hill, J. Improving the Spatial Resolution of Land Surface Phenology by Fusing Medium- and Coarse-Resolution Inputs. *IEEE Trans. Geosci. Remote Sensing* **2016**, *54* (7), 4153–4164. https://doi.org/10.1109/TGRS.2016.2537929.

(27) Nguyen, L. H.; Joshi, D. R.; Clay, D. E.; Henebry, G. M. Characterizing Land Cover/Land Use from Multiple Years of Landsat and MODIS Time Series: A Novel Approach Using Land Surface Phenology Modeling and Random Forest Classifier. *Remote Sens. Environ.* **2020**, *238*, 111017. https://doi.org/10.1016/j.rse.2018.12.016.

(28) Chen, X.; Wang, D.; Chen, J.; Wang, C.; Shen, M. The Mixed Pixel Effect in Land Surface Phenology: A Simulation Study. *Remote Sens. Environ.* **2018**, *211*, 338–344. https://doi.org/10.1016/j.rse.2018.04.030.

(29) Veloso, A.; Mermoz, S.; Bouvet, A.; Toan, T. L.; Planells, M.; Dejoux, J.-F.; Ceschia, E. Understanding the Temporal Behavior of Crops Using Sentinel-1 and Sentinel-2-like Data for Agricultural Applications. *Remote Sens. Environ.* **2017**, *199*, 415–426. https://doi.org/10.1016/j.rse.2017.07.015.

(30) Bradley, C.; Schwartz, M.; Xiao, X. Remote Sensing Phenology: Status and Way Forward. *Phenology of Ecosystem Processes—Applications in Global Change Research* **2009**, 231–246.

(31) de Beurs, K. M.; Henebry, G. M. Land Surface Phenology, Climatic Variation, and Institutional Change: Analyzing Agricultural Land Cover Change in Kazakhstan. *Remote Sens. Environ.* **2004**, *89* (4), 497–509. https://doi.org/10.1016/j.rse.2003.11.006.

(32) Zhang, X. Y.; Friedl, M. A.; Schaaf, C. B.; Strahler, A. H.; Hodges, J. C. F.; Gao, F.; Reed, B. C.; Huete, A. Monitoring Vegetation Phenology Using MODIS. *Remote Sens. Environ.* **2003**, *84* (3), 471–475. https://doi.org/10.1016/S0034-4257(02)00135-9.

(33) White, M. A.; de Beurs, K. M.; Didan, K.; Inouye, D. W.; Richardson, A. D.; Jensen, O. P.; O'Keefe, J.; Zhang, G.; Nemani, R. R.; van Leeuwen, W. J. D.; Brown, J. F.; de Wit, A.; Schaepman, M.; Lin, X.; Dettinger, M.; Bailey, A. S.; Kimball, J.; Schwartz, M. D.; Baldocchi, D. D.; Lee, J. T.; Lauenroth, W. K. Intercomparison, Interpretation, and Assessment of Spring Phenology in North America Estimated from Remote Sensing for 1982-2006. *Glob. Change Biol.* **2009**, *15* (10), 2335–2359. https://doi.org/10.1111/j.1365-2486.2009.01910.x.

(34) Wang, S.; Zhang, L.; Huang, C.; Qiao, N. An NDVI-Based Vegetation Phenology Is Improved to Be More Consistent with Photosynthesis Dynamics through Applying a Light Use Efficiency Model over Boreal High-Latitude Forests. *Remote Sens.* **2017**, *9* (7), 695. https://doi.org/10.3390/rs9070695.

(35) Lebrini, Y.; Boudhar, A.; Laamrani, A.; Htitiou, A.; Lionboui, H.; Salhi, A.; Chehbouni, A.; Benabdelouahab, T. Mapping and Characterization of Phenological Changes over Various Farming Systems in an Arid and Semi-Arid Region Using Multitemporal Moderate Spatial Resolution Data. *Remote Sens.* **2021**, *13* (4), 578. https://doi.org/10.3390/rs13040578.

(36) Jönsson, P.; Eklundh, L. TIMESAT—a Program for Analyzing Time-Series of Satellite Sensor Data. *Computers & Geosciences* **2004**, *30* (8), 833–845. https://doi.org/10.1016/j.cageo.2004.05.006.

(37) Ashourloo, D.; Nematollahi, H.; Huete, A.; Aghighi, H.; Azadbakht, M.; Shahrabi, H. S.; Goodarzdashti, S. A New Phenology-Based Method for Mapping Wheat and Barley Using Time-Series of Sentinel-2 Images. *Remote Sensing of Environment* **2022**, *280*, 113206. https://doi.org/10.1016/j.rse.2022.113206.

(38) Tuffery, L.; Davi, H.; López-García, N.; Rigolot, E.; Jean, F.; Stenger, A.; Lefèvre, F. Adaptive Measures for Mountain Mediterranean Forest Ecosystem Services under Climate and Land Cover Change in the Mont-Ventoux Regional Nature Park, France. *Reg Environ Change* **2021**, *21* (1), 12. https://doi.org/10.1007/s10113-020-01732-4.

(39) Trolard, F.; Bourrié, G.; Baillieux, A.; Buis, S.; Chanzy, A.; Clastre, P.; Closet, J.-F.; Courault, D.; Dangeard, M.-L.; Di Virgilio, N.; Dussouilliez, P.; Fleury, J.; Gasc, J.; Géniaux, G.; Jouan, R.; Keller, C.; Lecharpentier, P.; Lecroart, J.; Napoleone, C.; Mohammed, G.; Olioso, A.; Reynders, S.; Rossi, F.; Tennant, M.; de Vicente Lopez, J. The PRECOS Framework: Measuring the Impacts of the Global Changes on Soils, Water, Agriculture on Territories to Better Anticipate the Future. *Journal of Environmental Management* **2016**, *181*, 590–601. https://doi.org/10.1016/j.jenvman.2016.07.002.

(40) Séraphin, P.; Vallet-Coulomb, C.; Gonçalvès, J. Partitioning Groundwater Recharge between Rainfall Infiltration and Irrigation Return Flow Using Stable Isotopes: The Crau Aquifer. *Journal of Hydrology* **2016**, *542*, 241–253. https://doi.org/10.1016/j.jhydrol.2016.09.005.

(41) Weiss, M.; Baret, F.; Leroy, M.; Hautecoeur, O.; Bacour, C.; Prevot, L.; Bruguier, N. Validation of Neural Net Techniques to Estimate Canopy Biophysical Variables from Remote Sensing Data. *Agronomie* **2002**, *22* (6), 547–553. https://doi.org/10.1051/agro:2002036.

(42) *Zonal statistics in R | GeoProfesja*. http://geoprofesja.pl/en/zonal-statistics-in-r/ (accessed 2022-10-18).

(43) Rouse Jr, J. W.; Haas, R. H.; Schell, J. A.; Deering, D. W. *Monitoring the Vernal Advancement and Retrogradation (Green Wave Effect) of Natural Vegetation*; 1973.

(44) Gitelson, A. A.; Kaufman, Y. J.; Merzlyak, M. N. Use of a Green Channel in Remote Sensing of Global Vegetation from EOS-MODIS. *Remote Sens. Environ.* **1996**, *58* (3), 289–298. https://doi.org/10.1016/S0034-4257(96)00072-7.

(45) Huete, A.; Didan, K.; Miura, T.; Rodriguez, E. P.; Gao, X.; Ferreira, L. G. Overview of the Radiometric and Biophysical Performance of the MODIS Vegetation Indices. *Remote Sens. Environ.* **2002**, *83* (1–2), 195–213. https://doi.org/10.1016/S0034-4257(02)00096-2.

(46) Baret, F.; Guyot, G.; Major, D. J. TSAVI: A Vegetation Index Which Minimizes Soil Brightness Effects On LAI And APAR Estimation. In *12th Canadian Symposium on Remote Sensing Geoscience and Remote Sensing Symposium,*; 1989; Vol. 3, pp 1355–1358. https://doi.org/10.1109/IGARSS.1989.576128.

(47) Kaufman, Y.; Tanre, D. Atmospherically Resistant Vegetation Index (Arvi) for Eos-Modis. *IEEE Trans. Geosci. Remote Sensing* **1992**, *30* (2), 261–270. https://doi.org/10.1109/36.134076.

(48) Gitelson, A. A.; Keydan, G. P.; Merzlyak, M. N. Three-Band Model for Noninvasive Estimation of Chlorophyll, Carotenoids, and Anthocyanin Contents in Higher Plant Leaves. *Geophysical Research Letters* **2006**, *33* (11). https://doi.org/10.1029/2006GL026457.

(49) Gao, B. A Normalized Difference Water Index for Remote Sensing of Vegetation Liquid Water from Space. In *Imaging Spectrometry*; Descour, M. R., Mooney, J. M., Perry, D. L., Illing, L., Eds.; Spie - Int Soc Optical Engineering: Bellingham, 1995; Vol. 2480, pp 225–236. https://doi.org/10.1117/12.210877.

(50) Xiao, X. M.; Boles, S.; Liu, J. Y.; Zhuang, D. F.; Frolking, S.; Li, C. S.; Salas, W.; Moore, B. Mapping Paddy Rice Agriculture in Southern China Using Multi-Temporal MODIS Images. *Remote Sens. Environ.* **2005**, *95* (4), 480–492. https://doi.org/10.1016/j.rse.2004.12.009.

(51) Fisher, J. I.; Mustard, J. F. Cross-Scalar Satellite Phenology from Ground, Landsat, and MODIS Data. *Remote Sens. Environ.* **2007**, *109* (3), 261–273. https://doi.org/10.1016/j.rse.2007.01.004.

(52) Fisher, J. I.; Mustard, J. F.; Vadeboncoeur, M. A. Green Leaf Phenology at Landsat Resolution: Scaling from the Field to the Satellite. *Remote Sens. Environ.* **2006**, *100* (2), 265–279. https://doi.org/10.1016/j.rse.2005.10.022.

(53) Yang, X.; Mustard, J. F.; Tang, J.; Xu, H. Regional-Scale Phenology Modeling Based on Meteorological Records and Remote Sensing Observations. *J. Geophys. Res.-Biogeosci.* **2012**, *117*, G03029. https://doi.org/10.1029/2012JG001977.

(54) Zhong, L.; Gong, P.; Biging, G. S. Phenology-Based Crop Classification Algorithm and Its Implications on Agricultural Water Use Assessments in California's Central Valley. *Photogramm. Eng. Remote Sens.* **2012**, *78* (8), 799–813. https://doi.org/10.14358/PERS.78.8.799.

(55) Akbari, E.; Boloorani, A. D.; Samany, N. N.; Hamzeh, S.; Soufizadeh, S.; Pignatti, S. Crop Mapping Using Random Forest and Particle Swarm Optimization Based on Multi-Temporal Sentinel-2. *Remote Sens.* **2020**, *12* (9), 1449. https://doi.org/10.3390/rs12091449.

(56) Breiman, L. Random Forests. *Machine Learning* **2001**, *45* (1), 5–32. https://doi.org/10.1023/A:1010933404324.

(57) Meyer, H.; Reudenbach, C.; Hengl, T.; Katurji, M.; Nauss, T. Improving Performance of Spatio-Temporal Machine Learning Models Using Forward Feature Selection and Target-Oriented Validation. *Environ. Modell. Softw.* **2018**, *101*, 1–9. https://doi.org/10.1016/j.envsoft.2017.12.001.

(58) Jensen, J. R.; Lulla, K. Introductory Digital Image Processing: A Remote Sensing Perspective. *Geocarto International* **1987**, *2* (1), 65–65. https://doi.org/10.1080/10106048709354084.

(59) Genuer, R.; Poggi, J.-M.; Tuleau-Malot, C. Variable Selection Using Random Forests. *Pattern recognition letters* **2010**, *31* (14), 2225–2236.

(60) Usha, K.; Singh, B. Potential Applications of Remote Sensing in Horticulture—A Review. *Scientia Horticulturae* **2013**, *153*, 71–83. https://doi.org/10.1016/j.scienta.2013.01.008.

(61) Roland Colditz, R. An Evaluation of Different Training Sample Allocation Schemes for Discrete and Continuous Land Cover Classification Using Decision Tree-Based Algorithms. *Remote Sens.* **2015**, *7* (8), 9655–9681. https://doi.org/10.3390/rs70809655.

(62) Chen, B.; Jin, Y.; Brown, P. An Enhanced Bloom Index for Quantifying Floral Phenology Using Multi-Scale Remote Sensing Observations. *ISPRS Journal of Photogrammetry and Remote Sensing* **2019**, *156*, 108–120. https://doi.org/10.1016/j.isprsjprs.2019.08.006

Chapter 5

Characterization of grapevine canopy leaf area and inter-row management using Sentinel-2 time series.

5.1 Intention note

Data concerning vegetation cover and soil management are used in hydrological modelling. A wide spatial variability is generally observed for vineyards in Mediterranean regions (with grass or bare soils in inter-row, irrigated or not) which have an impact on water management. ., Remote sensing already has shown its ability and effectiveness in vegetation monitoring both spatial and temporal (Lanjeri et al., 2001; Primicerio et al., 2017).

Nevertheless, remote sensing signals can be difficult to analyse for heterogenous crops like grapevines and orchards having trees and backgrounds with grass or bare soils. (Borgogno-Mondino et al., 2018).

The study objective was to characterise canopy development and inter-row management of grapevine fields. The work is based on the analysis of the temporal profile of LAI averaged at plot scale. Ground observations were made on several fields in the Ouvèze area. These data were used to identify plots without grass and to better understand the spectral pattern. The main assumption was to consider that the background signal can be simulated by a double logistic model, with a plateau corresponding to the lowest level of LAI in summer. The background signal was then subtracted from the simulated canopy from the S2 LAI time series obtained for each plot of vineyards.

Résumé

Des données précises sur le couvert végétal sont essentielles à connaître pour la modélisation hydrologique ou la modélisation des productions. Notre étude s'est concentrée sur une analyse approfondie des données optiques satellitaires de la série chronologique Sentinel-2 (S2) en particulier l'indice de surface foliaire (LAI) pour caractériser des parcelles de vignes et la gestion de leur inter-rangs. Des observations de terrain ont été faites sur deux années -2021-2022) sur le bassin versant de de l'Ouvèze-Ventoux, dans le sud-est de la France, pour suivre la phénologie et le développement de 11 parcelles de vignes ayant des gestions différentes de l'inter-rang. La dynamique annuelle du LAI des parcelles a été ajustée avec un modèle à double logistique. Les observations de terrain ont permis de caractériser les paramètres du modèle qui correspondent à des parcelles avec des inter-rangs en sol nu. Le modèle correspondant a ensuite été soustrait aux profils temporels des parcelles de vignes et a permis de distinguer les parcelles enherbées des non enherbées. Les données pluviométriques ont été analysées en complément pour déterminer les explications possibles des variations dans le développement de l'herbe entre les rangs. Nous avons pu classer les

vignobles de u bassin de l'Ouvèze en 3 catégories : enherbée, partiellement enherbée et travaillée, et valider nos cartographies avec nos observations de terrain.

Mots-clés: télédétection, Sentinel-2, indice de surface foliaire, vigne, enherbement, canopée, gestion de l'inter-rang.

5.2 Graphical Abstract

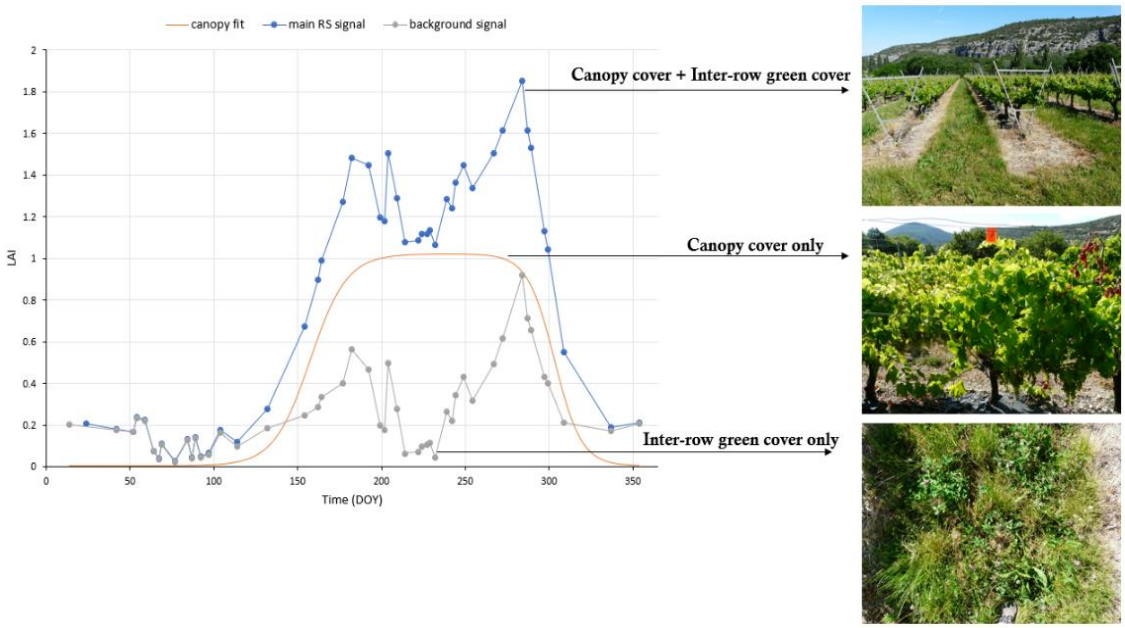

Characterisation of Grapevine Canopy Leaf Area and Inter-Row Management Using Sentinel-2 Time Series

Mukhtar Adamu Abubakar [1,2], André Chanzy[1*], Flamain Fabrice[1] and Dominique Courault[1]

[1] 1114 UMR INRAE-Avignon University EMMAH, Domaine St. Paul, 84914, Avignon, France

[2] Nasarawa State University Keffi, Faculty of Agriculture Shabu-Lafia Campus, Agronomy Department, Nasarawa State, Nigeria

DOI: https://doi.org/10.20870/oeno-one.2023.57.4.7703

*correspondence:
andre.chanzy@inrae.fr

Associate editor:
Bruno Tisseyre

Received:
2 August 2023

Accepted:
28 October 2023

Published:
23 November 2023

ABSTRACT

Accurate data on crop canopy are among the prerequisites for hydrological modelling, environmental assessment, and irrigation management. In this regard, our study concentrated on an in-depth analysis of optical satellite data of Sentinel-2 (S2) time series of the leaf area index (LAI) to characterise canopy development and inter-row management of grapevine fields. Field visits were conducted in the Ouveze-Ventoux area, South Eastern France, for two years (2021 and 2022) to monitor phenology, canopy development, and inter-row management of eleven selected grapevine fields. Regarding the S2-LAI data, the annual dynamic of a typical grapevine canopy leaf area was similar to a double logistic curve. Therefore, an analytic model was adopted to represent the grapevine canopy contribution to the S2-LAI. Part of the parameters of the analytic model were calibrated from the actual grapevine canopy dynamics timing observation from the field visits, while the others were inferred at the field level from the S2-LAI time series. The background signal was generated by directly subtracting the simulated canopy from the S2 LAI time series. Rainfall data were examined to see the possible explanations behind variations in the inter-row grass development. From the background signals, we could group the inter-row management into three classes: grassed, partially grassed, and tilled, which corroborated our findings on the field. To consider the possibility of avoiding field visits, the model was recalibrated on a grapevine field with a clear canopy signal and applied to two fields with different inter-row management. The result showed slight differences among the inter-row signals, which did not prevent the identification of inter-row management, thus indicating that field visits might not be mandatory.

KEYWORDS: Remote sensing, Sentinel-2, leaf area index, grapevine, characterisation, canopy, inter-row management

INTRODUCTION

Grapevine (*Vitis vinifera* L.) cultivation is one of the most widespread cultivations worldwide, and its practice in the Mediterranean is millennia-old (Corti *et al*., 2011). According to reports given by an international organisation of grapevine and wine (Roca, 2022) on the world, viticultural surfaces covered around 7.3 million hectares in 2021, with 3.3 million hectares within the EU (European Union) zone; Spain (13 % of the grapevine area) produced the most wine with France (11 %) in second.

OENO One | By the International Viticulture and Enology Society 2023 | volume 57–4

Grapevines mostly require good soils and, for table grapevines, good water resource management, too (Darouich *et al*., 2022). Conventionally, grapevines have been rainfed perennial woody crops as irrigation was prohibited by authorities for several wine qualities (Darouich *et al*., 2022). Nevertheless, because soil water stress seriously impacts the growth, yield, and grape quality (Zarrouk *et al*., 2012), irrigation practices have become more and more frequent, specifically across dry areas of South Europe (Esteban *et al*., 2001; Permanhani *et al*., 2016). Irrigation practices can vary a lot according to various factors: the soil type, the climatic demand, or the target in production quality. Inter-row management might differ by the management of the grass cover between the rows of grapevine. The grass can be kept in the field, leading to constant coverage that might have a positive impact on runoff, infiltration, and erosion, while a higher water consumption from the inter-row and an increased fire hazard might negatively impact the crop performance (Steenwerth and Belina, 2010; Whitmore and Schröder, 2007).

On the contrary, the grass is removed by frequent tillages, leading to opposite benefits and drawbacks. An intermediate situation is where part of the rows are tilled while in the other part, the inter-row is left grassed. In the context of climate change, there is an increasing need to irrigate perennial woody crops as vineyards that were rarely irrigated until now, especially with wine grapevine to gain in quality. Moreover, there is also a willingness to enhance ecosystem services of cropping systems, the management of inter-row being one of the levers to go in that direction. Therefore, delineating the green cover between the grapevine canopy and the vegetation in the background is an important issue for both the characterisation of the grapevine water need and, thus, the amount of irrigation and the detection of inter-row management practices. Moreover, Abubakar *et al*. (2023) have shown that inter-row management may lead to confusion in mapping the different perennial woody crops.

During the last decades, remote sensing is playing a significant role in crop supervision. Earth-observing (EO) satellites can record multispectral images with constant temporal revisit occurrence, documenting variations in spectral patterns among surfaces. This allows the detection of the spatial and temporal differences in crops. In recent times, the utilisation of remotely sensed information to promote decision and policy rulings has raised within the sectors of agriculture and forestry (Borgogno-Mondino *et al*., 2018; De Petris *et al*., 2019; Sarvia *et al*., 2019; Testa *et al*., 2014).

Regarding viticulture, airborne and spaceborne sensors can be utilised to characterise crop's yield spatial variability and describe soil features, crop varieties, and crop diseases (Arnó *et al*., 2009; Hall *et al*., 2003; Hall, 2018; Hall and Wilson, 2013; Karakizi *et al*., 2016a). Vegetation indices (VI) derived from multispectral reflectance can be exploited to acquire data on phenology, vegetation water content, and biomass over a growing season. In the past decades, several VI were unfolded (Gao, 1996 ; Huete, 1988 ; Motohka *et al*., 2010 ; Qi *et al*., 1994), with NDVI (normalised difference vegetation index) being the most widely used for crop growth dynamic descriptions. However, despite that fact, NDVI can be faced with some limitations like sensitivity restriction to vegetative photosynthetic dynamics (Wang *et al*., 2017), whereas biophysical variables like LAI (leaf area index) can be substituted to farmlands and were used advantageously to delineate different crop types (Abubakar *et al.*, 2022). Interpretation of the VI times series can bring advanced information on crop systems (Beniaich *et al*., 2022), management practices (Abubakar *et al*., 2022), irrigation needs (Darouich *et al*., 2022), and risk assessments on soil erosion (Rizzi *et al*., 2021).

The spatial resolution has a strong impact on the way to interpret remote sensing data, especially for perennial woody crops, which have spatial patterns (row, tree crown) that may be larger than the resolution. With a very high-resolution satellite (resolution lower than 5 m as WorldView-2 (Karakizi *et al*., 2016a)), it is possible to investigate within canopy details, for instance, the separation of the canopy and the soil background. However, such spaceborne sensors are mostly owned by private companies/firms, generating costs. Moreover, the revisit time might be large, preventing access to times series data capable of grasping the temporal feature over a crop cycle. Nonetheless, larger spatial resolution can be used to characterize vineyard inter-row management using time series, thanks to the difference in vegetation growth dynamics between grapevine and inter-row (Palazzi *et al.*, 2022). As an alternative, decametric resolution satellites such as the European Sentinel-2 (S2) can offer 10 m spatial resolution imagery and fine temporal revisits while being free of charge. Such spatial resolution does not permit a direct separation of the different field's components, but the free access and the possibility to access densely sampled times series are interesting properties to build applications.

Vaudour *et al.* (2010) used imageries coming from the SPOT satellite to zone viticultural terroirs in South Africa, while in Spain, Landsat images were used to detect grapevine fields by Rodriguez *et al*. (2006). Semmens *et al*. (2016) estimate daily field-scale evapotranspiration from satellite data coming from Landsat-8, MODIS (Moderate Resolution Imaging Spectroradiometer), and GEOS (Geosynchronous Equatorial Orbit Satellite) across two vineyards. Johnson *et al*. (2003) used multispectral high-resolution satellite imageries coming from IKONOS to characterise wine grapevine's leaf area. High-resolution satellite imageries were used, and it was observed that satellite information possesses the possibility to characterise or delineate quality parameters of wine grapevines (Kandylakis and Karantzalos, 2016). Landsat-8-derived NDVI (normalised difference vegetation index) was found to be highly correlated with aerial imagery-derived NDVI at the grapevine plot scale when evaluating grapevine vigour to build recommendation maps (Borgogno-Mondino *et al*., 2018). Nevertheless, some conducted research showed that the spatial resolution images coming from medium-resolution satellites are rarely adequate for grapevine field assessments because of the narrow spacing of the inter-row; such constraint is more evident among grapevine fields with huge heterogeneity, and higher resolution satellite information is capable of producing similar or equivalent results using aerial platforms (Erena *et al*., 2016; Matese and Filippo Di Gennaro, 2015). For instance, a detailed comparative analysis of grapevine multispectral imagery delivered by decametric satellite resolution (S2) and low-elevation UAV (unmanned aerial vehicle) platforms was proposed by Khaliq *et al* (2019). The success of S2 imagery and the UAV's high-resolution images was assessed while considering the known relation between NDVI and crop vigour. Comparisons were made between the information obtained from UAV and the S2 imagery by evaluating three different NDVI indices to accurately examine the grapevine's different spectral contribution in the surroundings by taking into note : (i) the total cropland surface (ii) the grapevine canopies only, and (iii) the grapevine inter-row. The results showed that the resolutions of the raw S2 satellite imagery might not be directly used to delineate grapevine variability. In reality, the inter-row surface contribution to the remotely sensed information might influence the NDVI estimation, leading to biased crop descriptors. Conversely, vigour maps calculated from the UAV imagery using pixel representation of crop canopies tend to be more linked to the in-field evaluation in comparison to the S2 satellite

imagery. In a different study on the characterisation of grapevines using high-resolution imagery, an object-based classification framework for grapevines was designed, developed, and evaluated to detect grapevine canopy and variety separation (Karakizi *et al*., 2016b). Innovative features (spectral, spatial, and textural), rules, segmentation scales, and a set of frameworks were suggested according to image analysis (object-based). The proposed methodology was evaluated on WorldView-2 (multitemporal) satellite imagery in Greece across four diverse regions for viticulture. The performed quantitative assessment showed the suggested approach detected over 89 % of grapevines with high completeness and correct detection rates. Evaluation of the grapevine canopy extraction was above 96 %, while the quantitative evaluation of the variety separation was above 85 % at the plot scale, although it is important to note that such satellite imagery with a very high spatial resolution (0.5 m) is not freely accessed. Anastasiou *et al*. (2018) aimed to assess spectral vegetation indices obtained via satellite and proximal sensing across different growth phases (veraison to harvest) of table grapevines of which NDVI and GNDVI (green normalised difference vegetation index) were computed by employing Landsat-8 satellite imagery and proximal sensing to examine the grapevine yield and quality characteristics. In this study, the proximal sensing was more accurate concerning the grape yield and quality in comparison to the satellite sensing.

However, in this current study, free, open-source multi-temporal data of S2 are used, and field-scale analysis was done. Time series of the leaf area index (LAI) and spectral bands are exploited in this study to characterise features of grapevine, particularly the canopy and inter-row coverage. At the field scale, analysis according to temporal evolutions of the LAI was used to examine inter-field differences of grapevine canopy and soil management strategies (i.e., identification of grassy and non-grassy inter-rows).

Recently, a phenology-based classification of perennial woody fruit crops (orchards, grapevines, and olives) based on S2 temporal profiles was conducted in South-Eastern France (Abubakar *et al*., 2023) with encouraging results. Despite the good results obtained, there is still room for improvement, especially among the grapevine class. The difficulty with the grapevine LAI signal is that confusion can occur between the grapevine canopy and the background leading to both signals having the same order of magnitude leading to some misclassifications. This is not the case with orchards that have a tree canopy contribution to the LAI signal significantly larger than that of the background. Consequently, we arrived at a different scientific question to be addressed in this current study concerning the grapevines classes. Can we separate the canopy signal and background signal, which depends on management practices, from the remote sensing (RS) LAI S2 data.

The objective of this paper is to develop a method based on decametric resolution remote sensing as that of Sentinel-2 or Landsat to characterise two features of interest for grapevine: the canopy leaf area to assess the transpiration and the resulting water need and the interrow management by identifying grassed and tilled interrows. The scientific issue is then to delineate in observed LAI the contribution from the vine and that from the background. In this study, we assumed that the LAI times series derived from remote sensing together with agronomic knowledge of the grapevine development across an annual cycle can be used to separate the contributions of the different vegetation components of a grapevine. The method was developed and implemented in the South-East of France.

MATERIALS AND METHODS

1. Description of the study sites and grapevine management

The research was carried out in the Ouvéze-Ventoux areas in the years 2021 and 2022. The area is located in southern France (44° 10' N and 5° 16' E) and covers a surface of 59 km² and an altitude ranging between 230 and 630 m a.s.l (Figure 1.) The study area encompasses forest and crops (mostly vineyards and orchards), the

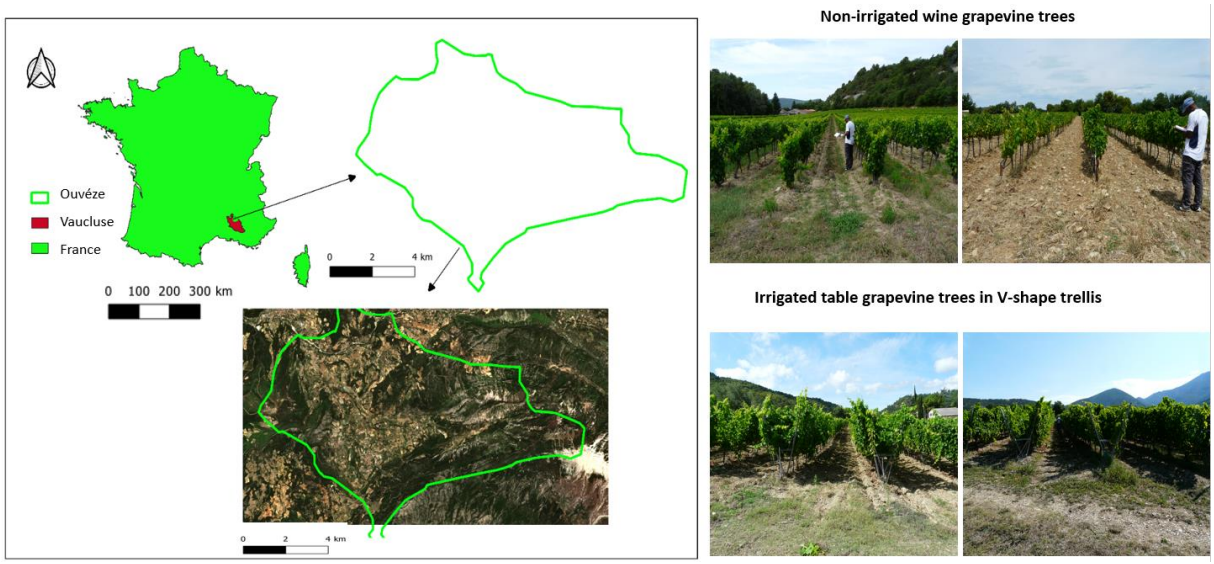

FIGURE 1. Map of France showing the location of the study site (Ouvèze-Ventoux) in the South-Eastern part of the country including photos of irrigated table and non-irrigated wine grapevine fields.

latter 57.7 % of the surface, 34 % of which are vineyards (Abubakar *et al*. 2023). The study site has a typical Mediterranean climate recognised by cold and moist winters with dry, hot summers; yearly rainfall is roughly 750 mm with a mean temperature of 12 °C.

The grapevines are planted in rows of 2 to 2.50 m apart for wine grapevines and 2.50 to 2.80 m apart for table grapevines. The ''V'' shape trellis was predominantly used for table grapevines. Part of the vineyards are irrigated (mostly the table grapevines) via drip irrigation. Irrigation strategies are different with small inputs in the case of wine grapevines to escape from very dry conditions while the amount of irrigation is much larger with table grapevine to maximise the fruit production. Inter/intra-row grass cover (background) development is governed by rainfalls and inter-row management. There are mainly three modes of inter-row management: tilled with regular harrowing to suppress weeds, grassed inter-row with regular mowing of the grass, and a mix of the two by tilling one inter-row over 2 or 3. Dry summer conditions lead to a drying out of the herbaceous stratum, with a very small remaining fraction of the green grass, whatever the inter-row management method.

2. Ground data

2.1 canopy development and phenology monitoring.

The experiment was conducted across two years (2021 and 2022). Eleven (11) plots of grapevines (4 table grapevines and 7 wine grapevines) were selected across the study area (Table 1). In each plot, five grapevine trees were randomly chosen to observe phenology and characterise the leaf development. On each grapevine tree, two branches were selected to count the leaves during the whole growing season (11 field visits every year) to characterise the dynamic of the leaf development. The standard protocol was to count the leaves number on the main branches and the sub-branches. In addition, specific observations were made to establish allometric

relationships to infer leaf surface area from the leaf counts. Therefore, at three dates across the grapevine cycle (20-05-2022, 05-07-2022, and 07-10-2022), the leaf lengths (from the petiolar sinus to the end of the apical lobe) of every leaf on a selection of monitored branches (from 58 to 30) were measured. The lengths thus measured were then converted into surface area using a relationship between length and surface area established on sets of leaves of different sizes taken from each of the plots. The results showed that a single relationship was sufficient to characterise the leaf area of the different grapevine varieties monitored in this work. At the end of the process, we obtained three allometric relationships for each of the leaf length measurement dates linking the leaf surface (cm^2 per branch) to the leaf number (Figure 2). Figure 2 exhibits a variation of the relationship across the year and, thus, the different relationships were estimated as follows. Up until March 20th, we used the allometric function established on 20-05-2022. From March 21st to October 6th, we applied the second relationship established on 05-07-2022, and finally, the relationship obtained on 07-10-2023 was applied after October 7th. The estimated leaf surface per branch was then averaged at the field level and then normalised using the maximum value of every time series.

2.2 Assessments of background coverage

Standardised RGB photos were taken using a digital camera to characterise the background coverage using vertical views in three locations in the plot inter-row, the location remaining the same across the season to maintain the same ROI (region of interest). To estimate the degree of soil surfaces covered by the background vegetation, the percentage of the ground cover was estimated using the SegVeg model for semantic segmentation of RGB photos into soil background portion, green vegetation portion, and senescent portion as described by Serouart et al. (2022). It is in conformity with the U-net model that delineates vegetation from the background (after training across a dataset that is very large and diverse) Pixels of the vegetation are subsequently

TABLE 1. Descriptions of the eleven selected grapevine fields.

Plot ID	Variety	Inter-row management strategy	Irrigation
45	Table grapevine	Grassed	Irrigated
203	Wine grapevine	Partially grassed	Non-irrigated
204	Wine grapevine	Constantly tilled	Non-irrigated
1901	Table grapevine	Grassed	Irrigated
2026	Wine grapevine	Tilled	Non-irrigated
2335	Wine grapevine	Tilled	Non-irrigated
3064	Table grapevine	Grassed	Irrigated
3121	Table grapevine	Tilled	Irrigated
3138	Wine grapevine	Tilled	Non-irrigated
3140	Wine grapevine	Tilled	Non-irrigated
3358	Wine grapevine	Partially grassed	Non-irrigated

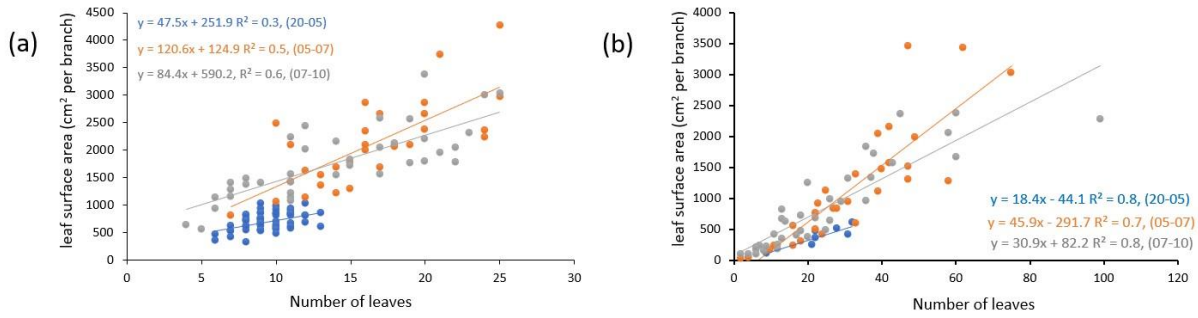

FIGURE 2. The three linear allometric relations (a) for main branches and (b) sub-branches used for the conversion portion, and senescent portion as described.

classified using a Support Vector Machine (SVM) shallow machine learning approach trained on grids extracted pixels applied to the RGB photos. We used an already trained SegVeg model (Serouart et al. 2022), leading to a vegetation cover fraction ranging from 0 to 1. The presence of senescent vegetation (pruned residues or dried grasses) was not taken into account in the vegetation cover. A qualitative assessment of the results was done, leading to the removal of images with shadows from the analysis.

3. Rainfall conditions at the experimental site.

Among the components of weather, only rainfall data was used. The rainfall data used in this study were extracted from the weather station of Entrecheaux for both years (2021 and 2022) located in the studied area with a distance to the fields that range from 1 to 5 km. The cumulated rainfall value for 2021 was 664.8 mm, and for 2022 was 754.8 mm, respectively. In particular, the year 2022 was wetter (more precipitation) than 2021 but also had the driest summer. Rainfall data analysis was useful to examine grass dynamics, especially in the summertime when grass regrowth might be stimulated by a rainfall event.

4. Satellite data

In this study, we used Sentinel-2 (S2) time series (optical images) collected from both Sentinel-2A and Sentinel-2B, considering all cloud-free images during the years 2021 and 2022. Images were provided by an open-source service centre named THEIA (https://www.theia-land.fr/, accessed on 17 January 2023). We worked with S2 level 2A, which is spatially registered and corrected for atmospheric effects. The products are delivered with a cloud mask used to filter the images. The number of used images varies across the two years; for instance, there were 50 and 53 available images in 2021 and 2022, respectively.

The leaf area index (LAI) utilised in this research was calculated via the BVNET algorithm (Weiss et al., 2002), which is based on the green (B3), red (B4), and near-infrared (B8) bands. The quality of this algorithm was proven and thus it was incorporated into the ESA (European Space Agency) S2 toolbox. The algorithm is based on the neural network trained on simulated spectral reflectance using the SAIL radiative transfer model (Weiss et al., 2002). The SAIL model is adapted to homogeneous canopies as field crops, and using it to structured plant cover such as orchards and vineyards remains questionable. However, in Abubakar et al. (2023), it was found that the LAI derived from the BVNET algorithm can track the leaf development dynamic. The LAI was computed on each 10m resolution pixel, and then the LAI average was computed for every field using the R function of zonal statistics (Zonal Statistics in R | GeoProfesja, 2016). To avoid any border effect, a buffer of 20 m from the field limit was removed before the averaging.

5. Analytic model and calibration

In this study, we assumed that the vine leaf area dynamic can be represented by a double logistic model (Fisher et al., 2006 ; Fisher and Mustard, 2007), which has proved to be efficient in describing the LAI dynamic of orchards and

vineyards (Abubakar et al., 2023). The analytic relationship is given in Equation 1.

$$Eq.\,1: V(t) = vmin + vamp\left(\frac{1}{1+e^{m1-n1t}} - \frac{1}{1+e^{m2-n2t}}\right)$$

Where V(t) represents a vegetation index (LAI in our case) at time t, *vmin* is the minimum V value, and *vamp* is the amplitude of V variations. Parameters m1, n1, m2, n2 are the curve-shape controlling parameters. The n1 and n2 parameters represent the slope at inflexion points, as shown below in Figure 3a, while m1 and m2 are the timing of the inflexion point. The problem with the vineyard is that there is a risk of confusion between the grassed background, which has its dynamic on the grapevine canopy since both components might have a similar weight in the overall LAI (Figure 3c). This hampers the possibility of determining the double logistic model parameters and consequently prevents identifying the vine canopy development. Such a feature was noticed in Abubakar et al. (2023) with the possibility of vineyard misclassification due to early grass development that provides leaf growth earlier than expected with grapevine. The results of the leaf development observations are displayed in Figure 3b. The observed leaf surface should be considered as a proxy of the LAI, whose main characteristic is to describe the temporal dynamic of the canopy development. The leaf surfaces were normalised using the maximum value observed in each field. Figure 3b clearly shows the relevance of using the double logistic model and shows a good synchronisation of the temporal patterns over the growing and plateau phases.

These observations were the foundation of the additional hypothesis used to constrain the fitting procedure. Based on the field observations, we can determine critical dates that correspond to *vmin, vmax=vmin+vamp*, and intermediate points in the growing and senescence phases corresponding to (*Vmin+¼Vamp*), ½, and ¾ of the amplitude (see Figure 3c). To determine the V value at those critical times, we need to

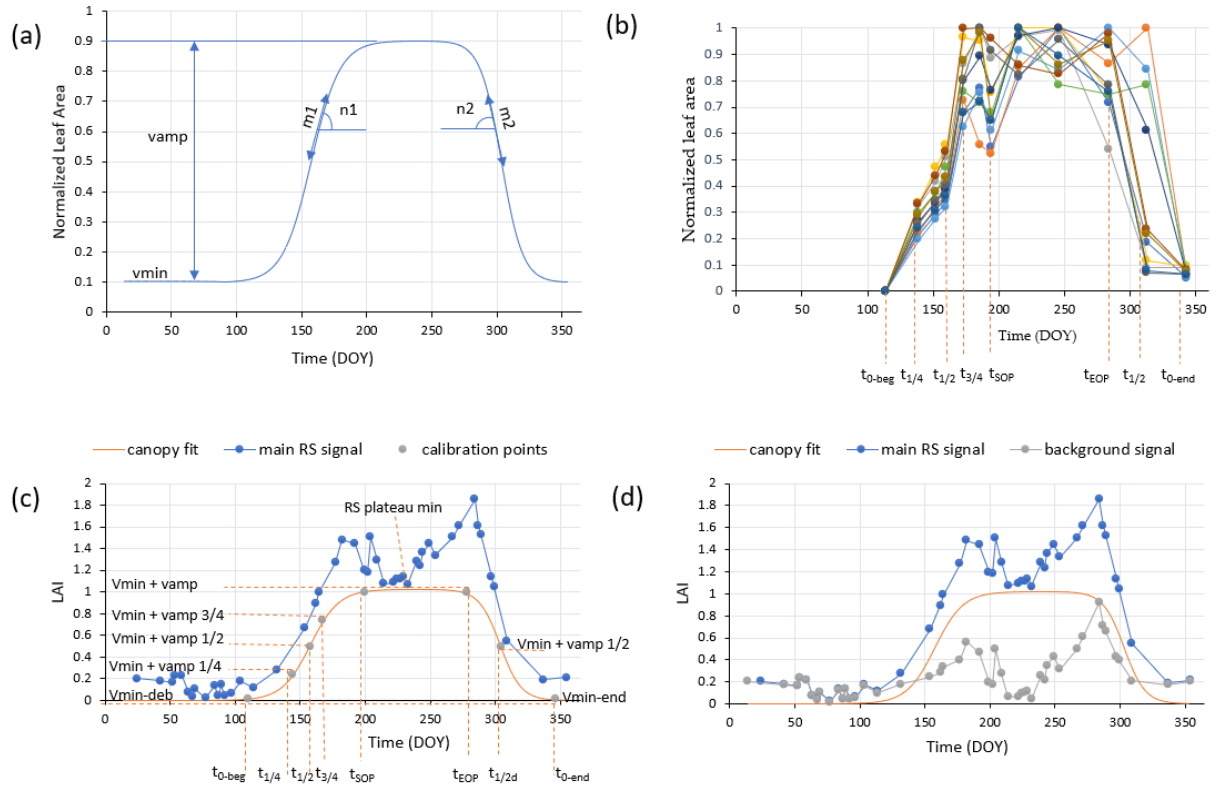

FIGURE 3. (a) analytic model showing Eq. 1 parameter effect (b) canopy developments from the field visits data showing selected time used for the model calibration (c) the simulated canopy from the S2

data showing the calibration points (d) the separation of canopy and background from S2 data of a given irrigated table grapevine field.

determine *Vmax and Vmin*. These values were taken from the LAI time series. *Vmin* was derived from a field with a tilled interrow, taking into account the field presenting a flat and the lowest LAI in winter. This value was then applied to all other fields. *Vmax* is characterised by every field's times series by taking the minimum value during the plateau phase. In doing so, the underlying assumption is that, whatever the inter-row management method, there is a point during the summer drought when the vegetation is completely dried out, allowing us to hypothesise that the grassed contribution to LAI is negligible.

From that hypothesis, we can generate a grapevine LAI time series at the critical times mentioned above. Then, the parameters n1, n2, m1, and m2 were determined using a non-linear fitting algorithm (nls function in R). The last step is to remove from the observed LAI time series the fitted vine LAI to obtain the LAI of the background (Figure 3d).

RESULTS

1. Grapevine canopy and background field observation

The data obtained on the evaluation of the grapevine leaf area were presented (Figure 3b) and partially discussed in the previous section. The measurements obtained on a sample of branches provide a good reflection of leaf evolution but do not allow us to compare LAI from one plot to another since the number of branches per grapevine is also an important datum that was not recorded. The evolution clearly shows the growth, plateau, and senescence phases. The first two phases are remarkably synchronous despite the diversity of the grape varieties used (different varieties for wine grapes and table grapes). More marked differences can be observed in the senescence phase. Between the two years, we noted a slight shift of a few days, with vegetation in 2022 ahead of 2021. The surface dynamic shows a drop at the beginning of the plateau, in line with thinning operation. Such an operation could have an impact on the detection of minimum LAI in the plateau phase.

The temporal patterns of the inter-row grass coverage are displayed in Figure 5 for the two years. The temporal patterns reflect the weather nature of the study area by having a significant drop in summer and a rise in both winter and autumn, as shown in Figure 5. From DOY 150 to 215, i.e., when the inter-row decline was observed, strong water deficits were recorded with cumulative daily rainfall of 54 mm (the potential evapotranspiration being 325 mm) in 2021 and 37.6 mm (the potential evapotranspiration being 315 mm) in 2022. Due to the significant variation in inter-row management strategies among the selected grapevines, the drop in the green vegetation still varies among fields with some having a drastic drop (for instance the constantly tilled plots), while in some fields the drop is not so drastic (for instance plots that have grassed inter-row). Such a drop in the summer confirms our hypothesis that in the summer, there are times when the grass contribution to LAI is negligible. However, the hypothesis is questionable with table grapevine fields 45, 1901, and 3064 that had a grassed inter-row and were irrigated. In that case, the grapevine canopy is very high, and the impact of the grassed inter-row might be minimised.

2. Delineation of canopy and soil background from the remote sensing data

The method was applied to each field, considering the specific *Vmax* for each of them. The canopy development for one of the selected grapevine is displayed below with all the calibration points (Figure 5). In this figure, we can make a qualitative assessment of the background dynamic as displayed by the picture. After tillage within some part of the growing season, there is re-emergence of the inter-row grasses coverage as seen in Figure 5 below ; which can be explained by rainfall that may stimulate the regrowth between the two tillage events shown in the two

mid photos. The regrowth of the grass shown in the last picture is also visible on the background LAI signal. When comparing the grapevine results, we can see that the timing of the growing and senescence phases was consistent. For the background, the overall trend is well reproduced, with high LAI in spring and fall while the grass cover decreases strongly in summer

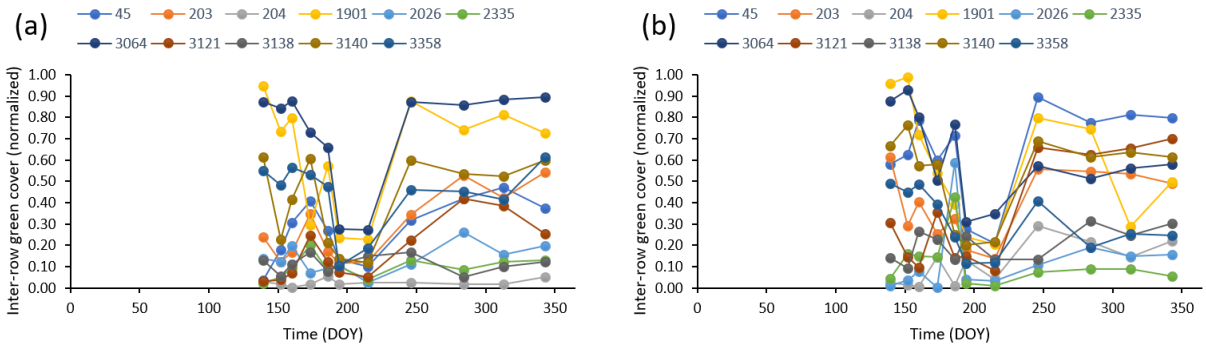

FIGURE 4. Temporal pattern of the inter-row green vegetation cover from the field visits data (with plot ID indicated above the figures) in 2021 (a) and 2022 (b).

Some variations in both signals were not always consistent due to some shifts in acquisition dates and very sharp variations in grass dynamics due to tillage and rainfall. The main parameters used including their timings are *vmin*_deb (110 DOY), *vmin*+*vamp*1/4 (144 DOY), *vmin*+*vamp*1/2 (158 DOY), *vmin*+*vamp*3/4 (167 DOY) *vmin*+*vamp*_SOP (199), *vmin*+*vamp*_EOP (272 DOY), *vmin*+*vamp*1/2 (304 DOY), *vmin*_end (346 DOY).

3. Evaluation of the vine LAI

The developped method was evaluated by considering the observations made on the 03/08/2023 when the canopy is expected to be fully developped. The average and standard deviation of the canopy width from the five selected grapevine tree was determined across each field. A relation was determined between the remotely sensed LAI (RS-LAI) and the average canopy width (of the same date) for each field with error bars on the ground measurements, as shown in Figure 6 below. The evaluation was done independently for table (Figure 6a) and wine grapevines (Figure 6b), as the grapevine trees are managed differently. The increase in the RS-LAI is somewhat directly linked to an increase in the canopy width, but the strong uncertainties on the ground observations might affect this evaluation strongly.

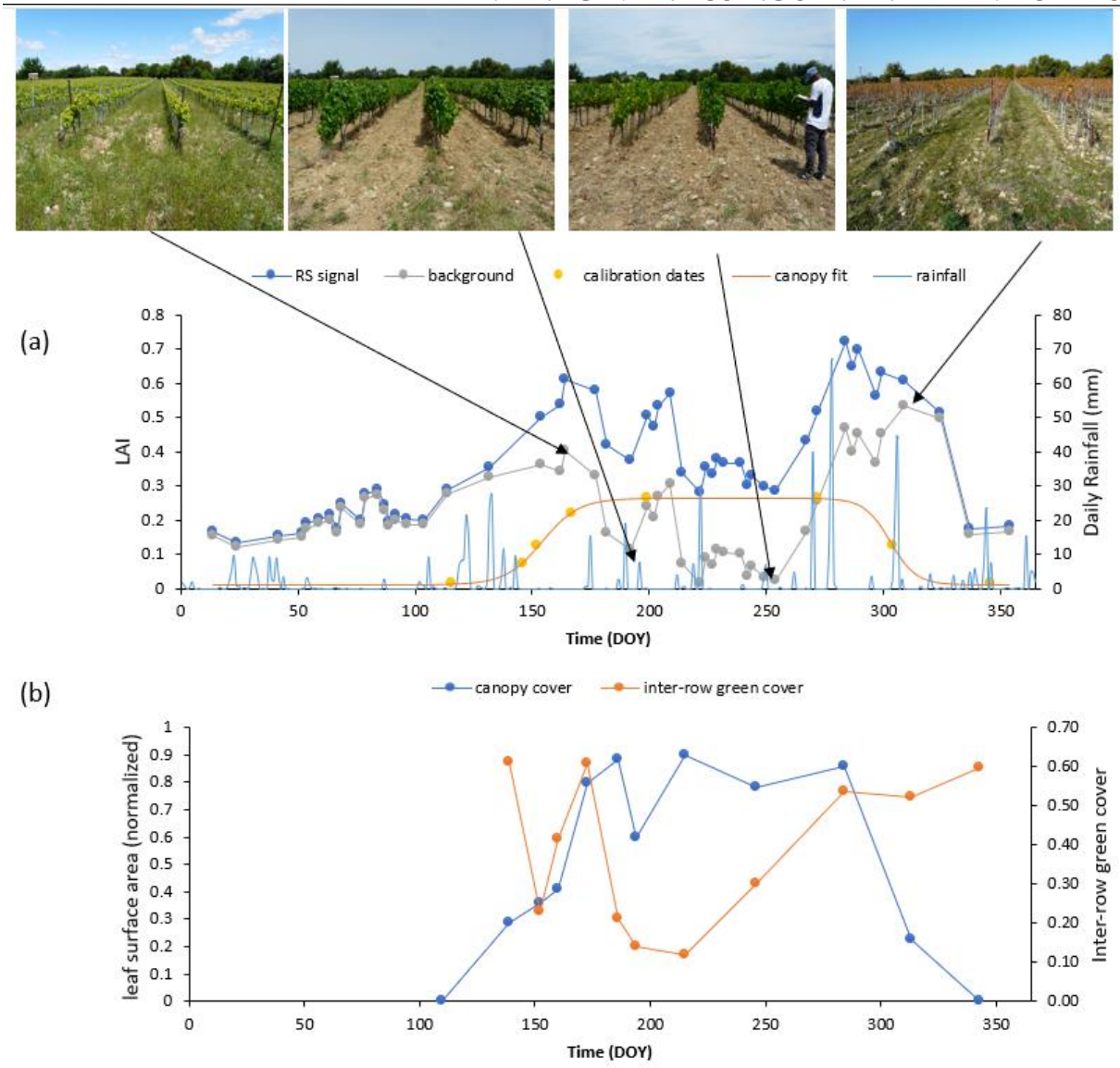

FIGURE 5. Results obtained with field ID 3140: (a) Separation of canopy and background green cover from remote sensing LAI signal and the rainfall data of a grapevine plot with field ID 3140. The points on the yellow curve are those used to calibrate the grapevine LAI curve. In (b), the curves correspond to the observed canopy leaf area and background green vegetation cover.

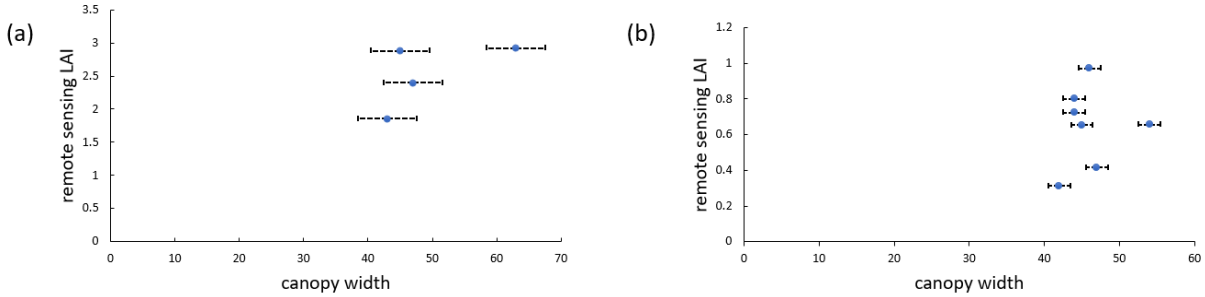

FIGURE 6. Table grapevine RS-LAI and canopy width relations (a) and wine grapevine RS-LAI and canopy width relations (b).

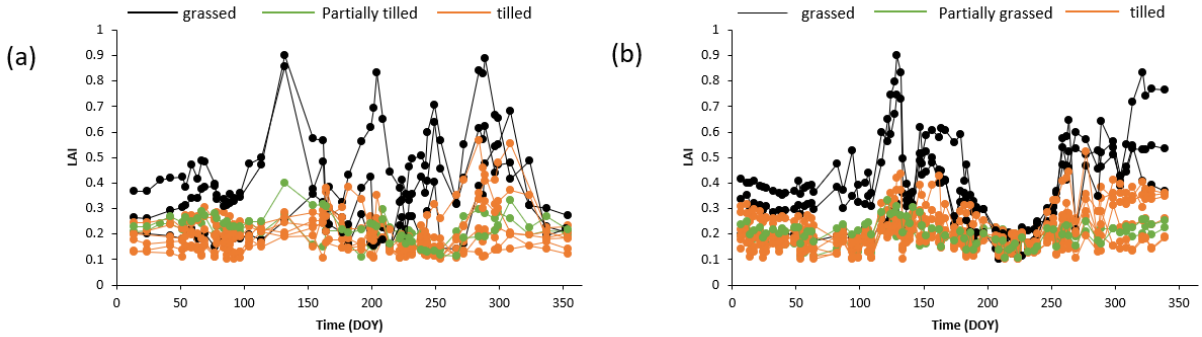

FIGURE 7. Temporal patterns of background LAI time series for 2021 (a) and 2022 (b). The black curves correspond to the grassed, green to the partially tilled, and orange to the tilled inter-row management.

4. Identification of inter-row management strategies from remote sensing data

The background LAI time series are displayed in Figure 7, and the colour scheme is used to distinguish the three management classes : tilled, partially grassed, and grassed. For the grassed class (black lines), we can observe strong variations in LAI that reflect growth, mowing, and summer senescence. Overall, the grassed class presented a yearly average LAI, which was significantly larger than the other modes, with an average of 0.36 compared to 0.19 to 0.21 values obtained with the other two classes. One can note that the differences were even larger when considering the spring period until DOY = 150. Therefore, the yearly (or spring average) average LAI over the year might be a useful metric to separate grassed and tilled inter-rows. As a matter of fact, the lowest yearly average in the grassed class (0.30) is always larger than the maximum obtained in the other class (0.24). On the other hand, the tilled and partially grassed classes are difficult to distinguish. A comparison of the retrieved LAI with the inter-row vegetation cover led to a significant relationship with an R^2 = 0.4. The quality of this comparison is affected by the uncertainties in the vegetation cover due to the sampling, the error in image processing, and the difference in time between the remote sensing data and the close field observation. However, a qualitative assessment made with the field pictures as shown in Figure 5 showed consistency between the background LAI time series and the grass development in the inter-rows.

DISCUSSION

1. **Impact of grapevine trimming and thinning management.**

Grapevine canopies are subjected to several management practices, such as pruning, trimming, or thinning, among others, for canopy structure manipulations. The shoot trimming is done to regulate the excess growth spread of the grapevines across the fields (regulate shoot vigour) by adopting several approaches of canopy management (shoot trimming or thinning) (Smart, 1985). Thinning or trimming of shoot remains one of the extensively adopted management strategies in viticulture to regulate canopy density, improve interception of sunlight, optimise photosynthetic dynamics, improve fruit microclimate, and eventually enhance fruit yield and quality of the wine (Costa et al., 2016). Figure 8 displays the temporal data obtained from the field visits and RS-LAI time series. With the field observation, one can notice that, in general, there is a slight decrease in the leaf surface area observations (highlighted with a red circle) on the sixth field visit which corresponds to 12–13 of July 2021. Such drop in the leaf surface area is ascribed to the first shoot thinning management, as demonstrated by the picture showing the removed shoots left on the ground. On the contrary, the RS-LAI signals from Figure 8 have failed to display such a reduction in leaf area. It is interesting to implement our approach that

needs to take profit of a minimum value, and it is interesting to have it not impacted by a thinning event. However, it also reflects that LAI estimated by remote sensing is not so sensitive to leaf area reduction within the grapevine canopies. This questions the LAI algorithm itself but also indicates that some management practices such as thinning and pruning can not be observable on the 10-metre resolution images delivered by the Sentinel 2 satellite

2. Is the proposed method dependent on field observations

The leaf growth is governed by the temperature (Malheiro et al., 2013) and is tightly linked to the phenology. It also depends on grapevine varieties, while water stress may impact the grapevine LAI dynamic. In our study, the timing of the plant development as the growth, the plateau, and the senescence phases were set up on ground observations. In other locations having different climates and grapevine varieties, there is a need to adapt the timing of the different phases. One can question the need for field observation and then the resulting burden of collecting leaf area in several fields. One can ask if such an observation step is mandatory or if we can infer the timing characteristics directly from the RS times series. In our data set, we can take profit from vineyards where the LAI time series is dominated by the grapevine canopy. A good candidate for that is a field with a LAI times series having low LAI in winter and spring and a LAI significantly higher during the crop seasons, as shown with field 3121 in Figure 9a. From that curve, we can determine the *Vmax* as done previously and then determine the time corresponding to the start and the end of the season (*t0-deb* and *t0-end*), the plateau (*tSOP* and *tEOP*), and the intermediate points during the growing and senescence phases (*t1/4, t1/2*, and *t3/4*). These points are displayed in the orange curves in Figure 9a. The differences in time between the remote sensing and field approaches reached a maximum of 17 days for *tSOP* and was, on average, equal to 10 days. The plateau duration was expended by 20 days, and the senescence phase was delayed when using the remote sensing time series in comparison to the field observations. If such differences in the development timing have no impact on the maximum LAI, their impacts on the vegetation component time series might be significant. Figure 9b displays the LAI times series of the background using the two methods (with or without field observation) on three fields representative of the three management classes. As expected, differences were found during the growing and senescence phases. However, such differences remain small in comparison to the differences observed between management practices and, thus, the possibility to identify grassed inter-row remains possible. Such a result is encouraging and opens the possibility of applying the method in different areas with the use of remote sensing data only. This is an important property for the model scalability and its implementation in wide areas.

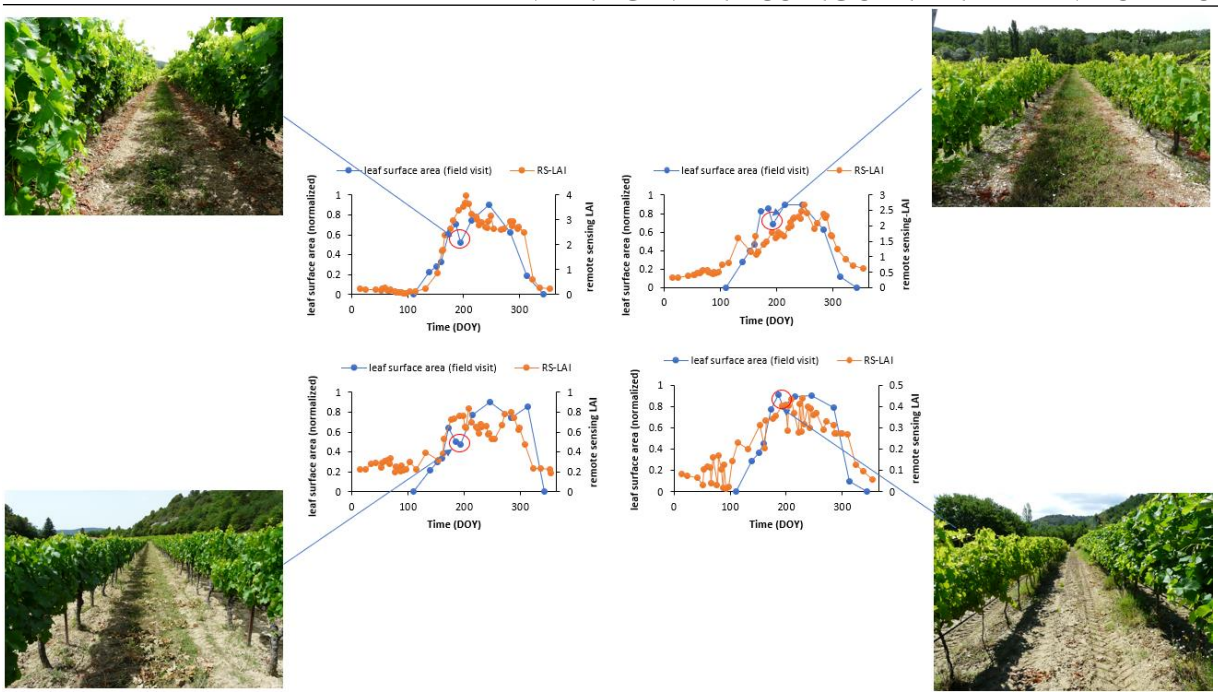

FIGURE 8. Temporal evolution of canopy dynamic and the temporal evolutions of the RS-LAI signal for the year 2021.

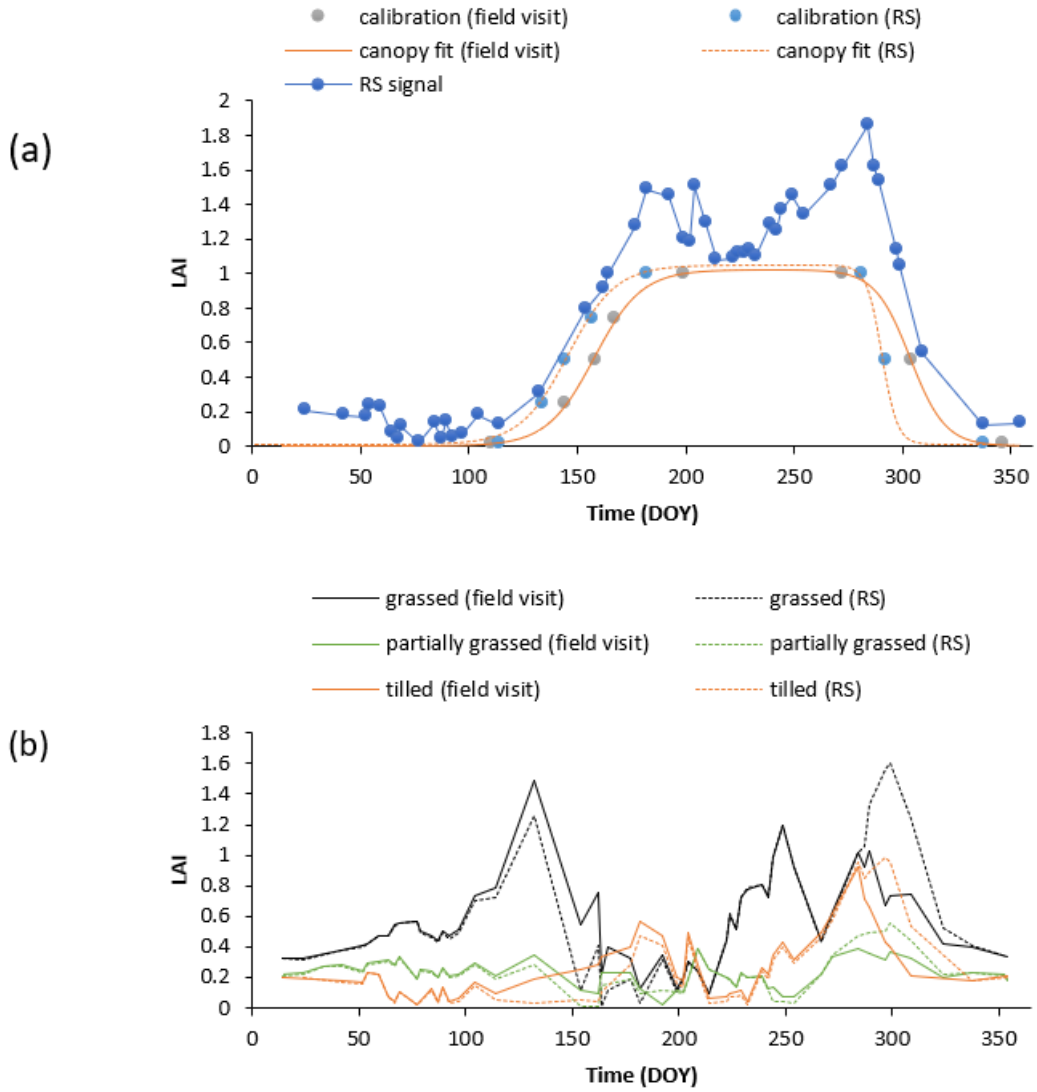

FIGURE 9. (a) RS-LAI signal of a clear and fully-grown grapevine tree where a good case was identified with calibration fit from field visit and RS data (b) comparison of the background LAI time series on three fields representative of the different management classes: Grassed inter-row (black for field 1901), tilled interrow (orange for field 3121), and partially tilled (green for field 203). The solid lines correspond to the implementation of the method using field observations, while the dashed lines correspond to the implementation using remote sensing only

CONCLUSIONS

In this work, we propose a method for characterising two important characteristics of grapevines, namely the LAI of the grapevine canopy and inter-row management. We showed that these data are accessible from the LAI time series derived from a decametric resolution satellite such as Sentinel 2, which has the advantage of offering frequent and free data over the whole globe but at a resolution that does not allow us to enter into the description of the constituent elements of a plant canopy such as the vineyards. The proposed method is based on assumptions about canopy dynamics supported by field observations, and on the presence of periods during the summer when the contribution of the herbaceous canopy may be neglected, due either to tillage or to the drying out of the grass as a result of water stress. The

method was applied to eleven (11) vineyards with different types of management and grape varieties. The results obtained led to interesting qualitative results on LAI, and we have succeeded in separating grass-covered vines from vines in which the inter-row is tilled. We have shown that we can dispense with field observation and base our methods solely on remote sensing data. These promising results now need to be evaluated against more quantitative data and applied on a larger scale.

ACKNOWLEDGMENTS

The authors are grateful to Petroleum Technology Development Funds (PTDF) under the Federal Ministry of Petroleum Resources, Nigeria, for awarding the overseas scholarship to the leading author in collaboration with INREA-EMMAH-Avignon and Avignon University. The work was done in the frame of the PRIMA project n°1633 IRRIWELL. The authors would like to thank and appreciate the respective selected grapevine farmers for the use of their grapevine fields for two years of experimentation and the Entrecheaux weather station for providing access to the rainfall data. We thank the reviewers for their kind and wise comments that helped us to improve the quality of the paper.

REFERENCES

Abubakar, M. A., Chanzy, A., Flamain, F., Pouget, G., & Courault, D. (2022). Detection of Irrigated Permanent Grasslands with Sentinel-2 Based on Temporal Patterns of the Leaf Area Index (LAI). Remote Sensing, 14(13), 3056. https://doi.org/10.3390/ rs14133056

Abubakar, M. A., Chanzy, A., Flamain, F., Pouget, G., & Courault, D. (2023). Delineation of Orchard, Vineyard, and Olive Trees Based on Phenology Metrics Derived from Time Series of Sentinel-2. Remote Sensing, 15(9), 2420. https://doi.org/10.3390/rs15092420

Anastasiou, E., Balafoutis, A., Darra, N., Psiroukis, V., Biniari, A., Xanthopoulos, G., & Fountas, S. (2018). Satellite and Proximal Sensing to Estimate the Yield and Quality of Table Grapes. Agriculture, 8(7), Article 7. https://doi.org/10.3390/ agriculture8070094

Arnó, J., Martínez Casasnovas, J. A., Ribes Dasi, M., & Rosell, J. R. (2009). Review. Precision viticulture. Research topics, challenges and opportunities in site-specific vineyard management. Spanish Journal of Agricultural Research, 7(4), 779. https://doi.org/10.5424/ sjar/2009074-1092

Beniaich, A., Silva, M. L. N., Guimaraes, D. V., Avalos, F. A. P., Terra, F. S., Menezes, M. D., Avanzi, J. C., & Candido, B. M. (2022). UAV-based vegetation monitoring for assessing the impact of soil loss in olive orchards in Brazil. Geoderma Regional, 30, e00543. https://doi.org/10.1016/j.geodrs.2022.e00543

Borgogno-Mondino, E., Lessio, A., Tarricone, L., Novello, V., & de Palma, L. (2018). A comparison between multispectral aerial and satellite imagery in precision viticulture. PRECISION AGRICULTURE, 19(2), 195–217. https://doi.org/10.1007/s11119- 017-9510-0

Corti, G., Cavallo, E., Cocco, S., Biddoccu, M., Brecciaroli, G., & Agnelli, A. (2011). Evaluation of erosion intensity and some of its consequences in vineyards from two hilly environments under a Mediterranean type of climate, Italy. Soil Erosion Issues in Agriculture, 113–160.

Costa, J. M., Vaz, M., Escalona, J., Egipto, R., Lopes, C., Medrano, H., & Chaves, M. M. (2016). Modern viticulture in southern Europe: Vulnerabilities and strategies for adaptation to water scarcity. Agricultural Water Management, 164, 5–18. https://doi. org/10.1016/j.agwat.2015.08.021

Darouich, H., Ramos, T. B., Pereira, L. S., Rabino, D., Bagagiolo, G., Capello, G., Simionesei, L., Cavallo, E., & Biddoccu, M. (2022). Water Use and Soil Water Balance of Mediterranean Vineyards under Rainfed and Drip Irrigation Management: Evapotranspiration Partition and Soil Management Modelling for Resource Conservation. Water, 14(4), 554. https://doi.org/10.3390/ w14040554

De Petris, S., Berretti, R., Sarvia, F., & Borgogno-Mondino, E. (2019). Precision arboriculture: A new approach to tree risk management based on geomatics tools. In C. M. U. Neale & A.

Maltese (Eds.), Remote Sensing for Agriculture, Ecosystems, and Hydrology Xxi (Vol. 11149, p. 111491G). Spie-Int Soc Optical Engineering. https://doi.org/10.1117/12.2532778

Erena, M., Montesinos, S., Portillo, D., Alvarez, J., Marin, C., Fernandez, L., Henarejos, J. M., & Ruiz, L. A. (2016). Configuration and Specifications of an Unmanned Aerial Vehicle for Precision Agriculture. In L. Halounova, V. Safar, C. K. Toth, J. Karas, G. Huadong, N. Haala, A. Habib, P. Reinartz, X. Tang, J. Li, C. Armenakis, G. Grenzdorffer, P. LeRoux, S. Stylianidis, R. Blasi, M. Menard, H. Dufourmount, & Z. Li (Eds.), XXIII ISPRS CONGRESS, COMMISSION I (Vol. 41, Issue B1, pp. 809–816). Copernicus Gesellschaft Mbh. https://doi.org/10.5194/ isprsarchives-XLI-B1-809-2016

Esteban, M. A., Villanueva, M. J., & Lissarrague, J. R. (2001). Effect of irrigation on changes in the anthocyanin composition of the skin of cv Tempranillo (Vitis vinifera L) grape berries during ripening. Journal of the Science of Food and Agriculture, 81(4), 409–420. https://doi.org/10.1002/1097-0010(200103)81:43.0.CO;2-H

Fisher, J. I., & Mustard, J. F. (2007). Cross-scalar satellite phenology from ground, Landsat, and MODIS data. Remote Sensing of Environment, 109(3), 261–273. https://doi.org/10.1016/j.rse.2007.01.004

Fisher, J. I., Mustard, J. F., & Vadeboncoeur, M. A. (2006). Green leaf phenology at Landsat resolution: Scaling from the field to the satellite. Remote Sensing of Environment, 100(2), 265–279. https://doi.org/10.1016/j.rse.2005.10.022

Gao, B. C. (1996). NDWI - A normalized difference water index for remote sensing of vegetation liquid water from space. Remote Sensing of Environment, 58(3), 257–266. https://doi.org/10.1016/ S0034-4257(96)00067-3

Hall, A. (2018). Remote Sensing Applications for Viticultural Terroir Analysis. Elements, 14(3), 185–190. https://doi.org/10.2138/ gselements.14.3.185 Hall, A., Louis, J., & Lamb, D. (2003). Characterising and mapping vineyard canopy using high-spatial-resolution aerial multispectral images. Computers & Geosciences, 29(7), 813–822. https://doi. org/10.1016/S0098-3004(03)00082-7

Hall, A., & Wilson, M. A. (2013). Object-based analysis of grapevine canopy relationships with winegrape composition and yield in two contrasting vineyards using multitemporal high spatial resolution optical remote sensing. International Journal of Remote Sensing, 34(5), 1772–1797. https://doi.org/10.1080/01431161.2012.726753

Huete, A. (1988). A Soil-Adjusted Vegetation Index (savi). Remote Sensing of Environment, 25(3), 295–309. https://doi. org/10.1016/0034-4257(88)90106-X

Johnson, L. F., Roczen, D. E., Youkhana, S. K., Nemani, R. R., & Bosch, D. F. (2003). Mapping vineyard leaf area with multispectral satellite imagery. COMPUTERS AND ELECTRONICS IN AGRICULTURE, 38(1), 33–44. https://doi.org/10.1016/S0168- 1699(02)00106-0

Kandylakis, Z., & Karantzalos, K. (2016). Precision Viticulture from Multitemporal, Multispectral Very High Resolution Satellite Data. In L. Halounova, V. Safar, P. L. N. Raju, L. Planka, V. Zdimal, T. S. Kumar, F. S. Faruque, Y. Kerr, S. M. Ramasamy, J. Comiso, Y. A. Hussin, P. S. Thenkabail, S. Lavender, A. Skidmore, P. Yue, P. Patias, O. Altan, & Q. Weng (Eds.), XXIII ISPRS

CONGRESS, COMMISSION VIII (Vol. 41, Issue B8, pp. 919–925). Copernicus Gesellschaft Mbh. https://doi.org/10.5194/isprsarchivesXLI-B8-919-2016

Karakizi, C., Oikonomou, M., & Karantzalos, K. (2016a). Vineyard Detection and Vine Variety Discrimination from Very High Mukhtar Abubakar et al. OENO One | By the International Viticulture and Enology Society 2023 | volume 57–4 | 13 Resolution Satellite Data. Remote Sensing, 8(3), 235. https://doi. org/10.3390/rs8030235

Karakizi, C., Oikonomou, M., & Karantzalos, K. (2016b). Vineyard Detection and Vine Variety Discrimination from Very High Resolution Satellite Data. REMOTE SENSING, 8(3), 235. https://doi.org/10.3390/rs8030235

Khaliq, A., Comba, L., Biglia, A., Aimonino, D. R., Chiaberge, M., & Gay, P. (2019). Comparison of Satellite and UAV-Based Multispectral Imagery for Vineyard Variability Assessment. REMOTE SENSING, 11(4), 436. https://doi.org/10.3390/rs11040436

Malheiro, A. C., Campos, R., Fraga, H., Eiras-Dias, J., Silvestre, J., & Santos, J. A. (2013). Winegrape Phenology and Temperature Relationships in the Lisbon Wine Region, Portugal. JOURNAL INTERNATIONAL DES SCIENCES DE LA VIGNE ET DU VIN, 47(4), 287–299.

Matese, A., & Filippo Di Gennaro, S. (2015). Technology in precision viticulture: A state of the art review. International Journal of Wine Research, 7, 69–81. https://doi.org/10.2147/IJWR.S69405

Motohka, T., Nasahara, K. N., Oguma, H., & Tsuchida, S. (2010). Applicability of Green-Red Vegetation Index for Remote Sensing of Vegetation Phenology. Remote Sensing, 2(10), 2369–2387. https://doi.org/10.3390/rs2102369

Palazzi, F., Biddoccu, M., Borgogno Mondino, E. C., & Cavallo, E. (2022). Use of Remotely Sensed Data for the Evaluation of InterRow Cover Intensity in Vineyards. Remote Sensing, 15(1), 41. https://doi.org/10.3390/rs15010041

Permanhani, M., Costa, J. M., Conceição, M. A. F., De Souza, R. T., Vasconcellos, M. A. S., & Chaves, M. M. (2016). Deficit irrigation in table grape: Eco-physiological basis and potential use to save water and improve quality. Theoretical and Experimental Plant Physiology, 28(1), 85–108. https://doi.org/10.1007/s40626-016- 0063-9

Qi, J., Chehbouni, A., Huete, A., Kerr, Y., & Sorooshian, S. (1994). A Modified Soil Adjusted Vegetation Index. Remote Sensing of Environment, 48(2), 119–126. https://doi.org/10.1016/0034- 4257(94)90134-1

Rizzi, J., Tarquis, A. M., Gobin, A., Semenov, M., Zhao, W., & Tarolli, P. (2021). Preface: Remote sensing, modelling-based hazard and risk assessment, and management of agro-forested ecosystems. Natural Hazards and Earth System Sciences, 21(12), 3873–3877. https://doi.org/10.5194/nhess-21-3873-2021

Roca, P. (2022). STATE OF THE WORLD VINE AND WINE SECTOR. 1–25. https://www.oiv.int/public/medias/8773/pptpressconf-2022-4-def.pdf

Rodriguez, J. R., Miranda, D., & Alvarez, C. J. (2006). Application of satellite images to locate and inventory vineyards in the designation of origin “Bierzo” in Spain. Transactions of the ASABE, 49(1), 277–290.

Sarvia, F., De Petris, S., & Borgogno-Mondino, E. (2019). Remotely sensed data to support insurance strategies in agriculture. In C. M. U. Neale & A. Maltese (Eds.), Remote Sensing for Agriculture, Ecosystems, and Hydrology Xxi (Vol. 11149, p. 111491H). Spie-Int Soc Optical Engineering. https://doi.org/10.1117/12.2533117

Semmens, K. A., Anderson, M. C., Kustas, W. P., Gao, F., Alfieri, J. G., McKee, L., Prueger, J. H., Hain, C. R., Cammalleri, C., Yang, Y., Xia, T., Sanchez, L., Alsina, M. M., & Velez, M. (2016). Monitoring daily evapotranspiration over two California vineyards using Landsat 8 in a multi-sensor data fusion approach. REMOTE SENSING OF ENVIRONMENT, 185, 155–170. https://doi.org/10.1016/j.rse.2015.10.025

Serouart, M., Madec, S., David, E., Velumani, K., Lopez Lozano, R., Weiss, M., & Baret, F. (2022). SegVeg: Segmenting RGB Images into Green and Senescent Vegetation by Combining Deep and Shallow Methods. Plant Phenomics, 2022. https://doi. org/10.34133/2022/9803570

Smart, R. (1985). Principles of Grapevine Canopy Microclimate Manipulation with Implications for Yield and Quality—A Review. American Journal of Enology and Viticulture, 36(3), 230–239.

Steenwerth, K. L., & Belina, K. M. (2010). Vineyard weed management practices influence nitrate leaching and nitrous oxide emissions. Agriculture, Ecosystems & Environment, 138(1–2), 127– 131. https://doi.org/10.1016/j.agee.2010.03.016

Testa, S., Mondino, E. C. B., & Pedroli, C. (2014). Correcting MODIS 16-day composite NDVI time-series with actual acquisition dates. European Journal of Remote Sensing, 47, 285–305. https://doi.org/10.5721/EuJRS20144718

Vaudour, E., Carey, V. A., & Gilliot, J. M. (2010). Digital zoning of South African viticultural terroirs using bootstrapped decision trees on morphometric data and multitemporal SPOT images. REMOTE SENSING OF ENVIRONMENT, 114(12), 2940–2950. https://doi. org/10.1016/j.rse.2010.08.001

Wang, S., Zhang, L., Huang, C., & Qiao, N. (2017). An NDVI-Based Vegetation Phenology Is Improved to be More Consistent with Photosynthesis Dynamics through Applying a Light Use Efficiency Model over Boreal High-Latitude Forests. Remote Sensing, 9(7), 695. https://doi.org/10.3390/rs9070695

Weiss, M., Baret, F., Leroy, M., Hautecoeur, O., Bacour, C., Prevot, L., & Bruguier, N. (2002). Validation of neural net techniques to estimate canopy biophysical variables from remote sensing data. Agronomie, 22(6), 547–553. https://doi.org/10.1051/agro:2002036

Whitmore, A. P., & Schröder, J. J. (2007). Intercropping reduces nitrate leaching from under field crops without loss of yield: A modelling study. European Journal of Agronomy, 27(1), 81–88. https://doi.org/10.1016/j.eja.2007.02.004

Zarrouk, O., Francisco, R., Pinto-Marijuan, M., Brossa, R., Santos, R. R., Pinheiro, C., Costa, J. M., Lopes, C., & Chaves, M. M. (2012). Impact of irrigation regime on berry development and flavonoids composition in Aragonez (Syn. Tempranillo) grapevine. Agricultural Water Management, 114, 18–29. https://doi. org/10.1016/j.agwat.2012.06.018

Zonal statistics in R | GeoProfesja. (2016, November 19). http://geoprofesja.pl/en/zonal-statistics-in-r/

General conclusions and perspectives

Shortage of water is among the major factors restricting agricultural development in the Mediterranean environment. This study addressed the **mapping of irrigated crop classes at the territory level and the characterization of vineyard components (canopy leaf area and identification of the inter-row management).** It aimed to propose different mapping approaches of the prevalent irrigated crop classes in the respective study areas like irrigated permanent grasslands, orchards, vineyards, and olive groves, using Sentinel 2 data.

In the course of this thesis, these proposed methodologies have been applied to our respective study sites: the plain of Crau and the basins of Ouvéze-Ventoux; where irrigation is a major issue to sustain agricultural production. The innovations in this thesis are to infer from Sentinel-2 (S2) time series agronomic or phenological traits (features) that are used to characterize the different irrigation systems. This was the case with irrigated grassland which presents a specific temporal signature with several mowing events that are easy to identify with a sharp drop in the amount of vegetation or with the phenology development which makes the distinction between orchard, vineyard, and olive groves possible. Such innovation is possible with the good temporal resolution offered by the S2 mission and the weather conditions that allow to exploit a large number of images. Among the different indices and biophysical variables that are accessible from remote sensing, the LAI led to interesting results on both the classification performances and the interest in having a meaningful variable that can be further used for agronomical analysis. Lastly, the temporal analysis of S2-LAI time series, as used for crop mapping, can also be used to characterize vineyards with two important characteristics, namely the LAI of the grapevine canopy and inter-row management It was shown that these characteristics are accessible from the LAI time series derived from a decametric-resolution satellite such as Sentinel-2, which does not allow us to enter into the description of the constituent elements of a plant canopy such as the vineyards. The proposed method is based on assumptions about canopy dynamics supported by field observations and the herbaceous canopy. The results obtained led to interesting qualitative results on vine LAI, and we have succeeded in separating grass-covered vines from vines in which the inter-row was tilled. We have shown that we can avoid collecting field observations and base our methods solely on remote sensing data. These promising results now need to be evaluated against more quantitative data and applied on a larger scale. Since this thesis gave information concerning irrigated crops and thus completely about water utilization management, the results can supplement studies in hydrology, agronomy, or water management.

Summary of the main findings

The first phase of the thesis was devoted to mapping irrigated permanent grasslands (IPG) at the plain of Crau. The developed method was tuned on a limited data set and can be replicated in different places when irrigated grassland is mowed at least two times a year with a classification scheme that is based on simple threshold detection applied to the number of mowing events. The developed method provides good results (Kappa ranging from 0.94-0.99), better than the results obtained using supervised classification (SVM) on soil LAI time series and comparable to the results provided by the THEIA land use map which covers the whole of the French territory using large ground-based data sets. An important part of the development was to handle noise from remote sensing. In spite of the good obtained results by the algorithm, some drawbacks were faced which can lead to failure to detect mowing

events like very low vegetation growth or biomass or heterogeneous plots, it tends to be faced with mowing detection failure. This can be viewed as a drawback however our analysis has demonstrated that the irrigated permanent grasslands class covers numerous management procedures. Such drawbacks might as well be advantageous to distinguish various production patterns. Moreover, it is possible to characterize practices from the detection of mowing events and to provide data to inform farming practices over large extents to implement crop models. Real land use change can be noticed but to confirm the change in land use, long time series are required to separate real changes from fields with lower irrigation or strong heterogeneities. In this study, we relied on agronomic traits that are typical of the irrigated grassland which makes the classification easier and can explain the good classification statistics, which were also found with other products such as the THEAI classification. However, it was expected that mapping the other irrigated crop types like orchards, vineyards, and olive groves would offer closer remote sensing signal making their characterization more challenging

In the second phase of the work, we have proposed a new approach to delineating deciduous (orchards and vineyards) and evergreen (olive groves) perennial woody trees by fitting an analytical model representing the plant development according to its phenology on LAI time series obtained from Sentinel-2 data. The parameters of such a model linked to phenological traits, were used as classifiers in the random forest algorithm. The obtained performances led to good overall accuracies (0.89-0.96) and Kappa (0.87-0.95), which was much better than the results derived from using the LAI times series as a classifier using the random forest method. This demonstrates the use of agronomic knowledge in the analysis of the temporal series, here by selecting a relevant analytical model to match the data, overpass machine learning method used with small training data sets. Our method is also significantly better than THEIA land use classification that is implemented across the territory of France using various sources of ground data. Additionally, the approach is not dependent on satellite acquisition dates. We can implement a random forest model derived from one year to another year by still obtaining reasonable precision.

In the third phase of the work, we suggested an approach that concentrated on an in-depth analysis of optical satellite data of Sentinel-2 (S2) time series of the leaf area index (LAI) to characterize canopy development and inter-row management of grapevine fields. Field visits were conducted in the Ouveze-Ventoux area, South Eastern France, for two years (2021 and 2022) to monitor phenology, canopy development, and inter-row management of eleven selected grapevine fields. Concerning the S2-LAI data, the annual dynamic of a typical grapevine canopy leaf area was found similar to a double logistic curve. Therefore, an analytic model was adopted to represent the grapevine canopy contribution to the S2-LAI. Part of the parameters of the analytic model were calibrated from the actual grapevine canopy dynamics timing observation from the field visits, while the others were inferred at the field level from the S2-LAI time series. The background signal was generated by direct subtraction of the simulated canopy from the S2 LAI time series. Rainfall data were examined to see the possible explanations behind variations in the inter-row grass development. From the background signals, we were able to group the inter-row management into three classes namely grassed, partially grassed, and tilled which corroborated our findings on the field. To consider the possibility of avoiding field visits, the model was recalibrated on a grapevine field with a clear

canopy signal and applied to two fields with different inter-row management. The result showed slight differences among the inter-row signals, which did not prevent the identification of inter-row management, thus indicating that field visits might not be mandatory.

Limitations of the study

Summarily, the presented findings (results) displayed in this work have demonstrated that multispectral remote sensing images and the use of LAI in particular allow to classify with a good level of precision Mediterranean crops and delineate parcels under irrigation (irrigated crops). These findings are in accordance with many past studies with similar emphases in the Mediterranean regions or under the climate of the Mediterranean. Nevertheless, the proposed approaches developed in this study (thesis) are nonetheless limited by some corresponding postulations which were mentioned and discussed below in a nutshell;

a) For instance, since the proposed approaches depend on specific agronomic or phenology timings, thus, when there is cloud coverage exactly corresponding to these crucial events (time of harvest or mowing, the onset of the season, etc.) the accuracies of the methods can be greatly affected as it was noticed with the first part of the work (developed grassland detection algorithm) and even to some extent the second part of the work (fruit trees delineation).

b) In general, there are difficulties in mapping young tree canopies and this might be due to the low contribution of the canopy and creating confusion with the background signals. Such limitation was also experienced with the grassland detection algorithm (mowing detection failure due to low vegetation growth mostly from poor management or levelling).

c) Classes of the orchards, vineyards, and olives were determined in a broad manner. For instance, there is a need for more clarity on the precise type of orchards (e.g plum, cherry, apricot, apple, nectarine, peach etc..) vineyards (separate between table and wine grapevines) and the same with olive class. This will give a clear pathway when estimating their respective water needs

d) There is a need for calibration between territories and in less extent between years. To maintain good accuracy there is a need for individual calibration across sites (due to the slight variation in micro-climate which consequently reflects on the phenology) and even across years.

e) Delineation of vineyard components needs validation over large data sets. The eleven selected fields might not be sufficient and there is a need for validation across vast extents to encounter different occurrences

Perspectives

The accessibility of remote sensing data with decametric resolution (spatial and temporal) like the Sentinel-2 mission provides an extraordinary avenue to improve the monitoring of crop water balance. The Sentinel-2 program mission made it practicable to obtain complete coverage of the main aspect of the Earth's surface for at least every 5 days with 13 multispectral independent bands with a GSD (ground sampling distance) of 10 m. Such spatial and temporal resolution might permit simultaneous supervision of crop

advancements and water status via the utilization of biophysical variables or spectral vegetation indices like NDVI or NDWI to mention a few and consequently estimation of crop water use.

Going by the respective results obtained from the three phases of this PhD thesis, it could be noticed that there is a need to be more curious about knowing the in-depth nature of the classified crops. For instance, in the second phase of the work irrespective of the good accuracy obtained, knowing the exact crop classes of the different classified orchards could as well be an adding value to the work (which was determined broadly). The ability to separate within the orchard class (cherry, plum, apricot, and apple trees) probably by exploiting a different vegetation index like the bloom index to make the separation according to time, colour, and intensity of blooming. Since floral phenology timing and intensity are linked to the reproduction of terrestrial ecosystems and are also highly responsive to climate change. Although flowering observational records are quite sparse which consequently affects our comprehension of spatiotemporal behaviours of floral phenology from local to regional extents. Remote sensing satellites can offer unique opportunities for spatiotemporal floral monitoring in a less expensive manner. For instance, Chen et al. (2019) proposed an enhanced bloom index (EBI) using remote sensing multispectral data to estimate the status of almond (Prunus dulcis) orchard flowering in the Central Valley of California. Their results showed that decametric S2 data displayed robustness of the EBI in displaying the flower information due to the relatively dense time series of S2 data being capable of grasping the blooming pattern of the almond orchards. EBI derived from satellite sensors like S2 is expected to capture the blooming data and thus, enhance our understanding and prediction of flowering responses to weather and yield.

Another way to classify the individual orchards could be by using textural feature analysis, which is a significant tool for classifying land cover types remotely having less inter-class variability or a huge intra-class heterogeneity (Myint et al., 2004). Very high-resolution aerial/satellite imageries could assist in generating the different classes by offering high-quality GLCM texture descriptors (Chen et al., 2019b; Chen et al., 2019).

Other issues (challenges) could be stated such as the imperative issues that might pertain to mixed pixel problems. Due to the complicated and diverse land cover types in the study areas, the issue of mixed pixels is a challenging incident that might lead to the wrong estimation of delineated maps. To address the problems of mixed pixels in future studies, subpixel analysis might be (presumably) crucial too.

The use of future very high-resolution optic satellite imageries that are cost-free and have a fine temporal frequency (finer than the Sentinel-2 mission in both resolution and frequency) can be merged with S2 data to improve time series acquisition. This will also counter the limitation of cloudy dates for instance in 2016 only one functional satellite of S2 was available (S2A) and that might explain the reasons behind the general low obtained accuracies.

The launch of the Franco-Indian mission (TRISHNA) in 2025 with thermal bands might be very promising to detect irrigated surfaces based on direct observation of crop stress might be interesting to delineate crop types that are not always irrigated as vineyards.

The different crop maps generated from this study (based on agronomic and phenology metrics) can be used to evaluate or estimate their respective water needs by adopting different modelling approaches such as the AquaCrop model, FAO-56 model, and STICS model to mention a few.

References

Abubakar, M.A, Chanzy, A., Pouget, G., Flamain, F., Courault, D., 2022. Detection of Irrigated Permanent Grasslands with Sentinel-2 Based on Temporal Patterns of the Leaf Area Index (LAI). https://doi.org/10.20944/preprints202205.0273.v1

Abubakar, M.A., Chanzy, A., Flamain, F., Pouget, G., Courault, D., 2023. Delineation of Orchard, Vineyard, and Olive Trees Based on Phenology Metrics Derived from Time Series of Sentinel-2. Remote Sensing 15, 2420.

Addabbo, P., Focareta, M., Marcuccio, S., Votto, C., Ullo, S.L., 2016. Contribution of Sentinel-2 data for applications in vegetation monitoring. Acta Imeko 5, 44–54.

Ahl, D.E., Gower, S.T., Burrows, S.N., Shabanov, N.V., Myneni, R.B., Knyazikhin, Y., 2006. Monitoring spring canopy phenology of a deciduous broadleaf forest using MODIS. Remote Sensing of Environment 104, 88–95. https://doi.org/10.1016/j.rse.2006.05.003

Akbari, E., Boloorani, A.D., Samany, N.N., Hamzeh, S., Soufizadeh, S., Pignatti, S., 2020. Crop Mapping Using Random Forest and Particle Swarm Optimization based on Multi-Temporal Sentinel-2. Remote Sens. 12, 1449. https://doi.org/10.3390/rs12091449

Ambika, A.K., Wardlow, B., Mishra, V., 2016. Remotely sensed high resolution irrigated area mapping in India for 2000 to 2015. Sci. Data 3, 160118. https://doi.org/10.1038/sdata.2016.118

Andreatta, D., Gianelle, D., Scotton, M., Vescovo, L., Dalponte, M., 2022. Detection of grassland mowing frequency using time series of vegetation indices from Sentinel-2 imagery. GIScience & Remote Sensing 59, 481–500. https://doi.org/10.1080/15481603.2022.2036055

Ashourloo, D., 2019. Automatic canola mapping using time series of sentinel 2 images. ISPRS Journal of Photogrammetry and Remote Sensing 14.

Ashourloo, D., Nematollahi, H., Huete, A., Aghighi, H., Azadbakht, M., Shahrabi, H.S., Goodarzdashti, S., 2022. A new phenology-based method for mapping wheat and barley using time-series of Sentinel-2 images. Remote Sensing of Environment 280, 113206. https://doi.org/10.1016/j.rse.2022.113206

Ashourloo, D., Shahrabi, H.S., Azadbakht, M., Aghighi, H., Matkan, A.A., Radiom, S., 2018. A Novel Automatic Method for Alfalfa Mapping Using Time Series of Landsat-8 OLI Data. IEEE J. Sel. Top. Appl. Earth Observations Remote Sensing 11, 4478–4487. https://doi.org/10.1109/JSTARS.2018.2874726

Ashourloo, D., Shahrabi, H.S., Azadbakht, M., Aghighi, H., Nematollahi, H., Alimohammadi, A., Matkan, A.A., 2019. Automatic canola mapping using time series of sentinel 2 images. ISPRS-J. Photogramm. Remote Sens. 156, 63–76. https://doi.org/10.1016/j.isprsjprs.2019.08.007

Ashourloo, D., Shahrabi, H.S., Azadbakht, M., Rad, A.M., Aghighi, H., Radiom, S., 2020. A novel method for automatic potato mapping using time series of Sentinel-2 images. Computers and Electronics in Agriculture 175, 105583. https://doi.org/10.1016/j.compag.2020.105583

Badeck, F., Bondeau, A., Böttcher, K., Doktor, D., Lucht, W., Schaber, J., Sitch, S., 2004. Responses of spring phenology to climate change. New Phytologist 162, 295–309. https://doi.org/10.1111/j.1469-8137.2004.01059.x

Baret, F., Guyot, G., Major, D.J., 1989. TSAVI: A Vegetation Index Which Minimizes Soil Brightness Effects On LAI And APAR Estimation, in: 12th Canadian Symposium on Remote Sensing Geoscience and Remote Sensing Symposium,. Presented at the 12th Canadian Symposium on Remote Sensing Geoscience and Remote Sensing Symposium, pp. 1355–1358. https://doi.org/10.1109/IGARSS.1989.576128

Bauer-Marschallingere, B., Freeman, V., Cao, S., Paulik, C., Schaufler, S., Stachl, T., Modanesi, S., Massario, C., Ciabatta, L., Brocca, L., Wagner, W., 2019. Toward Global Soil Moisture Monitoring With Sentinel-1: Harnessing Assets and Overcoming Obstacles. IEEE Trans. Geosci. Remote Sensing 57, 520–539. https://doi.org/10.1109/TGRS.2018.2858004

Bazzi, H., Baghdadi, N., Amin, G., Fayad, I., Zribi, M., Demarez, V., Belhouchette, H., 2021. An Operational Framework for Mapping Irrigated Areas at Plot Scale Using Sentinel-1 and Sentinel-2 Data. Remote Sensing 13, 2584. https://doi.org/10.3390/rs13132584

Bazzi, H., Baghdadi, N., Fayad, I., Zribi, M., Belhouchette, H., Demarez, V., 2020. Near real-time irrigation detection at plot scale using sentinel-1 data. Remote Sensing 12, 1456.

Bazzi, H., Baghdadi, N., Ienco, D., El Hajj, M., Zribi, M., Belhouchette, H., Jose Escorihuela, M., Demarez, V., 2019. Mapping Irrigated Areas Using Sentinel-1 Time Series in Catalonia, Spain. Remote Sens. 11, 1836. https://doi.org/10.3390/rs11151836

Bazzi, H., Baghdadi, N., Najem, S., Jaafar, H., Le Page, M., Zribi, M., Faraslis, I., Spiliotopoulos, M., 2022. Detecting Irrigation Events over Semi-Arid and Temperate Climatic Areas Using Sentinel-1 Data: Case of Several Summer Crops. Agronomy-Basel 12, 2725. https://doi.org/10.3390/agronomy12112725

Bolton, D.K., Gray, J.M., Melaas, E.K., Moon, M., Eklundh, L., Friedl, M.A., 2020. Continental-scale land surface phenology from harmonized Landsat 8 and Sentinel-2 imagery. Remote Sensing of Environment 240, 111685. https://doi.org/10.1016/j.rse.2020.111685

Borgogno-Mondino, E., Lessio, A., Tarricone, L., Novello, V., de Palma, L., 2018. A comparison between multispectral aerial and satellite imagery in precision viticulture. Precis. Agric. 19, 195–217. https://doi.org/10.1007/s11119-017-9510-0

Bourrelly, M., Borel, L., Devaux, J.P., Louis-Palluel, J., Archiloque, A., 1983. Dynamique annuelle et production primaire nette de l'écosystème steppique de Crau (Bouches du Rhône). Biologie et écologie méditerranéenne 10, 55–82.

Bousbih, S., Zribi, M., El Hajj, M., Baghdadi, N., Lili-Chabaane, Z., Gao, Q., Fanise, P., 2018. Soil moisture and irrigation mapping in A semi-arid region, based on the synergetic use of Sentinel-1 and Sentinel-2 data. Remote Sensing 10, 1953.

Bradley, C., Schwartz, M., Xiao, X., 2009. Remote Sensing Phenology: Status and Way forward. Phenology of Ecosystem Processes—Applications in Global Change Research 231–246.

Breiman, L., 2001. Random Forests. Machine Learning 45, 5–32. https://doi.org/10.1023/A:1010933404324

Brown, M.E., de Beurs, K.M., Marshall, M., 2012. Global phenological response to climate change in crop areas using satellite remote sensing of vegetation, humidity and temperature over 26 years. Remote Sens. Environ. 126, 174–183. https://doi.org/10.1016/j.rse.2012.08.009

Caffarra, A., 2023. Grapevine phenology : a biological clock to time vineyard management operations. itk - Predict and Decide. URL https://www.itk.fr/en/news/grapevine-phenology-a-biological-clock-to-time-vineyard-management-operations/ (accessed 5.31.23).

Chen, B., Jin, Y., Brown, P., 2019a. An enhanced bloom index for quantifying floral phenology using multi-scale remote sensing observations. ISPRS Journal of Photogrammetry and Remote Sensing 156, 108–120. https://doi.org/10.1016/j.isprsjprs.2019.08.006

Chen, B., Jin, Y., Brown, P., 2019b. Automatic mapping of planting year for tree crops with Landsat satellite time series stacks. ISPRS Journal of Photogrammetry and Remote Sensing 151, 176–188.

Chen, X., Wang, D., Chen, J., Wang, C., Shen, M., 2018. The mixed pixel effect in land surface phenology: A simulation study. Remote Sens. Environ. 211, 338–344. https://doi.org/10.1016/j.rse.2018.04.030

Chen, Y., Hou, C., Tang, Y., Zhuang, J., Lin, J., He, Y., Guo, Q., Zhong, Z., Lei, H., Luo, S., 2019. Citrus tree segmentation from UAV images based on monocular machine vision in a natural orchard environment. Sensors 19, 5558.

Chen, Y., Lu, D., Luo, L., Pokhrel, Y., Deb, K., Huang, J., Ran, Y., 2018. Detecting irrigation extent, frequency, and timing in a heterogeneous arid agricultural region using MODIS time series, Landsat imagery, and ancillary data. Remote Sens. Environ. 204, 197–211. https://doi.org/10.1016/j.rse.2017.10.030

Claverie, M., Vermote, E.F., Weiss, M., Baret, F., Hagolle, O., Demarez, V., 2013. Validation of coarse spatial resolution LAI and FAPAR time series over cropland in southwest France. Remote Sensing of Environment 139, 216–230. https://doi.org/10.1016/j.rse.2013.07.027

Congalton, R.G., 2001. Accuracy assessment and validation of remotely sensed and other spatial information. International Journal of Wildland Fire 10, 321–328. https://doi.org/10.1071/WF01031

Copernicus—The European Earth Observation Programme [WWW Document], n.d. URL https://defence-industry-space.ec.europa.eu/eu-space-policy/copernicus_en (accessed 3.1.23).

Courault, D., Bsaibes, A., Kpemlie, E., Hadria, R., Hagolle, O., Marloie, O., Hanocq, J.-F., Olioso, A., Bertrand, N., Desfonds, V., 2008. Assessing the potentialities of FORMOSAT-2 data for water and crop monitoring at small regional scale in South-Eastern France. Sensors 8, 3460–3481. https://doi.org/10.3390/s8053460

Courault, D., Hadria, R., Ruget, F., Olioso, A., Duchemin, B., Hagolle, O., Dedieu, G., 2010. Combined use of FORMOSAT-2 images with a crop model for biomass and water monitoring of permanent grassland in Mediterranean region. Hydrology and Earth System Sciences 14, 1731–1744. https://doi.org/10.5194/hess-14-1731-2010

Courault, D., Le Page, M., Jarlan, L., Khabba, S., 2020. Quels sont les capteurs et les méthodes disponibles en télédétection pour aider à la gestion de l'eau. L'eau en milieu agricole, éditions Quae.

de Beurs, K.M., Henebry, G.M., 2004. Land surface phenology, climatic variation, and institutional change: Analyzing agricultural land cover change in Kazakhstan. Remote Sens. Environ. 89, 497–509. https://doi.org/10.1016/j.rse.2003.11.006

De Vroey, M., Radoux, J., Defourny, P., 2021. Grassland Mowing Detection Using Sentinel-1 Time Series: Potential and Limitations. Remote Sens. 13, 348. https://doi.org/10.3390/rs13030348

Deines, J.M., Kendall, A.D., Hyndman, D.W., 2017. Annual Irrigation Dynamics in the US Northern High Plains Derived from Landsat Satellite Data. Geophys. Res. Lett. 44, 9350–9360. https://doi.org/10.1002/2017GL074071

Delegido, J., Verrelst, J., Alonso, L., Moreno, J., 2011. Evaluation of Sentinel-2 Red-Edge Bands for Empirical Estimation of Green LAI and Chlorophyll Content. Sensors 11, 7063–7081. https://doi.org/10.3390/s110707063

Dellery, 1964. Etude hydrogéologique de la Crau Rapport - Google Scholar [WWW Document]. URL https://scholar.google.com/scholar_lookup?title=Etude%20hydrog%C3%A9ologique%20de%20la%20Crau&publication_year=1964&author=B.%20Dellery&author=G.%20Durozoy&author=J.%20Forkasiewicz&author=C.%20Gouvernet&author=J.%20Margat (accessed 2.24.23).

Demarez, V., Helen, F., Marais-Sicre, C., Baup, F., 2019a. In-Season Mapping of Irrigated Crops Using Landsat 8 and Sentinel-1 Time Series. Remote Sens. 11, 118. https://doi.org/10.3390/rs11020118

Demarez, V., Helen, F., Marais-Sicre, C., Baup, F., 2019b. In-Season Mapping of Irrigated Crops Using Landsat 8 and Sentinel-1 Time Series. Remote Sens. 11, 118. https://doi.org/10.3390/rs11020118

Duchemin, B., Goubier, J., Courrier, G., 1999. Monitoring phenological key stages and cycle duration of temperate deciduous forest ecosystems with NOAA/AVHRR data. Remote Sensing of Environment 67, 68–82.

Dusseux, P., Vertes, F., Corpetti, T., Corgne, S., Hubert-Moy, L., 2014. Agricultural practices in grasslands detected by spatial remote sensing. Environ. Monit. Assess. 186, 8249–8265. https://doi.org/10.1007/s10661-014-4001-5

El Hajj, M., Baghdadi, N., Bazzi, H., Zribi, M., 2019. Penetration Analysis of SAR Signals in the C and L Bands for Wheat, Maize, and Grasslands. Remote Sens. 11, 31. https://doi.org/10.3390/rs11010031

El Hajj, M., Baghdadi, N., Zribi, M., Bazzi, H., 2017. Synergic use of Sentinel-1 and Sentinel-2 images for operational soil moisture mapping at high spatial resolution over agricultural areas. Remote Sensing 9, 1292.

Fader, M., Shi, S., von Bloh, W., Bondeau, A., Cramer, W., 2016. Mediterranean irrigation under climate change: more efficient irrigation needed to compensate for increases in irrigation

water requirements. Hydrol. Earth Syst. Sci. 20, 953–973. https://doi.org/10.5194/hess-20-953-2016

FAO-UNESCO, M., 1981. The FAO/UNESCO soil map of the world legend, in: South Pacific Regional Forum on Soil Taxonomy. Institute of Natural Resources, The University of the South Pacific Suva, Fiji, pp. 177–183.

Ferrant, S., Caballero, Y., Perrin, J., Gascoin, S., Dewandel, B., Aulong, S., Dazin, F., Ahmed, S., Marechal, J.-C., 2014. Projected impacts of climate change on farmers' extraction of groundwater from crystalline aquifers in South India. Sci Rep 4, 3697. https://doi.org/10.1038/srep03697

Ferrant, S., Selles, A., Le Page, M., Herrault, P.-A., Pelletier, C., Al-Bitar, A., Mermoz, S., Gascoin, S., Bouvet, A., Saqalli, M., Dewandel, B., Caballero, Y., Ahmed, S., Marechal, J.-C., Kerr, Y., 2017. Detection of Irrigated Crops from Sentinel-1 and Sentinel-2 Data to Estimate Seasonal Groundwater Use in South India. Remote Sens. 9, 1119. https://doi.org/10.3390/rs9111119

Ferrant, S., Selles, A., Le Page, M., Mermoz, S., Gascoin, S., Bouvet, A., Ahmed, S., 2019. Sentinel-1&2 for near real time cropping pattern monitoring in drought prone areas. application to irrigation water needs in telangana, south-india. International Archives of the Photogrammetry, Remote Sensing and Spatial Information Sciences 42, 285–292.

Fisher, J.I., Mustard, J.F., 2007. Cross-scalar satellite phenology from ground, Landsat, and MODIS data. Remote Sens. Environ. 109, 261–273. https://doi.org/10.1016/j.rse.2007.01.004

Fisher, J.I., Mustard, J.F., Vadeboncoeur, M.A., 2006. Green leaf phenology at Landsat resolution: Scaling from the field to the satellite. Remote Sens. Environ. 100, 265–279. https://doi.org/10.1016/j.rse.2005.10.022

Frantz, D., Stellmes, M., Roeder, A., Udelhoven, T., Mader, S., Hill, J., 2016. Improving the Spatial Resolution of Land Surface Phenology by Fusing Medium- and Coarse-Resolution Inputs. IEEE Trans. Geosci. Remote Sensing 54, 4153–4164. https://doi.org/10.1109/TGRS.2016.2537929

Gao, B., 1995. A normalized difference water index for remote sensing of vegetation liquid water from space, in: Descour, M.R., Mooney, J.M., Perry, D.L., Illing, L. (Eds.), Imaging Spectrometry. Spie - Int Soc Optical Engineering, Bellingham, pp. 225–236. https://doi.org/10.1117/12.210877

Gao, Q., Zribi, M., Escorihuela, M., Baghdadi, N., Segui, P., 2018. Irrigation Mapping Using Sentinel-1 Time Series at Field Scale. Remote Sensing 10, 1495. https://doi.org/10.3390/rs10091495

Gao, Q., Zribi, M., Escorihuela, M.J., Baghdadi, N., 2017. Synergetic use of Sentinel-1 and Sentinel-2 data for soil moisture mapping at 100 m resolution. Sensors 17, 1966.

Garrity, S.R., Bohrer, G., Maurer, K.D., Mueller, K.L., Vogel, C.S., Curtis, P.S., 2011. A comparison of multiple phenology data sources for estimating seasonal transitions in deciduous forest carbon exchange. Agric. For. Meteorol. 151, 1741–1752. https://doi.org/10.1016/j.agrformet.2011.07.008

Genuer, R., Poggi, J.-M., Tuleau-Malot, C., 2010. Variable selection using random forests. Pattern recognition letters 31, 2225–2236.

Gitelson, A.A., Kaufman, Y.J., Merzlyak, M.N., 1996. Use of a green channel in remote sensing of global vegetation from EOS-MODIS. Remote Sens. Environ. 58, 289–298. https://doi.org/10.1016/S0034-4257(96)00072-7

Gitelson, A.A., Keydan, G.P., Merzlyak, M.N., 2006. Three-band model for noninvasive estimation of chlorophyll, carotenoids, and anthocyanin contents in higher plant leaves. Geophysical Research Letters 33. https://doi.org/10.1029/2006GL026457

Gómez Giménez, M., de Jong, R., Della Peruta, R., Keller, A., Schaepman, M.E., 2017. Determination of grassland use intensity based on multi-temporal remote sensing data and ecological indicators. Remote Sensing of Environment 198, 126–139. https://doi.org/10.1016/j.rse.2017.06.003

Granero-Belinchon, C., Adeline, K., Lemonsu, A., Briottet, X., 2020. Phenological Dynamics Characterization of Alignment Trees with Sentinel-2 Imagery: A Vegetation Indices Time Series Reconstruction Methodology Adapted to Urban Areas. Remote Sensing 12, 639. https://doi.org/10.3390/rs12040639

Griffiths, P., Nendel, C., Hostert, P., 2019. Intra-annual reflectance composites from Sentinel-2 and Landsat for national-scale crop and land cover mapping. Remote Sensing of Environment 220, 135–151. https://doi.org/10.1016/j.rse.2018.10.031

Hagolle, O., Huc, M., Desjardins, C., Auer, S., Richter, R., 2017. MAJA Algorithm Theoretical Basis Document. https://doi.org/10.5281/zenodo.1209633

Hanes, J.M., Liang, L., Morisette, J.T., 2014. Land surface phenology, in: Biophysical Applications of Satellite Remote Sensing. Springer, pp. 99–125.

Hastie, T.J., 2017. Generalized Additive Models, 1er édition. ed. Routledge.

Henebry, G.M., Beurs, K.M. de, 2013. Remote sensing of land surface phenology: A prospectus, in: Phenology: An Integrative Environmental Science. Springer, pp. 385–411.

Hill, M.J., 2013. Vegetation index suites as indicators of vegetation state in grassland and savanna: An analysis with simulated SENTINEL 2 data for a North American transect. Remote Sens. Environ. 137, 94–111. https://doi.org/10.1016/j.rse.2013.06.004

Hoffman, R.O., Edwards, D.E., Wallin, G., Burton, T., 1975. Remote sensing instrumentation and methods used for identifying center pivot sprinkler irrigation systems and estimating crop water use, in: Proceedings of the International Seminar and Exposition on Water Resources Instrumentation.

Huete, A., Didan, K., Miura, T., Rodriguez, E.P., Gao, X., Ferreira, L.G., 2002. Overview of the radiometric and biophysical performance of the MODIS vegetation indices. Remote Sens. Environ. 83, 195–213. https://doi.org/10.1016/S0034-4257(02)00096-2

Immitzer, M., Vuolo, F., Atzberger, C., 2016. First Experience with Sentinel-2 Data for Crop and Tree Species Classifications in Central Europe. Remote Sens. 8, 166. https://doi.org/10.3390/rs8030166

Inglada, J., Vincent, A., Arias, M., Marais-Sicre, C., 2016. Improved Early Crop Type Identification By Joint Use of High Temporal Resolution SAR And Optical Image Time Series. Remote Sens. 8, 362. https://doi.org/10.3390/rs8050362

Inglada, J., Vincent, A., Arias, M., Tardy, B., Morin, D., Rodes, I., 2017. Operational High Resolution Land Cover Map Production at the Country Scale Using Satellite Image Time Series. Remote Sens. 9, 95. https://doi.org/10.3390/rs9010095

International Decade for Action on Water for Sustainable Development, 2018-2028 [WWW Document], n.d. URL https://www.un.org/en/events/waterdecade/background.shtml (accessed 4.14.22).

Jaunatre, R., 2012. Dynamics and restoration of a Mediterranean steppe after changes in land-use (La Crau, Southern-France). PhD Diss., Université d'Avignon et des Pays du Vaucluse, Avignon, FR.

Jensen, J.R., Lulla, K., 1987. Introductory digital image processing: A remote sensing perspective. Geocarto International 2, 65–65. https://doi.org/10.1080/10106048709354084

Jin, Z., Prasad, R., Shriver, J., Zhuang, Q., 2017. Crop model- and satellite imagery-based recommendation tool for variable rate N fertilizer application for the US Corn system. Precis. Agric. 18, 779–800. https://doi.org/10.1007/s11119-016-9488-z

Jönsson, P., Eklundh, L., 2004. TIMESAT—a program for analyzing time-series of satellite sensor data. Computers & Geosciences 30, 833–845. https://doi.org/10.1016/j.cageo.2004.05.006

Julien, Y., Sobrino, J.A., Jiménez-Muñoz, J.-C., 2011. Land use classification from multitemporal Landsat imagery using the Yearly Land Cover Dynamics (YLCD) method. International Journal of Applied Earth Observation and Geoinformation 13, 711–720. https://doi.org/10.1016/j.jag.2011.05.008

Karakizi, C., Karantzalos, K., Vakalopoulou, M., Antoniou, G., 2018. Detailed Land Cover Mapping from Multitemporal Landsat-8 Data of Different Cloud Cover. Remote Sens. 10, 1214. https://doi.org/10.3390/rs10081214

Karantzalos, K., Karmas, A., Tzotsos, A., 2017. Monitoring crop growth and key agronomic parameters through multitemporal observations and time series analysis from remote sensing big data. Advances in Animal Biosciences 8, 394–399. https://doi.org/10.1017/S2040470017001261

Kaufman, Y., Tanre, D., 1992. Atmospherically Resistant Vegetation Index (arvi) for Eos-Modis. IEEE Trans. Geosci. Remote Sensing 30, 261–270. https://doi.org/10.1109/36.134076

Khaliq, A., Comba, L., Biglia, A., Aimonino, D.R., Chiaberge, M., Gay, P., 2019. Comparison of Satellite and UAV-Based Multispectral Imagery for Vineyard Variability Assessment. Remote Sens. 11, 436. https://doi.org/10.3390/rs11040436

Kolecka, N., Ginzler, C., Pazur, R., Price, B., Verburg, P.H., 2018. Regional Scale Mapping of Grassland Mowing Frequency with Sentinel-2 Time Series. Remote Sens. 10, 1221. https://doi.org/10.3390/rs10081221

Kordi, F., Yousefi, H., 2022. Crop classification based on phenology information by using time series of optical and synthetic-aperture radar images. Remote Sens. Appl.-Soc. Environ. 27, 100812. https://doi.org/10.1016/j.rsase.2022.100812

Kumar, S.V., Peters-Lidard, C.D., Santanello, J.A., Reichle, R.H., Draper, C.S., Koster, R.D., Nearing, G., Jasinski, M.F., 2015. Evaluating the utility of satellite soil moisture retrievals over irrigated areas and the ability of land data assimilation methods to correct for unmodeled processes. Hydrology and Earth System Sciences 19, 4463–4478.

Kummu, M., Guillaume, J.H.A., de Moel, H., Eisner, S., Floerke, M., Porkka, M., Siebert, S., Veldkamp, T.I.E., Ward, P.J., 2016. The world's road to water scarcity: shortage and stress in the 20th century and pathways towards sustainability. Sci Rep 6, 38495. https://doi.org/10.1038/srep38495

Lanjeri, S., Melia, J., Segarra, D., 2001. A multi-temporal masking classification method for vineyard monitoring in central Spain. Int. J. Remote Sens. 22, 3167–3186. https://doi.org/10.1080/01431160152558305

Lawston, P.M., Santanello, J.A., Kumar, S.V., 2017. Irrigation Signals Detected From SMAP Soil Moisture Retrievals. Geophys. Res. Lett. 44, 11860–11867. https://doi.org/10.1002/2017GL075733

Le Page, M., Jarlan, L., El Hajj, M.M., Zribi, M., Baghdadi, N., Boone, A., 2020. Potential for the Detection of Irrigation Events on Maize Plots Using Sentinel-1 Soil Moisture Products. Remote Sens. 12, 1621. https://doi.org/10.3390/rs12101621

Lebrini, Y., Boudhar, A., Laamrani, A., Htitiou, A., Lionboui, H., Salhi, A., Chehbouni, A., Benabdelouahab, T., 2021. Mapping and Characterization of Phenological Changes over Various Farming Systems in an Arid and Semi-Arid Region Using Multitemporal Moderate Spatial Resolution Data. Remote Sens. 13, 578. https://doi.org/10.3390/rs13040578

Lee, K.-H., Anagnostou, E.N., 2004. A combined passive/active microwave remote sensing approach for surface variable retrieval using Tropical Rainfall Measuring Mission observations. Remote Sensing of Environment 92, 112–125. https://doi.org/10.1016/j.rse.2004.05.003

Lobert, F., Holtgrave, A.-K., Schwieder, M., Pause, M., Vogt, J., Gocht, A., Erasmi, S., 2021. Mowing event detection in permanent grasslands: Systematic evaluation of input features from Sentinel-1, Sentinel-2, and Landsat 8 time series. Remote Sens. Environ. 267, 112751. https://doi.org/10.1016/j.rse.2021.112751

Loveland, T.R., Reed, B.C., Brown, J.F., Ohlen, D.O., Zhu, Z., Yang, L., Merchant, J.W., 2000. Development of a global land cover characteristics database and IGBP DISCover from 1 km AVHRR data. Int. J. Remote Sens. 21, 1303–1330. https://doi.org/10.1080/014311600210191

Marras, P.A., Lima, D.C.A., Soares, P.M.M., Cardoso, R.M., Medas, D., Dore, E., De Giudici, G., 2021. Future precipitation in a Mediterranean island and streamflow changes for a small basin using EURO-CORDEX regional climate simulations and the SWAT model. Journal of Hydrology 603, 127025. https://doi.org/10.1016/j.jhydrol.2021.127025

Maselli, F., Battista, P., Chiesi, M., Rapi, B., Angeli, L., Fibbi, L., Magno, R., Gozzini, B., 2020. Use of Sentinel-2 MSI data to monitor crop irrigation in Mediterranean areas. International Journal of Applied Earth Observation and Geoinformation 93, 102216. https://doi.org/10.1016/j.jag.2020.102216

Masialeti, I., Egbert, S., Wardlow, B.D., 2010. A Comparative Analysis of Phenological Curves for Major Crops in Kansas. GISci. Remote Sens. 47, 241–259. https://doi.org/10.2747/1548-1603.47.2.241

Massari, C., Modanesi, S., Dari, J., Gruber, A., De Lannoy, G.J.M., Girotto, M., Quintana-Segui, P., Le Page, M., Jarlan, L., Zribi, M., Ouaadi, N., Vreugdenhil, M., Zappa, L., Dorigo, W., Wagner, W., Brombacher, J., Pelgrum, H., Jaquot, P., Freeman, V., Volden, E., Prieto, D.F., Tarpanelli, A., Barbetta, S., Brocca, L., 2021. A Review of Irrigation Information Retrievals from Space and Their Utility for Users. Remote Sens. 13, 4112. https://doi.org/10.3390/rs13204112

Mateo-Sanchis, A., Piles, M., Amoros-Lopez, J., Munoz-Mari, J., Adsuara, J.E., Moreno-Martinez, A., Camps-Valls, G., 2021. Learning main drivers of crop progress and failure in Europe with interpretable machine learning. Int. J. Appl. Earth Obs. Geoinf. 104, 102574. https://doi.org/10.1016/j.jag.2021.102574

Melaas, E.K., Sulla-Menashe, D., Gray, J.M., Black, T.A., Morin, T.H., Richardson, A.D., Friedl, M.A., 2016. Multisite analysis of land surface phenology in North American temperate and boreal deciduous forests from Landsat. Remote Sensing of Environment 186, 452–464. https://doi.org/10.1016/j.rse.2016.09.014

Merot, A., Bergez, J.-E., Capillon, A., Wery, J., 2008a. Analysing farming practices to develop a numerical, operational model of farmers' decision-making processes: An irrigated hay cropping system in France. Agricultural Systems 98, 108–118. https://doi.org/10.1016/j.agsy.2008.05.001

Merot, A., Bergez, J.-E., Capillon, A., Wery, J., 2008b. Analysing farming practices to develop a numerical, operational model of farmers' decision-making processes: An irrigated hay cropping system in France. Agricultural Systems 98, 108–118. https://doi.org/10.1016/j.agsy.2008.05.001

Meyer, H., Reudenbach, C., Hengl, T., Katurji, M., Nauss, T., 2018. Improving performance of spatio-temporal machine learning models using forward feature selection and target-oriented validation. Environ. Modell. Softw. 101, 1–9. https://doi.org/10.1016/j.envsoft.2017.12.001

Misra, G., Buras, A., Heurich, M., Asam, S., Menzel, A., 2018. LiDAR derived topography and forest stand characteristics largely explain the spatial variability observed in MODIS land surface phenology. Remote Sensing of Environment 218, 231–244. https://doi.org/10.1016/j.rse.2018.09.027

Misra, G., Cawkwell, F., Wingler, A., 2020. Status of Phenological Research Using Sentinel-2 Data: A Review. Remote Sens. 12, 2760. https://doi.org/10.3390/rs12172760

Mulla, D.J., 2013. Twenty five years of remote sensing in precision agriculture: Key advances and remaining knowledge gaps. Biosystems Engineering 114, 358–371. https://doi.org/10.1016/j.biosystemseng.2012.08.009

Myint, S.W., Lam, N.S.N., Tyler, J.M., 2004. Wavelets for urban spatial feature discrimination: Comparisons with fractal, spatial autocorrelation, and spatial co-occurrence approaches. Photogramm. Eng. Remote Sens. 70, 803–812. https://doi.org/10.14358/PERS.70.7.803

Nabil, M., Farg, E., Arafat, S.M., Aboelghar, M., Afify, N.M., Elsharkawy, M.M., 2022. Tree-fruits crop type mapping from Sentinel-1 and Sentinel-2 data integration in Egypt?s New Delta project. Remote Sens. Appl.-Soc. Environ. 27, 100776. https://doi.org/10.1016/j.rsase.2022.100776

Nasrallah, A., Baghdadi, N., El Hajj, M., Darwish, T., Belhouchette, H., Faour, G., Darwich, S., Mhawej, M., 2019. Sentinel-1 Data for Winter Wheat Phenology Monitoring and Mapping. Remote Sens. 11, 2228. https://doi.org/10.3390/rs11192228

Nguyen, L.H., Joshi, D.R., Clay, D.E., Henebry, G.M., 2020. Characterizing land cover/land use from multiple years of Landsat and MODIS time series: A novel approach using land surface phenology modeling and random forest classifier. Remote Sens. Environ. 238, 111017. https://doi.org/10.1016/j.rse.2018.12.016

Odenweller, J., Johnson, K., 1984. Crop Identification Using Landsat Temporal Spectral Profiles. Remote Sens. Environ. 14, 39–54. https://doi.org/10.1016/0034-4257(84)90006-3

Ozdogan, M., Gutman, G., 2008. A new methodology to map irrigated areas using multi-temporal MODIS and ancillary data: An application example in the continental US. Remote Sensing of Environment 112, 3520–3537. https://doi.org/10.1016/j.rse.2008.04.010

Ozdogan, M., Yang, Y., Allez, G., Cervantes, C., 2010. Remote sensing of irrigated agriculture: Opportunities and challenges. Remote sensing 2, 2274–2304.

Pageot, Y., Baup, F., Inglada, J., Baghdadi, N., Demarez, V., 2020. Detection of Irrigated and Rainfed Crops in Temperate Areas Using Sentinel-1 and Sentinel-2 Time Series. Remote Sens. 12, 3044. https://doi.org/10.3390/rs12183044

Palazzi, F., Biddoccu, M., Borgogno Mondino, E.C., Cavallo, E., 2022. Use of Remotely Sensed Data for the Evaluation of Inter-Row Cover Intensity in Vineyards. Remote Sensing 15, 41. https://doi.org/10.3390/rs15010041

Peña, M.A., Brenning, A., 2015. Assessing fruit-tree crop classification from Landsat-8 time series for the Maipo Valley, Chile. Remote Sensing of Environment 171, 234–244. https://doi.org/10.1016/j.rse.2015.10.029

Pena, M.A., Liao, R., Brenning, A., 2017. Using spectrotemporal indices to improve the fruit-tree crop classification accuracy. ISPRS-J. Photogramm. Remote Sens. 128, 158–169. https://doi.org/10.1016/j.isprsjprs.2017.03.019

Pervez, M.S., Brown, J.F., 2010. Mapping Irrigated Lands at 250-m Scale by Merging MODIS Data and National Agricultural Statistics. Remote Sens. 2, 2388–2412. https://doi.org/10.3390/rs2102388

Primicerio, J., Caruso, G., Comba, L., Crisci, A., Gay, P., Guidoni, S., Genesio, L., Aimonino, D.R., Vaccari, F.P., 2017. Individual plant definition and missing plant characterization in vineyards from high-resolution UAV imagery. Eur. J. Remote Sens. 50, 179–186. https://doi.org/10.1080/22797254.2017.1308234

Pun, M., Mutiibwa, D., Li, R., 2017. Land Use Classification: A Surface Energy Balance and Vegetation Index Application to Map and Monitor Irrigated Lands. Remote Sensing 9, 1256. https://doi.org/10.3390/rs9121256

Reed, B.C., Brown, J.F., VanderZee, D., Loveland, T.R., Merchant, J.W., Ohlen, D.O., 1994. Measuring phenological variability from satellite imagery. Journal of Vegetation Science 5, 703–714. https://doi.org/10.2307/3235884

Reed, B.C., Schwartz, M.D., Xiao, X., 2009. Remote sensing phenology: status and the way forward. Phenology of ecosystem processes: applications in global change research 231–246.

Richardson, K.J., Lewis, K.H., Krishnamurthy, P.K., Kent, C., Wiltshire, A.J., Hanlon, H.M., 2018. Food security outcomes under a changing climate: impacts of mitigation and adaptation on vulnerability to food insecurity. Clim. Change 147, 327–341. https://doi.org/10.1007/s10584-018-2137-y

Roland Colditz, R., 2015. An Evaluation of Different Training Sample Allocation Schemes for Discrete and Continuous Land Cover Classification Using Decision Tree-Based Algorithms. Remote Sens. 7, 9655–9681. https://doi.org/10.3390/rs70809655

Rouse Jr, J.W., Haas, R.H., Schell, J.A., Deering, D.W., 1973. Monitoring the vernal advancement and retrogradation (green wave effect) of natural vegetation.

Salinero-Delgado, M., Estévez, J., Pipia, L., Belda, S., Berger, K., Paredes Gómez, V., Verrelst, J., 2022. Monitoring Cropland Phenology on Google Earth Engine Using Gaussian Process Regression. Remote Sensing 14, 146. https://doi.org/10.3390/rs14010146

Santi, E., Dabboor, M., Pettinato, S., Paloscia, S., 2019. Combining Machine Learning and Compact Polarimetry for Estimating Soil Moisture from C-Band SAR Data. Remote Sens. 11, 2451. https://doi.org/10.3390/rs11202451

Schwartz, M.D., Reed, B.C., 1999. Surface phenology and satellite sensor-derived onset of greenness: An initial comparison. International Journal of Remote Sensing 20, 3451–3457. https://doi.org/10.1080/014311699211499

Schwieder, M., Wesemeyer, M., Frantz, D., Pfoch, K., Erasmi, S., Pickert, J., Nendel, C., Hostert, P., 2022. Mapping grassland mowing events across Germany based on combined Sentinel-2 and Landsat 8 time series. Remote Sensing of Environment 269, 112795. https://doi.org/10.1016/j.rse.2021.112795

Séraphin, P., Vallet-Coulomb, C., Gonçalvès, J., 2016. Partitioning groundwater recharge between rainfall infiltration and irrigation return flow using stable isotopes: The Crau aquifer. Journal of Hydrology 542, 241–253. https://doi.org/10.1016/j.jhydrol.2016.09.005

Serouart, M., Madec, S., David, E., Velumani, K., Lopez Lozano, R., Weiss, M., Baret, F., 2022. SegVeg: Segmenting RGB Images into Green and Senescent Vegetation by Combining Deep and Shallow Methods. Plant Phenomics 2022. https://doi.org/10.34133/2022/9803570

Sharma, A., Hubert-Moy, L., Buvaneshwari, S., Sekhar, M., Ruiz, L., Bandyopadhyay, S., Corgne, S., 2018. ambik. Remote Sensing 10, 893. https://doi.org/10.3390/rs10060893

Simonneaux, V., Duchemin, B., Helson, D., Er-Raki, S., Olioso, A., Chehbouni, A.G., 2008. The use of high-resolution image time series for crop classification and evapotranspiration estimate over an irrigated area in central Morocco. Int. J. Remote Sens. 29, 95–116. https://doi.org/10.1080/01431160701250390

Sonobe, R., Yamaya, Y., Tani, H., Wang, X., Kobayashi, N., Mochizuki, K., 2017. Assessing the suitability of data from Sentinel-1A and 2A for crop classification. GISci. Remote Sens. 54, 918–938. https://doi.org/10.1080/15481603.2017.1351149

Stumpf, F., Schneider, M.K., Keller, A., Mayr, A., Rentschler, T., Meuli, R.G., Schaepman, M., Liebisch, F., 2020. Spatial monitoring of grassland management using multi-temporal satellite imagery. Ecol. Indic. 113, 106201. https://doi.org/10.1016/j.ecolind.2020.106201

Taravat, A., Wagner, M., Oppelt, N., 2019. Automatic Grassland Cutting Status Detection in the Context of Spatiotemporal Sentinel-1 Imagery Analysis and Artificial Neural Networks. Remote Sensing 11, 711. https://doi.org/10.3390/rs11060711

Thenkabail, P.S., Schull, M., Turral, H., 2005. Ganges and Indus river basin land use/land cover (LULC) and irrigated area mapping using continuous streams of MODIS data. Remote Sensing of Environment 95, 317–341. https://doi.org/10.1016/j.rse.2004.12.018

Tian, J., Zhu, X., Chen, J., Wang, C., Shen, M., Yang, W., Tan, X., Xu, S., Li, Z., 2021. Improving the accuracy of spring phenology detection by optimally smoothing satellite vegetation index time series based on local cloud frequency. ISPRS Journal of Photogrammetry and Remote Sensing 180, 29–44. https://doi.org/10.1016/j.isprsjprs.2021.08.003

Tian, J., Zhu, X., Wu, J., Shen, M., Chen, J., 2020. Coarse-Resolution Satellite Images Overestimate Urbanization Effects on Vegetation Spring Phenology. Remote Sensing 12, 117. https://doi.org/10.3390/rs12010117

Toosi, A., Javan, F.D., Samadzadegan, F., Mehravar, S., Kurban, A., Azadi, H., 2022. Citrus orchard mapping in Juybar, Iran: Analysis of NDVI time series and feature fusion of multi-source satellite imageries. Ecol. Inform. 70, 101733. https://doi.org/10.1016/j.ecoinf.2022.101733

Trolard, F., Bourrié, G., Baillieux, A., Buis, S., Chanzy, A., Clastre, P., Closet, J.-F., Courault, D., Dangeard, M.-L., Di Virgilio, N., Dussouilliez, P., Fleury, J., Gasc, J., Géniaux, G., Jouan, R., Keller, C., Lecharpentier, P., Lecroart, J., Napoleone, C., Mohammed, G., Olioso, A., Reynders, S., Rossi, F., Tennant, M., de Vicente Lopez, J., 2016. The PRECOS framework: Measuring the impacts of the global changes on soils, water, agriculture on territories to better anticipate the future. Journal of Environmental Management 181, 590–601. https://doi.org/10.1016/j.jenvman.2016.07.002

Tucker, C., 1979. Red and Photographic Infrared Linear Combinations for Monitoring Vegetation. Remote Sens. Environ. 8, 127–150. https://doi.org/10.1016/0034-4257(79)90013-0

Tuffery, L., Davi, H., López-García, N., Rigolot, E., Jean, F., Stenger, A., Lefèvre, F., 2021. Adaptive measures for mountain Mediterranean forest ecosystem services under climate and land cover change in the Mont-Ventoux regional nature park, France. Reg Environ Change 21, 12. https://doi.org/10.1007/s10113-020-01732-4

Usha, K., Singh, B., 2013. Potential applications of remote sensing in horticulture—A review. Scientia Horticulturae 153, 71–83. https://doi.org/10.1016/j.scienta.2013.01.008

Van Der Perk, M., Jetten, V., Heskes, E., Segers, M., Wijntjens, I., 2004. Transport and retention of copper fungicides in vineyards, in: Golosov, V., Belyaev, V., Walling, D.E. (Eds.), Sediment Transfer Through the Fluvial System. Int Assoc Hydrological Sciences, Wallingford, pp. 437–443.

van Dijck, S.J.E., van Asch, Th.W.J., 2002. Compaction of loamy soils due to tractor traffic in vineyards and orchards and its effect on infiltration in southern France. Soil and Tillage Research 63, 141–153. https://doi.org/10.1016/S0167-1987(01)00237-9

Veloso, A., Mermoz, S., Bouvet, A., Toan, T.L., Planells, M., Dejoux, J.-F., Ceschia, E., 2017. Understanding the temporal behavior of crops using Sentinel-1 and Sentinel-2-like data for agricultural applications. Remote Sens. Environ. 199, 415–426. https://doi.org/10.1016/j.rse.2017.07.015

Verger, A., Filella, I., Baret, F., Penuelas, J., 2016. Vegetation baseline phenology from kilometric global LAI satellite products. Remote Sens. Environ. 178, 1–14. https://doi.org/10.1016/j.rse.2016.02.057

Vrieling, A., Meroni, M., Darvishzadeh, R., Skidmore, A.K., Wang, T., Zurita-Milla, R., Oosterbeek, K., O'Connor, B., Paganini, M., 2018. Vegetation phenology from Sentinel-2 and field cameras for a Dutch barrier island. Remote Sensing of Environment 215, 517–529. https://doi.org/10.1016/j.rse.2018.03.014

Wada, Y., Wisser, D., Eisner, S., Flörke, M., Gerten, D., Haddeland, I., Hanasaki, N., Masaki, Y., Portmann, F.T., Stacke, T., Tessler, Z., Schewe, J., 2013. Multimodel projections and uncertainties of irrigation water demand under climate change. Geophysical Research Letters 40, 4626–4632. https://doi.org/10.1002/grl.50686

Wang, C., Li, J., Liu, Q., 2017. Analysis on Difference of Phenology Extracted from Evi and Lai, in: 2017 Ieee International Geoscience and Remote Sensing Symposium (Igarss). Ieee, New York, pp. 5101–5104.

Wang, S., Zhang, L., Huang, C., Qiao, N., 2017. An NDVI-Based Vegetation Phenology Is Improved to be More Consistent with Photosynthesis Dynamics through Applying a Light Use Efficiency Model over Boreal High-Latitude Forests. Remote Sens. 9, 695. https://doi.org/10.3390/rs9070695

Weiss, M., Baret, F., 1999. Evaluation of Canopy Biophysical Variable Retrieval Performances from the Accumulation of Large Swath Satellite Data. Remote Sensing of Environment 70, 293–306. https://doi.org/10.1016/S0034-4257(99)00045-0

Weiss, M., Baret, F., Leroy, M., Hautecoeur, O., Bacour, C., Prevot, L., Bruguier, N., 2002. Validation of neural net techniques to estimate canopy biophysical variables from remote sensing data. Agronomie 22, 547–553. https://doi.org/10.1051/agro:2002036

White, M.A., de Beurs, K.M., Didan, K., Inouye, D.W., Richardson, A.D., Jensen, O.P., O'Keefe, J., Zhang, G., Nemani, R.R., van Leeuwen, W.J.D., Brown, J.F., de Wit, A., Schaepman, M., Lin, X., Dettinger, M., Bailey, A.S., Kimball, J., Schwartz, M.D., Baldocchi, D.D., Lee, J.T., Lauenroth, W.K., 2009. Intercomparison, interpretation, and assessment of spring phenology in North America estimated from remote sensing for 1982-2006. Glob. Change Biol. 15, 2335–2359. https://doi.org/10.1111/j.1365-2486.2009.01910.x

Whyte, A., Ferentinos, K.P., Petropoulos, G.P., 2018. A new synergistic approach for monitoring wetlands using Sentinels-1 and 2 data with object-based machine learning algorithms. Environ. Modell. Softw. 104, 40–54. https://doi.org/10.1016/j.envsoft.2018.01.023

Wriedt, G., Van der Velde, M., Aloe, A., Bouraoui, F., 2009. Estimating irrigation water requirements in Europe. Journal of Hydrology 373, 527–544. https://doi.org/10.1016/j.jhydrol.2009.05.018

Xiang, K., Ma, M., Liu, W., Dong, J., Zhu, X., Yuan, W., 2019. Mapping Irrigated Areas of Northeast China in Comparison to Natural Vegetation. Remote Sensing 11, 825. https://doi.org/10.3390/rs11070825

Xiao, X.M., Boles, S., Liu, J.Y., Zhuang, D.F., Frolking, S., Li, C.S., Salas, W., Moore, B., 2005. Mapping paddy rice agriculture in southern China using multi-temporal MODIS images. Remote Sens. Environ. 95, 480–492. https://doi.org/10.1016/j.rse.2004.12.009

Xie, Y., Lark, T.J., 2021. Mapping annual irrigation from Landsat imagery and environmental variables across the conterminous United States. Remote Sens. Environ. 260, 112445. https://doi.org/10.1016/j.rse.2021.112445

Yang, X., Mustard, J.F., Tang, J., Xu, H., 2012. Regional-scale phenology modeling based on meteorological records and remote sensing observations. J. Geophys. Res.-Biogeosci. 117, G03029. https://doi.org/10.1029/2012JG001977

Zeng, L., Wardlow, B.D., Xiang, D., Hu, S., Li, D., 2020. A review of vegetation phenological metrics extraction using time-series, multispectral satellite data. Remote Sens. Environ. 237, 111511. https://doi.org/10.1016/j.rse.2019.111511

Zhang, X.Y., Friedl, M.A., Schaaf, C.B., Strahler, A.H., Hodges, J.C.F., Gao, F., Reed, B.C., Huete, A., 2003. Monitoring vegetation phenology using MODIS. Remote Sens. Environ. 84, 471–475. https://doi.org/10.1016/S0034-4257(02)00135-9

Zheng, Y., Wu, B., Zhang, M., Zeng, H., 2016. Crop Phenology Detection Using High Spatio-Temporal Resolution Data Fused from SPOT5 and MODIS Products. Sensors 16, 2099. https://doi.org/10.3390/s16122099

Zhong, L., Gong, P., Biging, G.S., 2012. Phenology-based Crop Classification Algorithm and its Implications on Agricultural Water Use Assessments in California's Central Valley. Photogramm. Eng. Remote Sens. 78, 799–813. https://doi.org/10.14358/PERS.78.8.799

Zhu, Z., Wulder, M.A., Roy, D.P., Woodcock, C.E., Hansen, M.C., Radeloff, V.C., Healey, S.P., Schaaf, C., Hostert, P., Strobl, P., Pekel, J.-F., Lymburner, L., Pahlevan, N., Scambos, T.A., 2019. Benefits of the free and open Landsat data policy. Remote Sensing of Environment 224, 382–385. https://doi.org/10.1016/j.rse.2019.02.016

Zonal statistics in R | GeoProfesja, 2016. URL http://geoprofesja.pl/en/zonal-statistics-in-r/ (accessed 10.18.22).